Master of Science in Mining Engineering

November 2023

Master Thesis

Geochemical Mapping of the North-Central Portion of the Yukon-Tanana Upland, Alaska, United States: Application of Exploratory Data Analysis (EDA) to REE and PGE Mining Prospection

Supervisor:

Prof. Adriano Fiorucci

Candidate:

Cristian Leonardo Sanchez Siachoque

Abstract

The demand for Rare Earth Elements (REE) and Platinum Group Elements (PGE) in advanced technologies and clean energy has highlighted concerns about China's dominance in the REE market. To reduce dependence on foreign mineral supplies crucial for national security and the economy, the United States has sought to enhance its geological knowledge and identify undiscovered critical mineral resources.

This thesis focuses on the north-central region of the Yukon-Tanana Uplands in Alaska, a region of profound geological intrigue, holding the potential for significant critical mineral resource deposits. It employs advanced geochemical mapping techniques and Exploratory Data Analysis (EDA) to assess this potential with geochemical data provided by the Earth Mapping Resources Initiative (Earth MRI), carried out by the United States Geological Survey.

The study identifies distinct geochemical associations, including REE´s, REE pathfinders and PGE pathfinders, through multivariate analysis (PCA) and validates these associations through bivariate analysis. Tantalum (Ta) and Titanium (Ti) are excluded from further analysis due to weak correlations.

Univariate analysis generates two types of geochemical maps for REE and PGE associations, revealing distinct patterns and anomalies. Hafnium (Hf) and Zirconium (Zr) exhibit unique and different patterns within the REE group, while Chromium (Cr) differs from typical PGE patterns.

Using ArcGIS, the study combines dimensionally reduced geochemical elements from EDA to produce conclusive mining potential maps. The REE mining map identifies six anomalous zones, with only zones I and II as potential candidates for hosting REE mineralization. In the PGE mining map, three anomalous zones, including zones I and II, are recognized as viable PGE prospects.

Overlaying mining potential maps onto the geological map confirms the association of REE anomalous zones with Granitic peralkaline/alkaline rocks, known for their REE-hosting characteristics. Additionally, PGE occurrences are linked not only to igneous rocks but also to sedimentary and metamorphic rocks, especially those with mafic and ultramafic compositions, common PGE hosts.

Table of contents

List of figures

1. Introduction

The northern portion of the Yukon-Tanana Uplands in Alaska, United States, holds great potential for the discovery of abundant mineral resources, such as Earth Elements (REE), Platinum Group Elements (PGE), Gold, Cooper, Niquel, Molybdenum, Cobalt, etc. Recently, the rising demand for advanced technologies, clean energy solutions, and catalytic applications has accentuated the significance of Rare Earth Elements (REE) and Platinum Group Elements (PGE). These elements, although relatively scarce in the Earth's crust, play a critical role in modern industry, encompassing a wide spectrum of applications ranging from electronics, automotive, and energy sectors to catalysis and environmental technologies. Given their critical importance, the exploration and assessment of REE and PGE resources have gained prominence in the field of earth sciences.

The increasing global demand for REE and PGE resources has been further accentuated by China's near monopoly in their production and supply. It has raised significant concerns regarding the global supply chain's vulnerability. As a response to these concerns, the United States, along with other nations, has initiated actions to establish a more self-reliant and secure access to these critical resources. Earth Mapping Resources Initiative (Earth MRI), the source of the geochemical data of this thesis, is a giant and ambitious governmental project specially designed by the United States Geological Service for enhancing the knowledge of the geologic framework in the United States and to identify areas with the capacity to potentially harbor undiscovered critical mineral reserves, with the aim of reducing the country's dependence on foreign mineral supplies crucial for both the national security and economy. Earth MRI stands out as a multifaceted program encompassing a wide array of data collection methods, including geochemical surveys, geophysics, remote sensing, geological modeling, and more.

This thesis embarks on a comprehensive investigation, utilizing advanced geochemical mapping techniques, with a central focus on the application of Exploratory Data Analysis (EDA) for REE and PGE mining prospection. The objective is to enhance the understanding of the distribution and prospectivity of these critical minerals within this geologically complex region.

This comprehensive investigation applies various components of Exploratory Data Analysis (EDA), encompassing univariate, bivariate, and multivariate analyses. These analytical tools offer a structured approach to uncovering patterns, relationships, and hidden insights within the geochemical dataset, culminating in the generation of geochemical maps and mining potential maps. These maps serve as a vital tool for identifying anomalous zones, where elevated concentrations of REE and PGE are indicative of mineralization prospects.

As the chapters of this thesis unfold, the research will delve into the methodologies employed, the insights gained from EDA, and the broader implications for mining prospection. This thesis serves to contribute not only to scientific knowledge but also to the practical strategies that nations like the United States are adopting to ensure resource sustainability and national security in an increasingly competitive and resource-dependent world.

2. Yukon-Tanana Uplands Terrene

2.1 Main physiography

The study area, the North portion of the Yukon-Tanana uplands terrene spans over 75 miles from Fairbanks City to the Chena River State Area, Alaska, USA. The study area extends around an area of approximately 6,200 square miles. The Yukon-Tanana Upland is a huge region formed up of rounded hills and ridges that extend to heights of several thousand feet. The highest mountains, which range in elevation from 4,000 to 6,700 feet and are made of granite and gneiss, have been shaped and made steeper thanks to glacial erosion. The north-east tendency of the bedrock formations influences the dendritic drainage pattern present in the area. There are currently no glaciers, and there may be permanent snowbanks on higher heights. These circular ridges in the present in the zone, have ridge-crest heights of 1,500–3,000 feet and rise up to 500–1,500. [1] The whole area is part of the Yukon drainage basin. Both north and south oriented streams drain into the Yukon River flow in narrow V-shaped terraced canyons. The majority of the region's streams follow paths that are parallel to the bedrock's structural tendencies. Drainage divisions are extremely variable. Small streams typically go southward laterally.[1] The uplands currently undergo a continental climate with long, cold winters and brief, cool summers. The region experiences temperatures between a minimum winter low of —70° F and a maximum summer high of around 100° F. [2]

2.2 Geological Context

The predominant rocks in the region include quartzitic, pelitic, calcareous, and mafic metasedimentary rocks, with a little quantity of mafic to felsic meta-igneous rocks. Mesozoic and Cenozoic granitic rocks as well as tiny amounts of intermediate and mafic rocks have heavily intruded these rocks **(Figure 1)**. The eastern portion of the region is rich in volcanic rocks from the Cretaceous and Tertiary periods. Nonmarine sedimentary rocks from the Late Cretaceous and Tertiary times were deposited in tiny basins that were frequently surrounded by volcanic rocks and/or faults. Alpine-type ultramafic rocks can be found in patches, primarily in the northern half of the region, along with greenstones, basalts, gabbros, cherts, graywackes, and other sedimentary rocks. (Tempelman-Kluit, 1976 and Churkin and others, 1982). [3]

Unconsolidated deposits

Qs Unconsolidated surficial deposits, undivided (Quaternary)

These deposits are a mix of unconsolidated materials, such as alluvial, colluvial, marine, lacustrine, eolian, and swamp deposits. They also present glacial and periglacial deposits from both the Holocene and Pleistocene periods. These deposits evidence presence of volcanic debris and block and ash flows that have been reworked over time.

QTs Poorly consolidated surficial deposits (Quaternary, Pleistocene, and uppermost Tertiary)

Alaska's erosional remnant deposits encompass from silt to coarse-gravel and semi-consolidated sandstone to conglomerate. These deposits present fluvial, glaciofluvial, colluvial, eolian, and shallow-marine deposits, as well as local tuffaceous deposits. The unit includes several named formations, such as the Faneto Formation, Kougarok Gravel, Chariot, Saligvik, and Ilyirak Gravels, and the Gubik Formation. Some deposits exhibit folding or tilting, reflecting tectonic movement. Additionally, exhibits marine

deposits which are rich in fossils, but age control is not well defined. Some deposits are thought of as outwash deposits from glaciated highlands southwest of the Kuskokwim River. Other deposits include bedded sand and gravel, semi-consolidated marine beach deposits, and the Gubik Formation. (Powers and others, 1960).
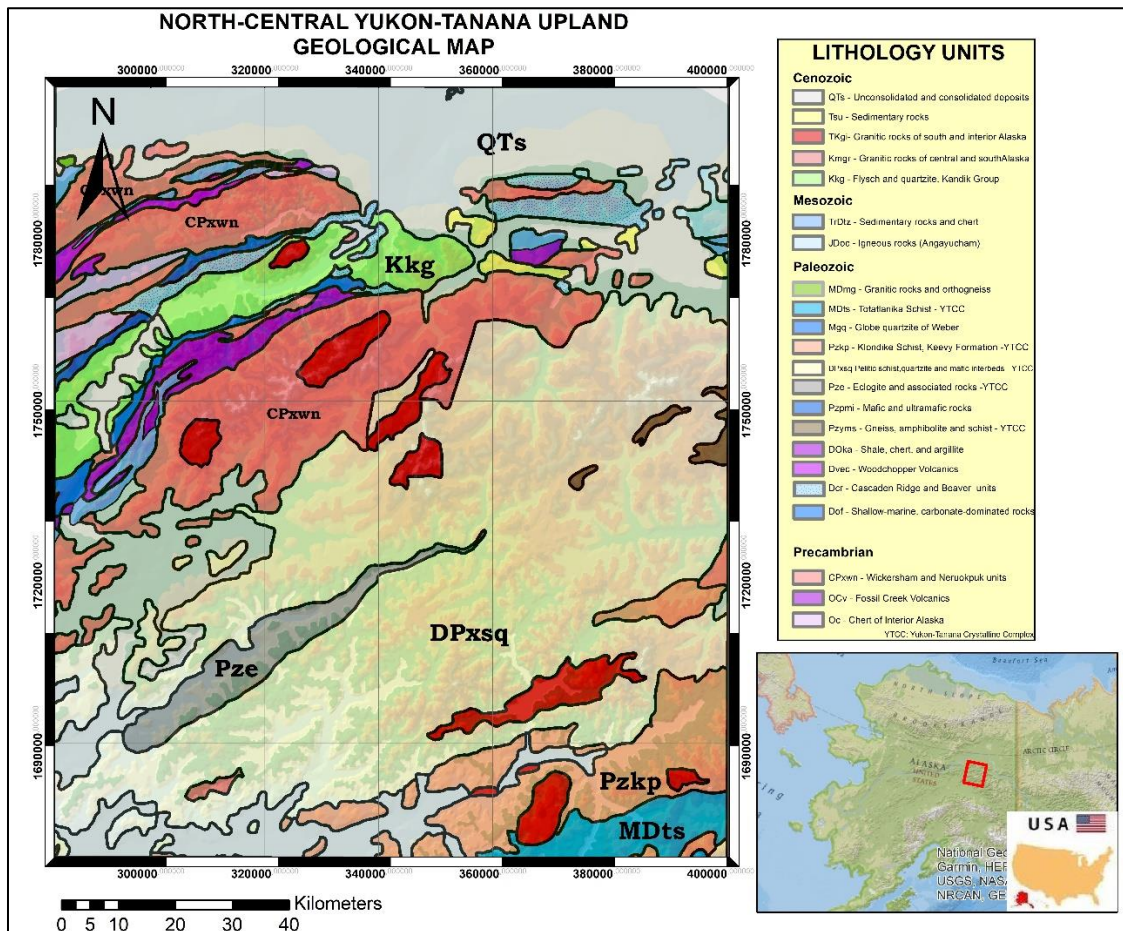
Figure 1: Geological map of the Study zone

Sedimentary rocks

Dcr - Cascaden Ridge and Beaver Bend combined correlative units (Devonian): The Cascaden Ridge unit, mostly described by Weber and others (1992), includes gray and olive-gray shale, siltstone, and graywacke in the Livengood quadrangle. Moreover, another secondary component includes gray limestone and polymictic granule- and pebble-conglomerate with a graywacke matrix. The Beaver Bend unit is made up of conglomerate, graywacke, siltstone, and slate. Moreover, the Beaver Bend unit contains plant fragments and is assigned a Devonian age. On the general map, is part of unit DZyf.

DZkb Older carbonate strata of the Porcupine River sequence of Brosgé and Reiser (1969) and equivalent units (Middle Devonian to Neoproterozoic?): Named the Salmontrout Limestone, it is a poorly known unit in the Yukon Flats basin, it is characterized by a a thick sequence of limestone, dolostone, and minor calcareous shale and black chert. It is about 600 ft thick and is a biohermal Limestone (Churkin and Brabb, 1965; Oliver and others, 1975). The Table Mountain quadrangle presents gray, foliated, thin-bedded, platy, and recrystallized micritic limestone. On the general map, is part of unit DZyf.

Metamorphic rocks

Pze Eclogite and associated rocks (Paleozoic): The assemblage basically is a metamorphic sequence of biotite-muscovite schist, micaceous marble, black quartzite, and amphibolite in thin interlayers. It´s assigned a epidote-amphibolite facies rocks, sharing lithologic similarities with the structurally underlying quartz and pelitic schist (Swainbank and Forbes, 1975; Brown and Forbes, 1986; Weber and others, 1992; Foster and others, 1994). The protolith of eclogite comprises quartz-rich and pelitic to calcareous pelitic sedimentary rocks, impure limestone, and mafic volcanic and volcaniclastic rocks. Pressure and temperature conditions estimations are from 590 °C and 5.5 to 7.5 kbar.

Kkg Flysch and quartzite, Kandik Group, and equivalents (Lower Cretaceous, Albian to Valanginian): The Kandik Group encompass several units such as the Keenan Quartzite, Biederman Argillite, and Kathul Graywacke. Keenan Quartzite is a massive, resistant quartzite and sandstone with abundant Buchia sublaevis of Valanginian age (Brabb, 1969). Biederman Argillite is a 1,500 m thick and interbedded, with a few beds of chert-pebble conglomerate, siliceous shale, chert-limestone breccia, and limestone. Kathul Graywacke is made up of several thousand feet dark-greenish-gray, feldspathic graywacke, conglomerate, dark-gray argillite and olive-gray shale and mudstone.

Mgq Globe quartzite of Weber and others (1992) (Mississippian): Defined as a fine- to medium-grained dense quartzite, vitreous, additionally, includes monocrystalline quartz grains and scanty chert grains. Shares lithologic and stratigraphic features to Keno Hill Quartzite in Yukon, Canada, and it is also found in Livengood and Tanana quadrangles (Weber and others, 1992; Dover, 1994).

Pzyms Mafic schist and amphibolite (Devonian or older Paleozoic): Named as Green Quartz-Chlorite-Carbonate schist, it comprises a green, metamorphosed mafic pyroclastic rock found in several locations. It is associated with amphibolitic schist,marble, quartzite, and pelitic schist. It exhibits variations in color and texture, with dark green, fine- to coarse-grained, strongly foliated hornblende-biotite gneiss and augen gneiss (Wilson and others, 1998; see also Foster and others, 1983). The unit also presents a green and white metaigneous rock.

Pzkp - Keevy Peak Formation and similar rocks (early Paleozoic): The unit consists in several deformed siliceous and carbonaceous array of phyllite, meta-argillite, quartzite, metachert, and interlayered calcareous phyllite, marble, and mafic and felsic metavolcanic rocks ranging at lower to upper greenschist facies. (Foster, 1992; Dusel-Bacon and others, 1993). It contains the Keevy Peak Formation in the Healy and Denali quadrangles. The unit typically crops up nearby to the Totatlanika Schist (MDts).

DPxsq Quartzite and pelitic schist (Devonian and older): This fossilized rock is primarily exhibiting a series of quartzite, schistose quartzite, and quartz-mica schist, with other elements including gritty quartzite, chlorite schist, calc-silicate schist, marble, magnetite-biotite schist, amphibolite, and greenstone (Nokleberg and others, 1992a; Smith and others, 1994). It is associated with the Fairbanks schist and surrounding areas. Other cropping areas are in the southern Big Delta quadrangle and Eagle quadrangle.

PzPyqm - Pelitic schist, including Chena River sequence (Devonian and older): This unit is considered a medium- to high-grade pelitic schist associated with quartzite, quartz schist, calc-silicate rocks, marble, amphibolite, graphitic schist, and augen gneiss interlayers. It shares significant similitudes in lithology, polymetamorphic history, and metamorphic grade with metaplutonic rocks of unit MDag Foster and others (1983)

MDts Totatlanika Schist (Early Mississippian to Late Devonian): The Totatlanika Schist is a low-grade rock formation that has undergone multiple deformations and can locally exhibit mylonitic textures It comprises gritty semischist with quartz "eyes," chloritic quartzo-feldspathic schist, augen gneiss, phyllitic schist, phyllite, metavolcanic rocks, quartzite, marble, and greenstone. Fossil age is not well defined, conodonts dated from Middle Devonian to Early Mississippian. Foster (1992)

CPxwn Wickersham and Neruokpuk units (Cambrian and Proterozoic): The Wickersham unit, also referred as the Hyland Group in Yukon, Neruokpuk Schist of Leffingwell, Nilkoka Group in central Alaska, and the informal Wickersham unit in Alaska, is a clastic sequence of poorly sorted quartzite, feldspathic quartzite, grit, calcareous siltstone, fine-grained sandstone,dark limestone and chert. It is made up of the presence of maroon and green slate and grit. In central Alaska, the unit typically is characterized by a gray, maroon, and green slaty argillite interlayered with gray and greenish-gray grit and quartzite, phyllite, slate, minor limestone, and chert (Foster and others, 1983; Weber and others, 1992). In northeast Alaska, the Neruokpuk Schist of Leffingwell exhibits a lithologic transition from south to north, with exposures of interbedded thin- to thick-bedded, resistant massive quartz wacke and semischist, phyllite and argillite, and calcareous sandstone. Additionally, the unit also contains siltstone, red, green, and black phyllitic slate, and rare limy beds. On the other hand, the Wickersham unit is exposed south of or within strands of the Tintina Fault System in east-central Alaska, and north of the fault system in Yukon.

Igneous rocks

OCv Fossil Creek Volcanics and similar rocks (Ordovician and Cambrian): The Fossil Creek Volcanics in east-central Alaska can be divided in two main members: volcanic and sedimentary. The volcanic member exhibits alkali basalt, agglomerate, and volcaniclastic conglomerate, while the sedimentary member is composed of shale, chert, and limestone. The unit is located in the White Mountains stratigraphic belt and northeast Alaska, with features such as mafic vesicular flows, basaltic tuffs, and calcareous volcanic wacke.

DPxsq - Granitic rocks of interior Alaska (Tertiary, Paleocene, to Cretaceous, Maastrichtian): Rock association characterized by granitic plutons, ranging from granite to quartz monzonite, are normally found in interior Alaska and the Yukon. These plutons consist of both mafic and alkalic varieties and occur in a wide belt paralleling the Tinitna and Denali Fault Systems. They are quite related to the Alaska-Aleutian batholith and arc magmatism. These plutons crosscut rocks normally without offset. They are subdivided into the following units: Tpgr, Tpg, TKg, TKgd, and TKgb

Tpg Peralkaline granite (Tertiary, Paleocene?): Based on a medium-grained hypidiomorphic granular granite with subhedral to euhedral perthite. It has correlation with the Alaska-Aleutian Range batholith and may correlate with plutons of unit Tgw (Nelson and others, 1983). The Middle Fork granite, a perthite-arfvedsonite-granite phase, assigns K/Ar ages of 57.7±1.7 and 55.6±1.7 Ma.

PzPmi Mafic igneous rocks, central and northeast Alaska (early Paleozoic and (or) late Proterozoic): The unit exhibits a series of gabbro and diabase sills and serpentinite, cropped out in a linear belt in the Livengood and northwest Circle quadrangles. Gabbro and diabase present colors dark olive green and greenish gray to dark greenish-black, moreover they are medium- to coarse-grained, and are graded as diorite. Serpentinite is intruded by dikes of clinopyroxene gabbro, microgabbro, and diorite. (Weber and others, 1988, 1992; Reifenstuhl and others, 1998a; Athey and others, 2004)

Dvec - Woodchopper Volcanics and Schwatka unit of Weber and others (1992) (Devonian): The Woodchopper Volcanics are aged as Late Devonian formation in the Charley River quadrangle, composed by a amygdaloidal basalt, pillow basalt, and aquagene tuff. They are associated to dark-gray laminated shale with minor interbeds of limestone. Instead, the Schwatka unit, mapped in Livengood and Circle quadrangles, is offset from the Woodchopper Volcanics by the Tintina Fault System and is made up of massive basalt flows, agglomerate, tuff, and limestone.[4]

3. REE and PGE Geochemistry and mineral deposits

3.1 Geochemistry of Rare Elements

Commonly the REE (i.e., the lanthanides and the group 3b elements, Sc, and Y) have a 3+ valence in most environments, except the Ce and Eu. Cerium works in 4+ state and Eu in 2+ state. Zirconium and Hf are tetravalent (4+), and Nb and Ta are pentavalent (5+). These last are known as High field strength elements (HFSE) and have high ionic potential and moderate ionic radii, making them incompatible with common rock-forming silicates. They are also referred to as 'hard' cations in hydrothermal fluids. Zirconium and Hf behave in a similar way because they share same valence and ionic radii. In certain geological settings, Ce and Eu can exhibit valences of 4+ and 2+ respectively, which results in unusual behavior compared to other rare earth elements (REE). These deviations are referred to as anomalies and are determined by comparing the actual normalized concentration of these elements to their estimated concentration based on interpolation between La and Pr, or between Sm and Gd, respectively. These anomalies commonly occur when a substantial proportion of Eu2+ or Ce4+ is present in a fluid or magma, leading to distinct behavior for these elements. For instance, if conditions favor the presence of a significant amount of Eu2+, the incorporation of divalent Eu into calcium-rich minerals like calcic plagioclase can end up in negative Eu anomalies. On the other hand, the dissolution of primary Eu-enriched minerals can lead to an enrichment of Eu (positive anomalies) in a fluid. The ratios of Eu2+/Eu3+ and Ce3+/Ce4+ in a fluid or magma are influenced by factors such as redox conditions and temperature. These ratios are indicative of the prevailing conditions and can contribute to the observed anomalies in the behavior of Eu and Ce.

3.2 Concentrations of rare elements in magmatic rocks

The concentration of rare elements, including rare earth elements (REE) and high field strength elements (HFSE), are normally low, except for Y and Zr. On the other hand, ocean island basalt (OIB) shows higher concentrations of rare elements compared to N-MORB. A typical OIB contains approximately 280 ppm Zr, 48 ppm Nb, and REE abundances from 80 to 0.3 ppm. Although ore deposits are not directly associated with these rock types, they are commonly found in carbonatites, peralkaline granites (Syenite and nepheline), feldspathoid-bearing rocks, or peraluminous granites and pegmatites. Rare-element pegmatites exhibit two distinct suites: LCT (Li–Cs–Ta), NYF (Nb–Y–F. Carbonatites normally are rich in light rare earth elements (LREE), with concentrations of La and Ce over 1000 ppm, instead Yb concentrations are close to 2 ppm. Moreover, carbonatites may host various ppm of Niobium and Zirconium. Peralkaline granites are characterized by a more enriched trace-element signature, with REE concentrations from hundred to 1000 ppm, and 50–100 ppm for Yb. They also present roughly 1000 ppm of niobium, various thousand for Zirconium, and less than 100 ppm of Tantalum and Hafnium.

3.3 REE deposits characteristics and types

Normally, Rare-element deposits mineralize in primary or secondary deposits, the primary deposits occur commonly in igneous rocks. Moreover, Primary deposits can be found principally in carbonatites, peralkaline granitic- silica-undersaturated rocks, and meta luminous and peraluminous granitic rocks. On the other hand, Secondary deposits evidence high considerable concentrated rare-element mineralization, for example placers are typical sources of Ta, Zr, and Hf, as well as supergene laterites clays which can host REE.

Carbonatites and genetically related rocks

Carbonatite is a term used to describe igneous rocks that contain 50% or more carbonate minerals (calcite, dolomite), while rocks with less than 50% carbonate are just genetically associated to carbonatites. Metasomatic and hydrothermal deposits related to carbonatites have not well-defined origins but are related to carbonatitic sources. Rare-metal deposits with carbonatitic affinity can be found into several categories, such as Nb and REE deposits, Zr and Nb deposits, complex rare-element deposits, and weathering crusts.

Peralkaline granitic and Silicate-hosted deposits

Silicate intrusions normally host mineralization of REE, Nb, and Zr in rocks ranging from alkaline to peralkaline or ultra-alkaline. The most significant deposits are in peralkaline and ultra-alkaline rocks, with ultra-alkaline rocks predominating. World deposit examples include Khibiny and Lovozero intrusions in Russia, Ilı́maussaq intrusion in Greenland, and Nechalacho layered suite at Thor Lake in Canada. Peralkaline granites also contain important Ta mineralization, with Ghurayyah, Khaldzan-Buregtey, and Motzfeld with the largest reserves of Ta.

Peraluminous granite-hosted deposits

Peraluminous granites are known for their significant reserves of tantalum (Ta), either as primary commodities or as by-products. The mineralization in these granites is primarily composed of disseminated Ta-Nb-Sn oxide minerals, with the presence of tungsten-tin (W Sn) minerals like wolframite and cassiterite often found in peripheral quartz veins. These Deposits are zoned with depth, with some zonation related to magmatic processes. Instead, the upper zone, rich in Fe and W, is thought to be correlated with hydrothermal fluid activity.[5]

3.4 REE pathfinders

Frequently some elements often co-occur or exhibit similar geochemical behavior to REEs, making them useful indicators in identifying potential REE-rich deposits. According to (Baralam 2022) summary of REE pathfinder element depending on the type of deposit is:[6]

Type of deposit	Common host minerals	Pathfinder elements
Carbonatite rocks	Bastnäsite group, ancylite, monazite, (fluor)apatite, pyrochlore, xenotime, florencite.	Na, Mg, Fe, P, Ba, F, S, Sr, Ca, Nb, Th, U, Zr, Cu, Ta, Ti, V, Mn, Pb.
Igneous rocks (including hydro-thermal rocks)	Bastnäsite group, aegirine, eudialyte, loparite, allanite, calcite, allanite, Fe-rich olivine, fayalite, monazite, fergusonite, zircon, xenotime, fluorapatite, ancylite, gadolinite, euxenite, mosandrite.	Na, K, Fe, Al, Zr, Ti, Nb, Ta, Li, F, Cl, Si, Th, U, P, Cs, Rb, Sn, W, Mo, Be, Ga, Hf, Mn, B.
Placers and paleo-placers including regoliths which are not laterites but *in-situ* weathered overburden.	Monazite, xenotime, allanite, euxenite.	Ti, Nb, Zr, Au, Sn, Th, U, Pb, F.
Laterites	Monazite, apatite, pyrochlore, crandallitegroup, bastnäsite group, churchite, rhabdophane, plumbogummite, zircon, florencite, xenotime, cerianite.	Fe, Al, Nb, Zr, Ti, Sn, Mn, P, low Si, negative Ce anomaly.
Ion-adsorption	Clay minerals (mainly kaolinite and halloysite).	High Si (>75%), low P.
Iron oxide-associated (including IOCG) deposits	Bastnäsite, synchysite, monazite, xenotime, florencite, britholite.	Fe, Cu, U, Au, Ag, Ba, F, P, S.
Deep-sea mineral deposits (poly-metallic nodules, crusts and marine mud)	Vernadite, Todorokite, Fe-oxyhydroxide, Carbonate fluorapatite	Mn, Fe, P, Cu, Ni, Co.

Table 1: *Different types of REE deposits, pathfinder minerals and Elements [6]*

3.5 Platinum-group elements (PGE) geochemistry

The platinum group elements (PGE) encompass six metallic elements, Ru, Rh, Pd, Os, Ir, and Pt, which share similar physical and chemical properties. These elements normally coexist within single mineral deposits. The PGE can be organized in two subgroups: the iridium subgroup (Os, Ir, Ru) and the palladium subgroup (Rh, Pt, Pd). This division is based on the coherent behavior of each subgroup's members during magmatic processes. In addition, they form over 100 PGE-bearing minerals, moreover, the PGE are also found in native metals, alloys, and complex solid solutions. PGE also exhibits variable associations with elements such as Co, Cr, Cu, Ni, Ti, and V in deposits related to mafic to ultramafic (MUM) rocks. [6] The deposits can be classified into two groups according to Naldrett (1981). The first group consists of ores where nickel (Ni) and copper (Cu) are the primary products, while the noble metals (platinum group elements (PGE) and gold (Au)) are considered byproducts. These deposits normally have more than 10% sulfide minerals. They typically present irregular orebodies shapes associated with small intrusions. Additionally, they can also be found at the base of lava channels formed by komatiite, basaltic komatiite, and picrite. Locating these deposits can be challenging due to their irregular nature. The second group comprises deposits where the PGE are the primary products, while Ni and Cu are considered byproducts. These are known as PGE reef-type deposits, such as the UG-2 and Merensky reefs of the Bushveld Complex or the JM reef of the Stillwater Complex in Montana. Exploration and research on PGE deposits have experienced a significant surge in the past 10-15 years. However, despite these advancements, the origin of many deposits and occurrences still lacks clarity. This is primarily due to the identification of a wide range of mineralization styles. Among these styles, deposits and occurrences that are primarily of magmatic origin and associated with mafic-ultramafic intrusions are the most significant and prevalent.

3.6   PGE deposits characteristics and types

PGE deposits and occurrences is divided into eight groups: PGE enriched intervals along the base of intrusions, mineralized intervals within ultramafic silicate cumulates, chromitites, layers associated with layered mafic-ultramafic cumulates, PGE enriched intervals in upper, gabbroic-dioritic portions, deposits related to late magmatic and hydrothermal fluids, unmineralized intrusions, and PGE as byproducts in some magmatic Ni-Cu sulfide deposits and occurrences.

PGE mineralization at the base/sidewall of intrusions

This particular type of mineralization is characterized by the presence of disseminated sulfide mineralization, and in some cases, massive sulfide mineralization. located at or near the base or sidewall of the intrusions. The ores are predominantly found within heterogeneous gabbroic rocks, and less commonly, ultramafic rocks, which exhibit varying textures, modes, and grain sizes. These rocks are often referred to as "vary-textured" or "taxitic" rocks. Additionally, they frequently contain xenoliths of the surrounding country rocks and veins of felsic intrusive, which may represent partial melts of the floor rocks.

PGE mineralization in peridotites and pyroxenites within the lower portions of intrusions

The occurrence occurs at varying distances above the base of the intrusion, ranging from several hundred meters to 1000 meters. It exhibits wide zones, normally several tens of meters, where disseminated sulfides are found within peridotites or pyroxenites. The sulfide content in these zones is below 5%, and the PGE grades can be various parts per million (ppm). Currently, the only economically viable example of this type of mineralization is the MSZ in the Great Dyke.

13

PGE mineralization in chromitites

Chromitites found in layered intrusions generally exhibit higher concentrations of PGE compared to the surrounding silicate host lithologies. In the case of the Bushveld Complex, the grades of the main seams can vary from approximately 0.1 parts per million (ppm) total PGE in the LG1 seam to around 6-7 ppm in the UG2 seam). The chromitite stringers of the Merensky Reef, which are less than 2 centimeters in width, can contain up to 50 ppm of PGE (Barnes and Maier, 2002a). Currently, the only significant chromitite being mined for its PGE content is the UG2 chromitite. It represents the largest known resource of PGE globally, with a width of approximately 1 meter and extending over several hundred kilometers.

Fig. 1. Schematic diagram showing occurrence of PGE mineralization in mafic–ultramafic intrusions and their feeder conduits. See Table 1 for further characterization of reefs. J-M = J-M reef of Stillwater complex; SJ = Sompujärvi reef of Penikat intrusion; SK = Siika Kämä reef of Portimo intrusion; LG = lower group chromitites (Bushveld); MG = middle group chromitites (Bushveld). Figure modelled after Hoatson and Sun (2002).

Figure 2: Schematic diagram showing occurrence of PGE in Mafic and Ultramafic Intrusions [8]

PGE mineralization in the mafic, central portion of intrusions

The Merensky Reef and J-M Reef of the Stillwater Complex are two of the world's most significant PGE deposits. These reefs occur above intrusions, showing evidence of magma replenishments and mixing among diverse magma types. The mineralization may be found within various rock types, including harzburgites, pyroxenites, troctolites, norites, gabbros, and anorthosites. The ore zone appears near the base of cyclic units, ranging from chromitite to anorthosite.[8]

Ni-Cu-PGE-Cr-V bearing layered mafic-ultramafic intrusions cases.

Layered mafic-ultramafic intrusions are home to some of the world's largest ore deposits, for instance those located in the Bushveld Complex of South Africa, the Great Dyke of Zimbabwe, and the Stillwater Complex of Montana. More and less 400 intrusions have been discovered around the planet, but few have been well-studied. Deposits such as Monchepluton, the 1.85–1.88 Ga Chineysky intrusion and the 728 Ma Yoko-Dovyren intrusion, contain considerable Cu-Ni, V-Ti, and PGE ore deposits which have been mined in the past and/or presently. The mafic-ultramafic deposit monchepluton, in the Kola Peninsula, has been the most

studied and mined, dating back to the 1930s. On the other hand, The Yoko-Dovyren intrusion, discovered 60 km to the NE of Lake Baikal, exhbits Cu-Ni sulfide occurrences since 1915, in the 1960s the mining started when the vast Ni-Cu-(PGE) sulfides were mapped. Another well-known mafic deposit is the Chineysky gabbronorite-anorthosite layered intrusion, in eastern Siberia, which is the Russia's largest V deposit. [9]

Stella-type reefs

Normally, the upper parts of intrusions are not targets for PGE reefs, due to low-grade Pd-Au found in several intrusions which are uneconomic. However, PGE-rich reefs, such as the Stella intrusion in South Africa, are potentially economically viable. This suggests that the upper parts of layered intrusions may are important targets for PGE reefs.

Hydrothermal PGE mineralization

Primary magmatic PGE mineralization often exhibits a low-temperature hydrothermal overprint; however, some cases have registered configurations where hydrothermal processes are the main factor in the creation of PGE concentrations. Some deposits give evidence of element remobilizations from originally magmatic PGE in shear zones or faults. For example, a well-known type of hydrothermal Au-Pd mineralization mineralize in quartzite-hematite veins associated to metamorphosed and deformed Lake Superior type Fe formations at Conceicao and Caue, Brazil. Additionally, there are cases where hydrothermal PGE mineralization with grades up to 1 ppm mineralize in thin sulfidic layers within P-rich black shales located in continental rift zones.

PGE as byproduct in magmatic Ni–Cu deposits

The most studied and accepted model for magmatic Ni-Cu deposit associated with PGE as a by-product is related to heating crustal rocks which involve large volumes of fertile mantle-derived silicate magma, normally occurring within intersection between a mantle plume within the continental rift system. The magma may become supersaturated in sulfur, forming an immiscible sulfide melt. This sulfide melt can be entrained by silicate magma, equilibrating with a large volume of silicate magma, and extracting metals. This model explains why massive or semi-massive sulfide ores are rare in large, layered intrusions. This magma has the potential to become supersaturated with sulfur, allowing the formation of a separate sulfide melt which is immiscible with silicate magma. Moreover, this sulfide melt often is incorporated into silicate magma, interacting with silicate magma, and extracting metals in the process. This model is the base to explain the scarcity of massive or semi-massive sulfide ores within extensive layered intrusions.[8]

3.7   PGE Pathfinders

According to authors such as (Melanie B et al 2016,[7]), elements such as Gold (Au), Nickel (Ni), Copper (Cu), Sulfur (S), Tellurium (Te), Bismuth (Bi), Titanium (Ti), Arsenic (As), Lead (Pb), Zinc (Zn), Cobalt (Co), Chromium (Cr), and Vanadium (V) have been identified as potential indicators for the presence of Platinum Group Elements (PGE) mineralization or as useful tools for identifying areas with the potential for PGE enrichment.[7]

4. Exploratory Data Analysis (EDA)

Exploratory data analysis (EDA) is a crucial step in any research analysis and has the purpose of examining data in to find distributions, outliers, and anomalies in order to test a hypothesis. It offers tools for visualizing and comprehending data through visual representations, aiding to support a hypothesis. EDA facilitates the recognition of natural patterns by analysis and often includes feature selection techniques. EDA has become widely accepted as the gold standard methodology for analyzing datasets. According to Howard Seltman from Carnegie Mellon University, EDA encompasses any method of examining data that does not involve formal statistical modeling and inference. EDA is an essential initial step following data collection and pre-processing, data is visualized, plotted, and manipulated without making assumptions. Its purpose is to assess data quality and aid in model building. EDA techniques primarily rely on graphics, as they provide an incomparable power to explore and gain insights from the data **(Table 2)**. There are various ways to categorize the numerous EDA techniques available. The goals of EDA can be summarized as follows:

1. Enhance understanding of the database and its structure, aiming to maximize insights gained.
2. Visualize and identify potential relationships, both in terms of direction and magnitude, between the variables.
3. Identify outliers and anomalies, which are values that significantly deviate from the rest of the observations.
4. Extract and generate relevant variables that hold significance in scientific context.

Type of data	Suggested EDA techniques
Categorical	Descriptive statistics
Univariate continuous	Line plot, Histograms
Bivariate continuous	2D scatter plots
2D arrays	Heatmap
Multivariate: trivariate	3D scatter plot or 2D scatter plot with a 3rd variable represented in different color, shape or size
Multiple groups	Side-by-side boxplot

Table 2: Suggested EDA techniques depending on the type of data [10]

Objective	Suggested EDA techniques
Getting an idea of the distribution of a variable	Histogram
Finding outliers	Histogram, scatterplots, box-and-whisker plots
Quantify the relationship between two variables (one exposure and one outcome)	2D scatter plot +/curve fitting Covariance and correlation
Visualize the relationship between two exposure variables and one outcome variable	Heatmap
Visualization of high-dimensional data	t-SNE or PCA + 2D/3D scatterplot
-SNE t-distributed stochastic neighbor embedding, *PCA* Principal component analysis	

Table 3: Most useful EDA techniques depending on the objective [10]

4.1 Multivariate Analysis

Multivariate analysis is based on examining and comprehending data with multiple variables at once. These analyses employ various methods, such as correlation analysis, PCA, factor analysis, cluster analysis, CCA, discriminant analysis, multivariate regression analysis, and MDS, in order to unveil patterns, identify outliers, and grasp the data's structure. The ultimate goal is to facilitate informed decision-making across diverse domains. **(Table 4)**

4.1.1 Pearson and Spearman Correlation Coefficient Matrix

The association between two variables can be described using a numerical value known as the linear correlation coefficient, quantifying the level of "proportional connection" between them. This coefficient ranges from -1 to 1, representing scenarios where the variables show perfect inverse or direct proportionality, respectively. When there are more than two variables, a correlation matrix can be created. At the point where row j intersects with column i, the value of the correlation coefficient between variables numbered j and i is inserted. The Pearson rank correlation coefficient matrix is used when the data is treated follows a normal distribution. Instead, the Spearman rank correlation matrix is implemented when the data distribution is not normal.

VARIABLE	Cd	Co	Cr	Cu	Ni	Pb	Zn
Cd	1.00	0.26	0.58	0.15	0.49	0.22	0.62
Co	0.26	1.00	0.48	0.19	0.74	0.16	0.44
Cr	0.58	0.48	1.00	0.21	0.71	0.26	0.61
Cu	0.15	0.19	0.21	1.00	0.22	0.82	0.66
Ni	0.49	0.74	0.71	0.22	1.00	0.27	0.59
Pb	0.22	0.16	0.26	0.82	0.27	1.00	0.67
Zn	0.62	0.44	0.61	0.66	0.59	0.67	1.00

Table 4: Correlation matrix among elements [10]

Pearson's Correlation Coefficient Matrix:

Pearson's correlation coefficient evaluates the strength and direction of a linear relationship between two continuous variables. It follows the next formula for two variables X and Y:

$$r = \frac{\sum (X_i - \bar{X})(Y_i - \bar{Y})}{\sqrt{\sum (X_i - \bar{X})^2 \sum (Y_i - \bar{Y})^2}}$$

Therefore, in a correlation matrix using Pearson's coefficient, each cell holds the Pearson correlation coefficient calculated from the respective pair of variables.

Spearman's Correlation Coefficient Matrix:

Spearman's rank correlation coefficient measures the strength and direction of a monotonic (not necessarily linear) relationship between two variables. It's useful working with ordinal or ranked data. The formula to calculate Spearman's rank correlation coefficient for two variables X and Y implies firstly rank the values and then calculate Pearson's correlation on each rank:

$$\rho = 1 - \frac{6 \sum d^2}{n(n^2-1)}$$

Therefore, *d* is the difference between the ranks of each pair of variables, on the other hand *n* is the count of data points. As a consequence, in a correlation matrix using Spearman's coefficient, each cell calculates the Spearman rank correlation coefficient for each pair of variables, evaluated based on the ranks of the data.[10] [11]

4.1.2 Principal component analysis (PCA)

PCA is a method employed to minimize large numbers of variables to uncorrelated ones, by the plotting of variation diagrams. It reduces bias in geochemical data by transforming potentially correlated variables into principal components, which are uncorrelated factors. The PCA pulls out variance and tries to find a second linear combination to interpret the remaining variance. Principal components, variance-focused method is the result from both common and unique variance of variables. Eigenvectors, principal component coefficients or loadings, express the relative significance of each component and its variability within the data set. Hence, they are calculated according to the number of variables used in geochemical surveys. Before applying the PCA technique, it advisable to check the data, set up the number of factors needed to explain the pattern or relationships between variables, and perform log-ratio transformation to avoid uninterpretable results. [13]
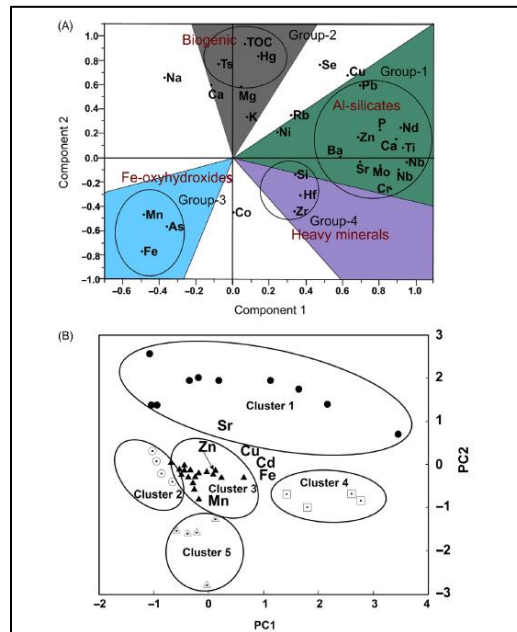
Figure 3: (A) Example of PCA for geochemical elements (B) Score plot for events PC1 and PC2 [13]

4.2 Bivariate Analysis

Bivariate analysis in exploratory data analysis (EDA) analyzes the connection and relationship between two variables. It aims to understand how the values of one variable relate to the values of another variable. This analysis aids reveal patterns, associations, and dependencies between the variables. Techniques commonly employed in bivariate analysis include scatter plots, correlation analysis, and cross-tabulation.

By exploring the relationship between two variables, bivariate analysis provides insights into potential connections and dependencies in certain dataset.

4.2.1 Scatterplots

These plots involve visualizing the values of one variable in relation to another, requiring both variables to have been measured at the same locations. It allows for a pairwise examination or 'correlation' between the two variables and facilitates the detection of outliers. In geochemistry, there is a strong correlation between elements concentrations: when one of these variables increases, the other tends to increase as well, confirming the positive slope of the regression line.
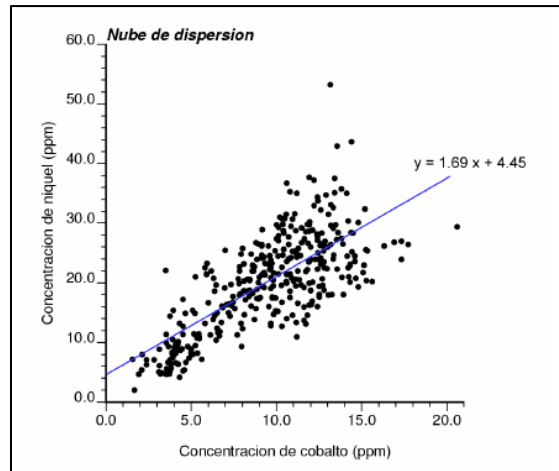
Figure 4: Scatter plot for Ni and Co concentrations [14]

4.2.2 Curve Fitting

Curve fitting is a method used to measure the relationship between two variables or how those values change over time. Commonly, the best method implemented is the linear regression line. A linear regression line (or best-fit line) is the line that best represents the general trend or relationship between the two variables in the scatter plot. It's calculated by using a mathematical method that minimizes the sum of the squared distances between the data points and the line. Hence, when a scatter plot shows a positive correlation, the resulting linear regression line will possess a positive slope, providing insight into the direction and strength of the relationship between the two variables. To quantitatively measure the strength of the relationship between two variables in a linear regression model, the coefficient of determination, denoted as R^2, is employed. R^2 serves as a valuable metric for assessing how well the regression model fits the observed data. It quantifies the proportion of the variance in the dependent variable that can be explained by the independent variable in the linear regression model. R^2 is calculated using the formula:

$$R^2 = 1 - \frac{SS_{res}}{SS_{tot}}$$

Where SS_{res} is the sum of squared residuals (errors) and SS_{tot} is the total sum of squares. R^2 ranges from 0 to 1 (0%-100%). A higher R^2 value indicates a better fit of the model to the data. In simpler terms, R^2 illustrates the proportion of the variance in the dependent variable that is predictable from the independent variable. For instance, an R^2 of 0.80 (or 80%) implies that 80% of the variance in the dependent variable is explained by the independent variable(s) in the model. Another useful regression line application is the

predictive Analysis, once a linear regression model is set up, it can be employed for predicting purposes. Given the value of one chemical element, the regression line function can estimate the value of the other element, proving insights in prediction, forecasting and modeling. [14]

4.3 Univariate Analysis

Univariate data analysis involves examining and analyzing a single variable within a dataset. Its main objective is to gain insights into the distribution, central tendency, variability, and other characteristics of that particular variable. Univariate analysis focuses on one variable at a time, allowing deeper investigations of its properties and patterns. Univariate analysis can be non-graphical and graphical. A non-graphical method for exploring variables in univariate analysis involves constructing a table that displays the count and frequency of data for each category. Sample statistics are used to describe the characteristics of a sample using a limited set of parameters. They can provide clear ideas about the central tendency of the data (such as arithmetic mean, median, and mode), its variability (variance, standard deviation, interquartile range, maximum and minimum values), or certain aspects of its distribution (skewness, kurtosis). It is important to note that these statistics are applicable only to quantitative variables and not categorical variables.

4.3.1 Non-graphical Univariate EDA

Central tendency measures

The arithmetic mean, also known as the mean, is calculated by summing all the data values and dividing the sum by the total number of values. On the other hand, the median represents the middle value in a sorted list of all the values. The median is considered more "robust" than the mean because it is less influenced by extreme values and outliers. This means that even if there are extreme values in the dataset, the median tends to provide a more representative measure of the central tendency.
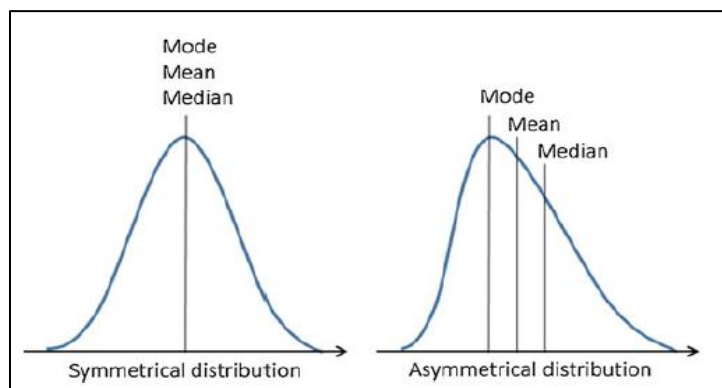
Figure 5: Symmetrical vs asymmetrical distribution, showing mode, mean and median [10]

Variance and Standard Deviation

The variance ($s2$) for an entire population, is calculated by the sum of squares and divided by the population size *(n)*. However, when working with observed data, the conventional formula for variance uses *n-1* in the denominator instead of *n*. This adjustment is made in order to achieve "unbiasedness," it means, the average should match the corresponding population value ($s2$). The sample variance (s2) is an unbiased estimator of the population variance. Therefore, the standard deviation is obtained by calculating the square root of

the variance. It shares the same units as the original data, making it more easily interpretable. The sample standard deviation is typically denoted by the symbol *s*.

$$s^2 = \frac{\sum_{i=1}^{n}(x_i - \underline{x})^2}{(n-1)}$$

Interquartile range (IQR)

The interquartile range (IQR) is determined by considering the data located between the 1st (Q_1) and 3rd (Q_3) quartiles. Similar to how the median is considered more robust than the mean, the interquartile range (IQR) is a more robust measure of spread compared to variance and standard deviation. As a result, the IQR is often preferred, especially for small or asymmetrical distributions. Its robustness allows it to be less influenced by extreme values or outliers, making it a reliable choice for assessing the spread of data in certain scenarios.

$$IQR = Q_3 - Q_1$$

Skewness/kurtosis

Skewness quantifies the degree of asymmetry in a distribution, while kurtosis provides a summary statistic that conveys information about the tails (i.e., the smallest and largest values) of the distribution. Both skewness and kurtosis serve as useful tools for describing the distribution of data when graphical methods are not applicable or available. They offer alternative means of communicating important characteristics of the data's distribution. [10]

Criteria for verifying a normal distribution.

In order to have a normal distribution or approximate normality, the mean, mode, and median should be similar, is accepted a minimal difference between them of 1 unit. Since the skewness allows the verification of data normality, in the case of horizontal asymmetry, it means that the data does not form a normal distribution, Wester-Oliver propose evaluating the following: If skewness < 0.5, the probability distribution function is accepted as normal, and a data analysis method can be applied to the data. On the contrary, if $0.5 < |$ skewness $|$, it is necessary to perform a data transformation by using some normalization method (the square root, log, etc.) [12]

4.3.2 Graphical Univariate EDA

Histograms

Histograms are effective exploratory data analysis (EDA) methods that offer valuable insights into the distribution, central tendency, spread, modality, and outliers within a dataset. They are graphical representations in the form of bar plots, where each bar represents the frequency or proportion of cases within specific subgroups of an exposure variable. The number of bins significantly impacts the appearance of the histogram, and it is recommended to experiment with different values. Histograms serve multiple purposes, including confirming the accuracy of operations, identifying outliers, and displaying data distribution in various formats.
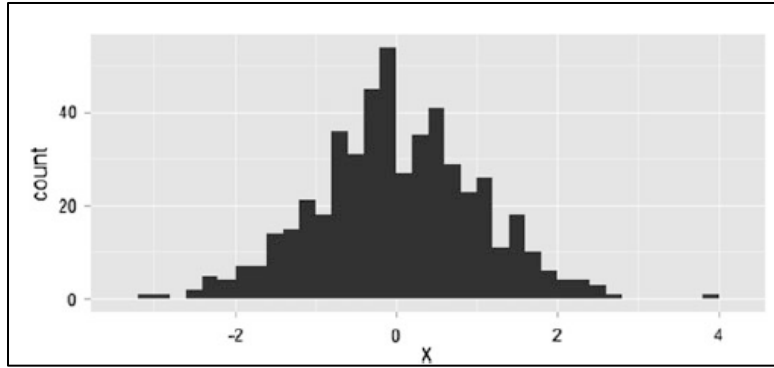
Figure 6: Example of histogram [10]

Boxplots

Turkey boxplots are useful for analyzing central tendency, symmetry, skewness, and outliers, but can skips presence of multimodality. They are an effective EDA technique due to their work with robust statistics such as median and IQR. Outliers are plotted beyond 1.5 IQRs above or below Q3, and their location is a suggestion of potential errors.
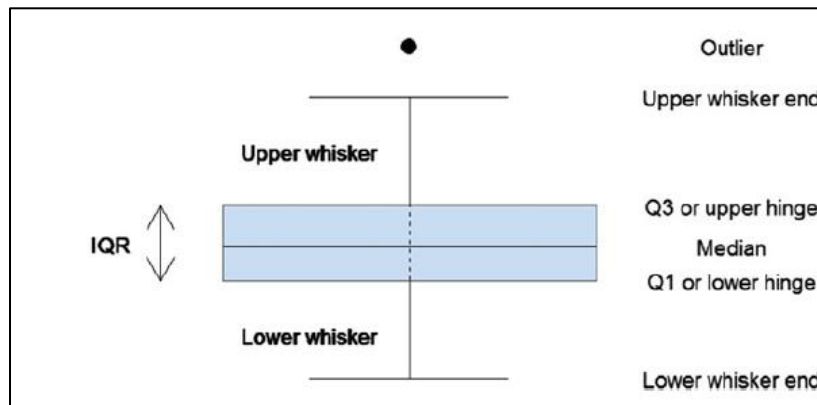
Figure 7: Example of boxplot with annotations [10]

Probability Plots

Probability plots are graphical tests used to evaluate data distribution, often used for normality and residual analysis. They can recognize skewness, kurtosis, fat tails, outliers, and bimodality. Quantitative statistical tests like Pearson Chi2, Shapiro-Wilk, and Kolmogorov-Smirnov as well are used for normality testing. However, deviation from normal distribution can render other statistical tools useless. Sometimes data sets can be transformed to a more normal distribution or discretized into a finite set. [14]
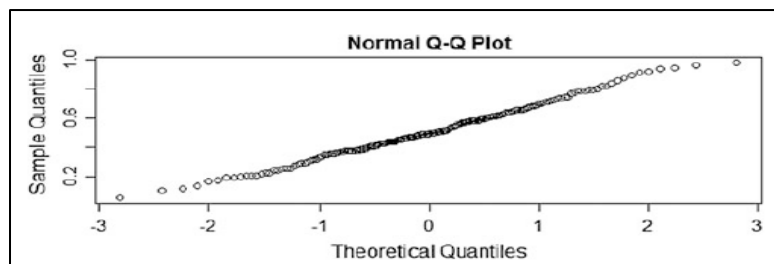
Figure 8: Example of Probability plot [10]

5. Mining Prospectivity Mapping

Mineral prospectivity mapping (also referred to as mineral potential mapping) is an approach utilized to identify the probable locations of mineral deposits within a specific study area. It involves the integration of various geoscience datasets and employs mathematical tools like weights-of-evidence, artificial neural networks, logistic regression, and fuzzy logics, all within a geographic information system (GIS). This method plays a significant role in mineral exploration and is increasingly becoming more popular. By combining geological, geochemical, and geophysical methods, it aims to predict the likelihood of finding an ore body in a given area. Mineral prospectivity mapping has been implemented in different regions worldwide, such as French Guiana by the Bureau de Recherches Géologiques et Minières (BRGM), China, the United States, as well as in certain areas of Africa like Rwanda. Geologists in various parts of the world are familiar with the effectiveness of mineral prospectivity mapping. The specific data and information needed will primarily vary based on the type of mineral or group of minerals being sought after and the deposit type. In a GIS environment, the information or criteria are stored as layers. For instance, Cassard et al. (2008) employed geological criteria (lithostratigraphy and stratigraphy), geophysical criteria, and geochemical criteria to plot mining portential maps for French Guiana in their search for gold within Precambrian orogenic settings. By utilizing mineral prospectivity mapping software, it becomes possible to generate a visual representation of a map indicating areas that are favorable for mineral occurrences. This map is produced after processing all the relevant criteria. An example of such a map can be seen in next Figure, where the highest scores are depicted in red color, indicating the greatest likelihood of discovering the desired mineral, such as gold in this particular case.
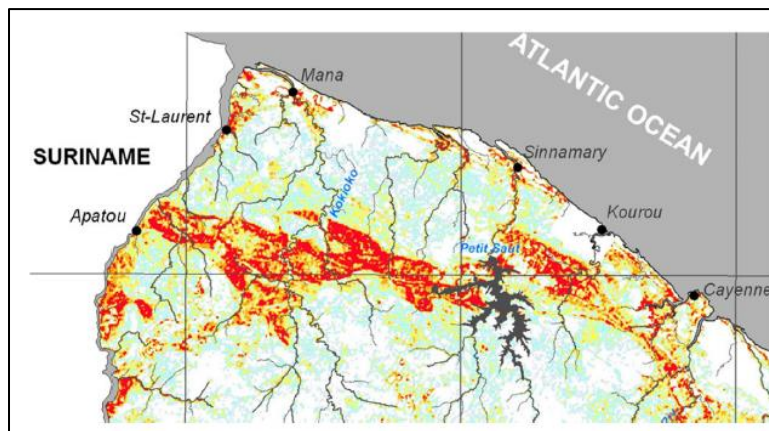
Figure 9: Example of mineral prospectivity map. Reddish color represents areas with the highest favorability. [13]

5.1 Geochemical mapping

Geochemical mapping involves the processes of collecting, analyzing, and mapping the distribution of chemical elements and compounds in Earth's surface materials. Its primary objective is to illustrate spatial variations and concentrations within a certain geographic area. Data from chemical analysis is employed to elaborate maps, commonly with Geographic Information Systems (GIS), offering insights not only for mineral exploration, but also for environmental assessments, agriculture, and public health. Geochemical maps can uncover anomalies that indicate geological features, mineral deposits, or environmental issues, providing tools for decision-making. A geochemical map visually depicts the distribution of specific chemical elements across a geographic area. It implements color-coding to indicate concentration levels,

with warm colors indicating higher concentrations and cool colors for lower levels. Contour lines are employed to show areas of equal concentration. Data points from sample locations are plotted on the map to indicate the data source. In cases of scarce or uneven data, interpolation is employed to estimate concentrations between sample points.

Geochemical anomaly

Geochemical anomalies are a crucial technique used by mineral explorers to find deposits. These anomalies are zones or areas of abnormal high or low values of elements or minerals compared to the general element background values. Conventional methods only detect positive geochemical anomalies and do not account for negative anomalies. The abnormal concentration of elements or comes normally from soils, waters, sediments, or rocks lying inside the deposits or by the surrounding area. Higher or lower values in a dataset would evidence the presence of anomalies, instead, lower values would imply mineral alterations. This approach could be confusing because not all highest values mean mineralized zones, and abnormally higher values could be related to geogenic and anthropogenic processes. Typically, an anomaly is defined as values above threshold limit, which are the upper limit of the background values. Therefore, rocks genetically associated would share the same background values and threshold values for certain elements or minerals. Nevertheless, this is not consistently true., due to rocks of the same family vary background values according to the elements and the localities. Traditionally (Aitchison, 1986; Filzmoser and Hron, 2008; Reimann et al., 2002), threshold values have been determined through the use of frequency-based models, such as:

$$\text{Threshold} = \text{Mean} + 2 \times \text{ standard deviation}$$

Sinclair (1974) argued that combining anomalous values with background values would complicate results and overlook the origin nature of geochemical data. Therefore, the previous equation for calculating threshold values has led to skip potential deposits which have remained undiscovered around the globe. Hence, this approach uses Percentiles to calculate threshold values:

$$\text{Threshold} = Q3 + (Q3 - Q1) \times 1.5$$

Q_3 and Q_1 represent the 75th and 25th percentiles of the element concentrations, respectively. [13]

5.2 Interpolation Methods

Inverse Distance Interpolation (IDI)

It's a spatial interpolation technique employed in GIS and geo statistics that estimates values at locations without measured data. This method assigns weights to nearby sample points based on the inverse of their distances, with closer points having a more substantial impact. The estimated value is computed as 13a weighted average of the known values at the nearby sample points. The mathematical expression for estimated value *(Z)* at a location can be expressed as:

$$Z = \frac{\sum_{i=1}^{n} \frac{Z_i}{d_i^p}}{\sum_{i=1}^{n} \frac{1}{d_i^p}}$$

Where Z_i is the known value at sample point *i*. d_i is the distance between the unmeasured location and sample point *i*. *p* is a positive exponent, normally 2 for the inverse square of the distance, but I can vary.[15]

Kriging Ordinary interpolation

Kriging is a geostatistical interpolation technique utilized for spatial estimation and prediction. It includes spatial autocorrelation and gives the best linear unbiased predictions (BLUPs) at unobserved locations within a certain spatial domain. Spatial autocorrelation evaluates the relationship between data points at varying distances. It serves as the basis for kriging, helping to determine the spatial dependence structure within the dataset. It forms the base of the kriging method, assisting in the identification of the spatial correlation structure present in the dataset. The ordinary kriging estimation of a variable Z at an unmeasured location is based on a linear combination of values at nearby measured locations. The equations for ordinary kriging estimate at an unmeasured location Z_0 can be expressed as:

$$Z_0 = \sum_{i=1}^{n} \lambda_i Z_i$$

Where Z_0 is the kriging estimate at the unmeasured location. λ_i represents the kriging weights assigned to each of the n measured locations. Z_i is the known value at the i-th measured location.

5.3 Variogram Modelling

The variogram is a crucial instrument in geo statistics, illustrating how the variance between data points changes with spatial distance. Analyzing the variogram implies computing the semi variance at varying spatial intervals. It mainly consists of three essential elements: sill, range, and nugget effect. The sill denotes the highest observed variability in the dataset, it means the point at which the semi variance stabilizes, defining the range of spatial correlation. A greater sill value is more pronounced spatial dependence. On the other hand, the range defines the distance where spatial correlation plateaus, reaching the sill. This parameter is critical due to it defines the scope of spatial impact. Finally, the nugget effect represents variability at extremely short distances, normally it is attributed to measurement errors or true discontinuities along short distances. A notable nugget effect signifies weak or null spatial correlation over short distances.
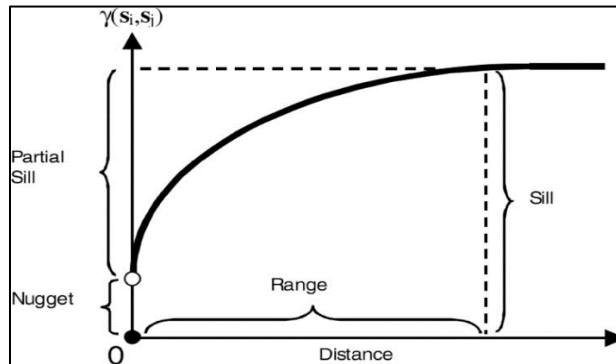
Figure 10: Variogram parameters [14]

In order to evaluate the reliability of the variogram models created, the average standard error gives an error estimation, it measures the 'average' disparity between the measured values and the estimated values.

$$\varepsilon_{XY} = \sqrt{\frac{\sum (Y - \overline{Y})^2}{n - 2}}$$

Where ε_{XY} is the estimation error, $(Y - \overline{Y})^2$ is the squared difference between the measured values and the estimated values and *n* is the data number. Therefore, the smallest standard error between the theoretical semi variogram models (spherical, Gaussian, and exponential) indicates that the selected method matches the best the studied element.

Variogram Models

Most used variogram models encompass exponential, spherical, Gaussian, and circular, they serve to fit the variogram and estimate the parameters: sill, range, and nugget effect. These models help to describe the spatial dependence between the variables having each one unique feature:

Exponential: The exponential variogram model portrays a rapid decrease in spatial correlation as the distance between data points increases. It means nearby points are stronger correlated than those farther apart, but the correlation decreases rapidly with distance.

Spherical: This model exhibits a practical limit to spatial correlation at a certain range. further this range, spatial correlation levels decrease, therefore, the influence of neighboring points is limited within this range.

Gaussian: It works on the assumption of a normal distribution around the spatial influence. It represents a brief decline in spatial correlation compared to the exponential model, which indicates a steady decrease in correlation regarding the increasing distance.

Circular: Itis suitable for represent circular or directional spatial dependence patterns. It works with premise of the spatial correlation may vary according to the direction of the data points, forming circular patterns of influence. [14]
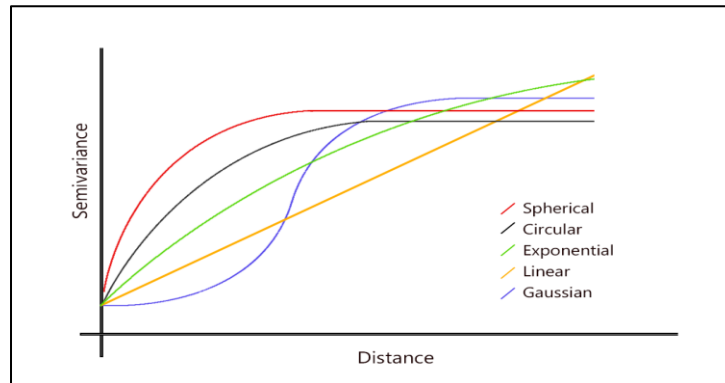
Figure 11: *Types of variogram models*

5.4 Map Algebra

The Raster Calculator within ArcGIS allows users to conduct map algebra operations on raster data (Maps). This involves selecting input raster layers, utilizing the Expression Builder to create mathematical or logical expressions, executing the computations, and producing an output raster (final map) based on the specified operations. The tool's flexibility works with a spectrum of operations, from simple arithmetic to complicated calculations, playing a crucial role in raster analysis and extracting meaningful information from raster datasets.

6. Results and discussion

6.1 Fieldwork, sampling, and chemical analyses

The data collection was carried out by the Alaska state geological survey. 1076 samples were collected encompassing an area of 15981,8 km2 in the portion north-central of the Yukon-Tarana uplands terrane, central-eastern region of Alaska, United States of America. Consequently, the sampling density was roughly 15 samples per square kilometer. 94.4% of samples were collected in stream/river places, the remaining 5,6% were conducted in quarries/mines or from an unknown source. **(Figure 12)**
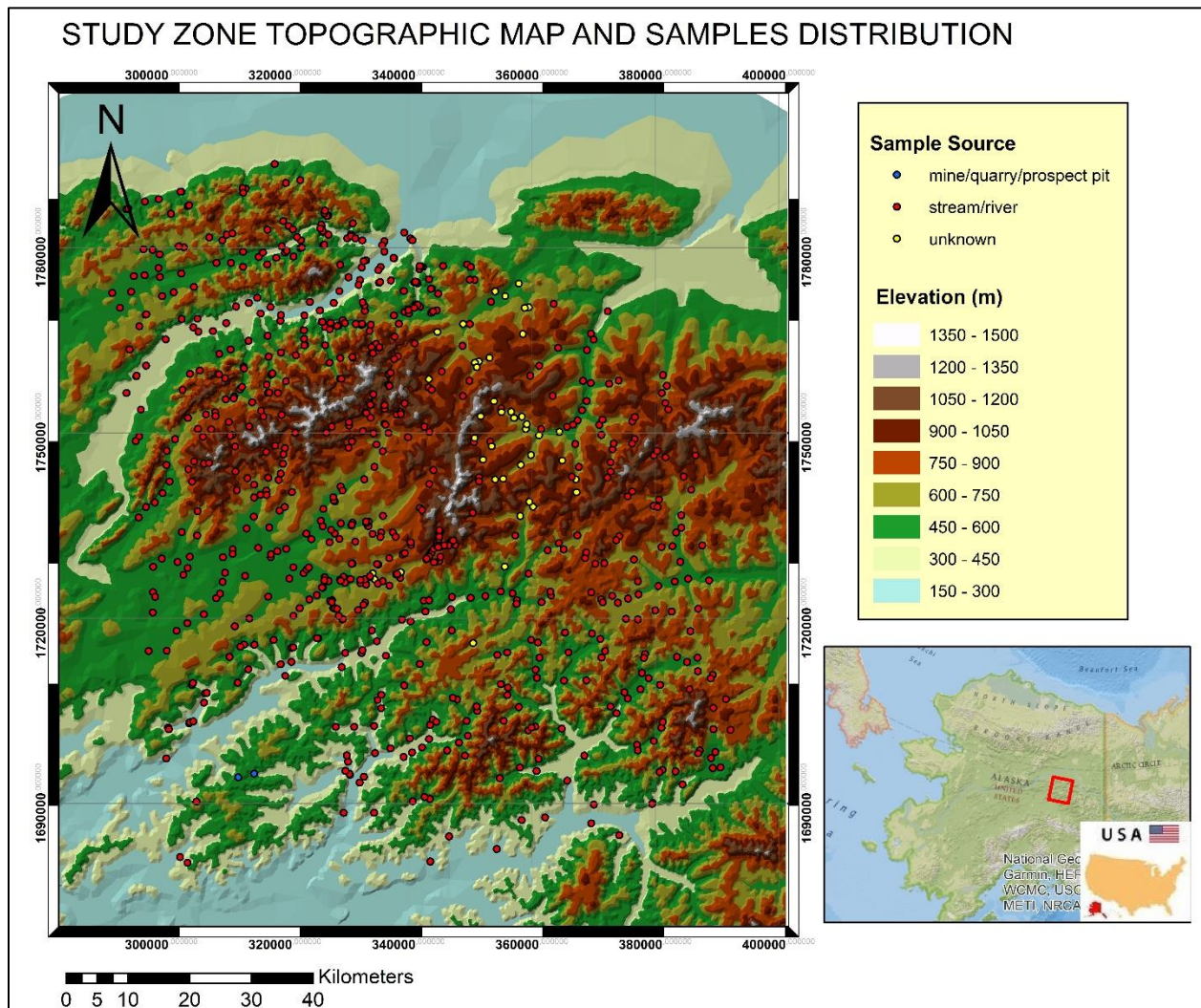
Figure 12: Topographic and sampling map for study zone

Following data collection, the collected samples underwent digestion processes essential for preparing geological samples for subsequent analysis, breaking them down into a suitable form for measuring specific elements or compounds. Diverse digestion methods were strategically employed based on the inherent characteristics of the respective samples. Primarily, three distinct methods were utilized: **Inductively**

Coupled Plasma Optical Emission Spectroscopy (ICPOES MS-60): It is a sophisticated analytical technique employed to determine the elemental composition of samples by analyzing the light emitted by ions within an inductively coupled plasma. **Aqua Regia Digestion:** involves the use of aqua regia, a highly corrosive mixture of nitric acid and hydrochloric acid. This technique is instrumental in dissolving samples, thereby preparing them comprehensively for subsequent analysis. **Fire Assay for Gold (Au), Palladium (Pd), and Platinum (Pt) Analysis (C-FA-AU-PD-PT):** known as Fire Assay, is primarily utilized for the analysis of precious metals such as gold (Au), palladium (Pd), and platinum (Pt).

6.2 Data preprocessing

Data preprocessing is a fundamental step preceding exploratory data analysis (EDA), particularly in the context of geochemical raw data. Its primary purpose is to refine and enhance the raw data, rendering it suitable for analysis and modeling. The main objective of data preprocessing is to transform the raw data into a structured format that optimizes the performance and precision of subsequent analyses and employed models. Essentially, data preprocessing encompasses several vital objectives, namely Data Cleaning (involving the handling of missing or null values, identification and appropriate treatment of outliers, removal of duplicates, etc.), data standardization, and data transformation (such as log transformation). A notable trouble encountered with the collected data in this survey was the presence of negative values. Among the 61 elements analyzed, 25 elements exhibited negative values. To address this issue, the negative values were systematically substituted with half of the detection limit specified for each corresponding element within the geochemical survey (for instance, -1 was replaced with 0.5). Additionally, within the 25 elements, certain elements manifested a significant proportion of their data in the form of negative values, (as denoted in red within the table). Consequently, these elements *(Ag, Be, In, Mo, Re, Se and Te)* were deemed to be skewed and hence were excluded from the exploratory data analysis, ensuring a rigorous and focused analytical approach. **(Table 5)**

Variable	Problem	Value	Count	%	Replacement Value	Rows without problems
Ca pct	Negative	-0.01	3	0.3	0.005	1073
P pct	Negative	-0.01	11	1	0.005	1065
Ag ppm	Negative	-1	978	90.9	0.5	98
As ppm	Negative	-5	78	7.2	2.5	998
Be ppm	Negative	-5	1002	93.1	2.5	74
Bi ppm	Negative	-0.1	81	7.5	0.05	995
Cd ppm	Negative	-0.2	315	29.3	0.1	761
Cr ppm	Negative	-10	1	0.09	5	1075
Cu ppm	Negative	-5	15	1.4	2.5	1061
Ge ppm	Negative	-1	57	5.3	0.5	1019
In ppm	Negative	-0.2	1054	98	0.1	22
Li ppm	Negative	-10	8	0.7	5	1068
Mn ppm	Negative	-10	2	0.2	5	1074
Mo ppm	Negative	-2	898	83.5	1	178
Ni ppm	Negative	-5	1	0.09	2.5	1075
Pb ppm	Negative	-5	5	0.5	2.5	1071
Re ppm	Negative	-0.02	1065	99	0.01	11
Sb ppm	Negative	-0.1	3	0.3	0.05	1073
Sc ppm	Negative	-5	30	2.8	2.5	1046
Se ppm	Negative	-5	1067	99.2	2.5	9
Sn ppm	Negative	-1	70	6.5	0.5	1006
Ta ppm	Negative	-0.5	110	10.2	0.25	966
Te ppm	Negative	-0.5	1065	99	0.25	11
Tl ppm	Negative	-0.5	344	32	0.25	732
W ppm	Negative	-1	164	15.2	0.5	912

Table 5: Data cleaning

Before proceeding to Exploratory Data Analysis (EDA), the last step in data preprocessing involves log-transforming the complete dataset. This transformation is implemented to achieve several important objectives: stabilizing variance, transforming relationships into a more linear form, normalizing distributions, mitigating the influence of extreme values, and improving interpretability. Log transformation is effective for visualizing data that spans a wide range of values, addressing skewed data and enhancing linearity for regression analysis. To summarize, this technique treats the data in order to improve the quality and interpretability for subsequent analysis.

6.3 Exploratory Data Analysis Results

6.3.1 Multivariate Data Analysis Results

Pearson Correlation Matrix

The first step in the multivariate analysis is the creation of the correlation matrix, between the final 54 elements, REE and its subdivisions LREE and HREE. As the entire dataset was log-transformed, the matrix selected was the Pearson correlation matrix. Its robust algorithm is suitable for previously treated data. It quantifies the strength and direction of the linear relationship between pairs of variables in a dataset. For each pair of variables in the dataset, it calculates the Pearson correlation coefficient (r). The Pearson correlation coefficient ranges from -1 to 1. r=1 indicates a perfect positive linear relationship (as one variable increases, the other also increases proportionally). Instead, r=−1 indicates a perfect negative linear relationship (as one variable increases, the other decreases proportionally). r=0 indicates no linear relationship between the variables. The correlation matrix is visualized as a heatmap. Positive correlations are shown in color gradient, perfect correlation coefficient r=1, are indicated with perfect red color, as the correlation coefficient decreases the color is less red. (Annex 11.1)

PCA results

Principal Component Analysis (PCA) is a robust statistical method employed to reduce dimensionality and visually represent complex, high-dimensional data. It aids in recognizing patterns and associations within diverse chemical elements or compounds. Following the data preprocessing, the main input data for the PCA is the Pearson correlation matrix as this matrix provides insights into the relationships between different chemical elements. The PCA starts computing the eigenvalues and corresponding eigenvectors of the correlation matrix **(Table 6)**. Each eigenvector indicates a principal component, and the eigenvalue associated with each eigenvector represents the amount of variance explained by that principal component. Next, it sorts the eigenvectors in descending order of their corresponding eigenvalues. The eigenvectors with higher eigenvalues (larger variance) are more important in explaining the variability in the data.

Component	Eigenvalues	Percent	Cumulative %
PC1	22,87	38,11	38,11
PC2	9,42	15,69	53,80
PC3	5,92	9,87	63,68
PC4	3,24	5,40	69,08
PC5	2,08	3,47	72,54
PC6	1,87	3,12	75,66
PC7	1,59	2,65	78,31
PC8	1,11	1,85	80,16
PC9	1,03	1,71	81,87
PC10	1,00	1,67	83,54

Table 6: *PCA Eigenvalues*

The primary objective is to preserve a significant proportion of the total variance utilizing a minimal number of principal components. Consequently, three key eigenvectors, denoted as PC1, PC2, and PC3, have been chosen. These eigenvectors represent 38.11%, 15.69%, and 9.87% of the overall variability within the geochemical dataset, respectively. The net contribution of these selected components amounts to 63.68% of the entire dataset's variability.

Visualization and Interpretation

In order to visualize the clusters, patterns, or trends in the data for understanding the relationships and structures present in the geochemical dataset. The PCA generates 2 plots according to the number of Principal components chosen: PC1 vs PC2 plot and PC1 vs PC3 plot.
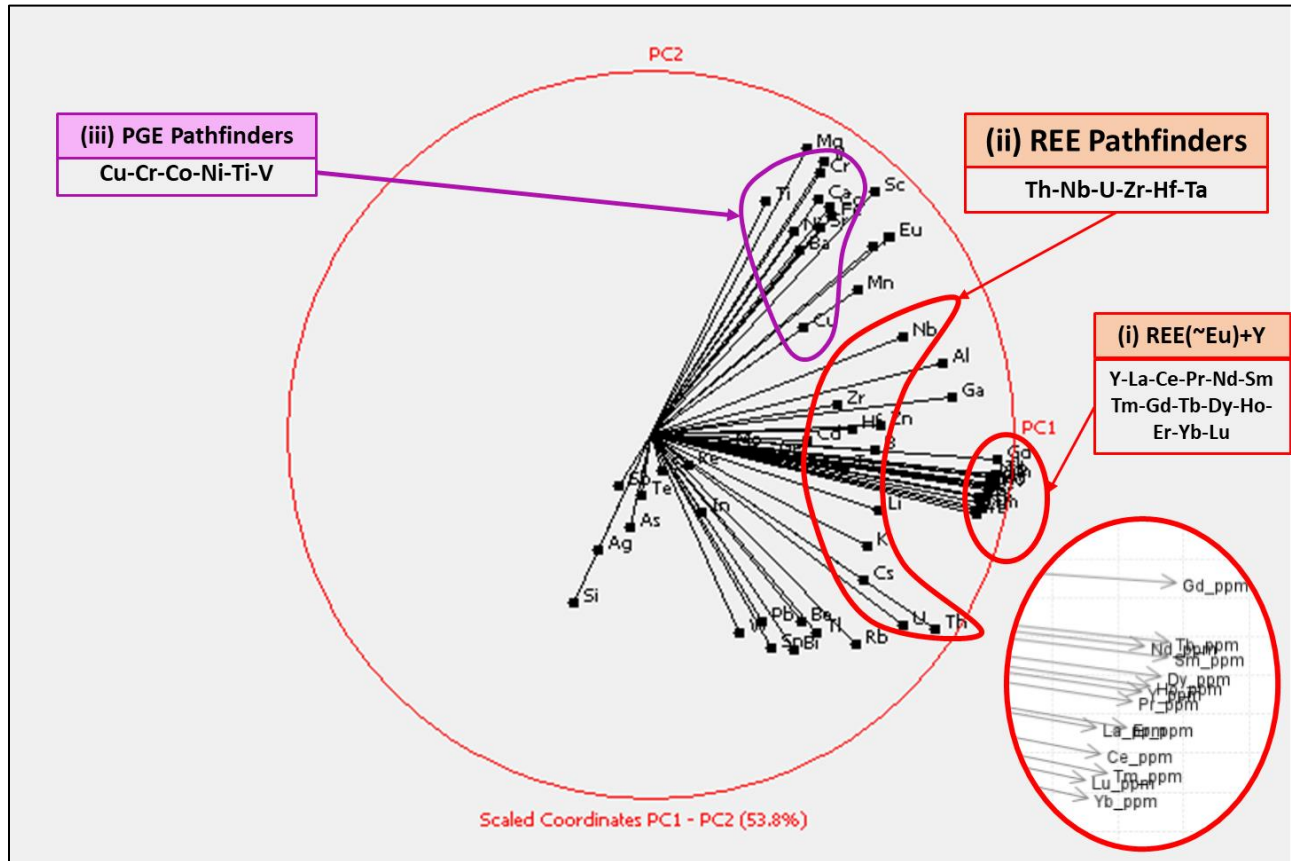
Figure 13: PC1 – PC2 plot

Analyzing the first plot (PC1 vs PC2), 3 geochemical associations are clearly identified: (i) (REE-Eu) + Y, (ii) REE path finders and (iii) PGE path finders. **(Figure 13)**

(i)   The REE´s and *Yttrium (Y)* are spotted in the immediate neighborhood area of PC1 axis, it is imperative to reiterate that proximity to the unit circle signifies a stronger association with the respective principal component.
Notably, all 14 REEs measured in the survey (Pm was not surveyed) are present in the PC1 domain, with the exception of *Europium (Eu)*. Despite being classified as a rare earth element and sharing chemical properties because of their placement in the f-block of the periodic table alongside other REEs, all possessing partially filled 4f orbitals, Europium exhibits distinctive behavior. Eu shows a unique behavior primarily due to its anomalous electronic configuration and divalent state. Europium has an anomalous half-filled $4f^7$ configuration, sets it apart from

the REEs resulting in distinct chemical and magnetic properties compared to other REEs with varying electron arrangements Notably, Europium stands as the only REE commonly found in two oxidation states: Eu^{2+} and Eu^{3+}. The prevalence of the divalent Eu^{2+} state occurs in reducing conditions, while the trivalent Eu^{3+} state is notably more stable in oxidizing conditions. Additional factors contributing to Europium's distinct behavior encompass variations in stability, magnetic behavior, and the lanthanide contraction. Collectively, these aspects highlight the unique behavior of Europium among the REEs.

Although *Yttrium (Y)* is commonly associated with rare earth elements (REE) due to its chemical characteristics and occurrence alongside them in mineral deposits, Yttrium is not considered a true rare earth element t. This is primarily because it does not fall into the category of lanthanides. The rare earth elements are specifically the lanthanides, which are the elements with atomic numbers from 57 (Lanthanum, La) to 71 (Lutetium, Lu) on the periodic table. Yttrium holds an atomic number of 39, placing it outside this range. Technically classified as a transition metal.

(ii)   Adjacent to the previously mentioned Rare Earth Element (REE) association, positioned toward the center of the circular domain within PC1, a distinct group of elements emerges. These elements encompass *Niobium (Nb), Zirconium (Zr), Hafnium (Hf), Tantalum (Ta), Thorium (Th),* and *Uranium (U).* Among them, Niobium, Zirconium, Hafnium, and Tantalum are categorized as *High Field Strength Elements (HFSE)*. This categorization is indicative of their high field strength, elevated ionic charge, and relatively diminutive ionic radius. In contrast, Thorium and Uranium diverge from HFSE and belong to the actinide series, a subset of 15 elements residing within the f-block of the periodic table. Both elements are radioactive, exhibiting radioactive decay and emitting radiation over time. However, it is worth noting that all six of these elements, as indicated by *(Karl et al, 2016 [7]),* serve as valuable Rare Earth Element pathfinders. They are useful indicators in identifying potential REE-rich deposits. Their association with REE is crucial for exploration and understanding the formation of these economically valuable mineral deposits.

(iii)   The third and last geochemical association spotted in the PC1 vs PC2 plot consist of: *Cooper (Cu), Chromium (Cr), Cobalt (Co), Niquel (Ni), Titanium (Ti) and Vanadium (V)*. They are situated within the domain of PC2, signifying they are associated with a mineralization event totally different from the 2 previous associations (i) and (ii). Notably, these six elements, as outlined by (*Karl et al, 2016 [7]*), can be regarded as pathfinders for Platinum Group Elements (PGE). Their presence serves as a strong indicator of potential PGE mineralization, providing valuable insights for prospecting and exploration purposes.

The PC1 vs PC3 plot only displays the associations (i) and (ii), both linked to a common mineralization event—specifically, Rare Earth Element (REE) mineralization denoted by PC1. In the proximity of PC3, not nearby elements are observed. **(Figure 14)**

PC1 encompasses the associations (i) and (ii), it is interpreted characterized as Rare Earth Element (REE) Mineralization, accompanied by its characteristic pathfinder elements *(Th-Nb-U-Zr-Hf-Ta)*. This mineralization is attributed to protracted fractional crystallization of enriched magmas; the outcome is the development of alkaline intrusive rocks that tend to contain considerable elevated abundances of incompatible elements.
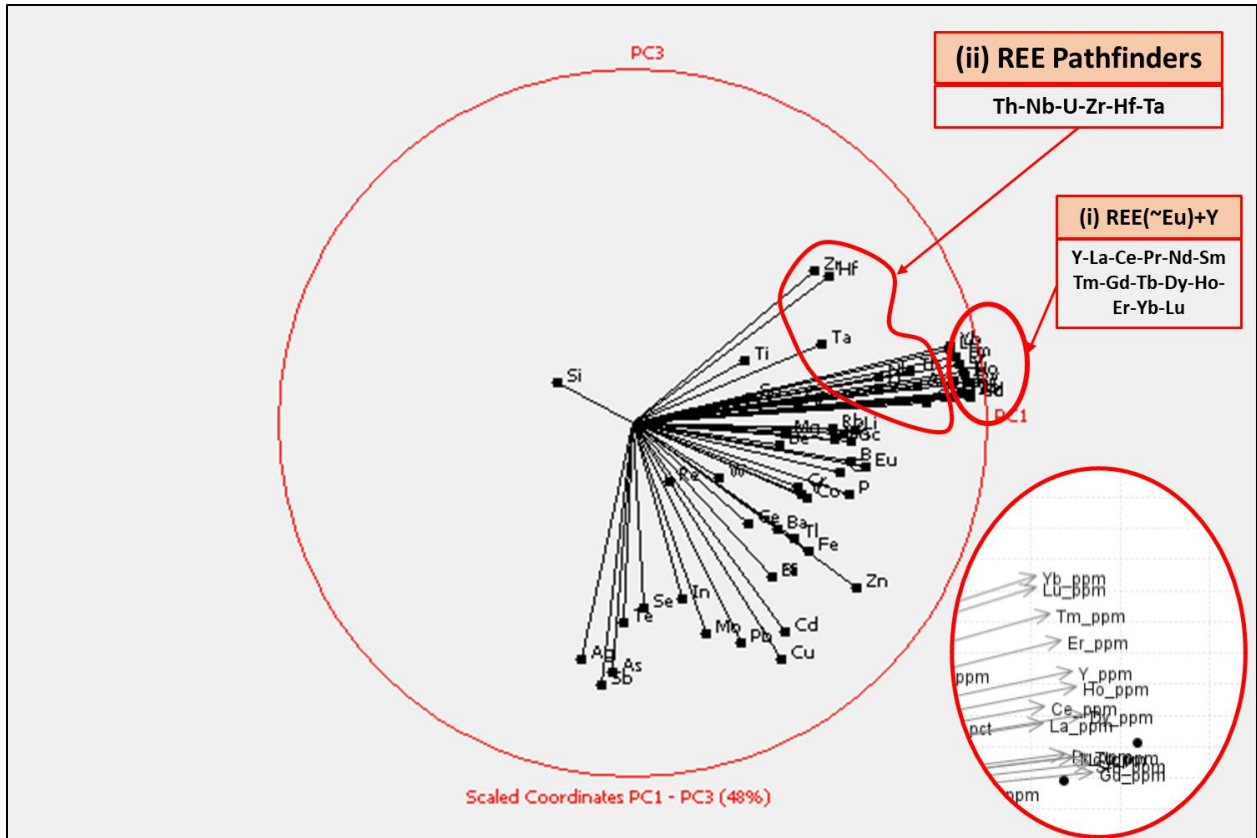
Figure 14: PC1 – PC3 plot

Component/Event	Percent	Association	Interpretation
PC1	38,11	(i) (REE~Eu) + Y	Protracted fractional crystallization of enriched magmas; development of alkaline intrusive rocks that tend to contain elevated abundances of incompatible elements.
		(ii) (Th-Nb-U-Zr-Hf-Ta) **REE pathfinders**	
PC2	15,69	(iii) Cu-Cr-Co-Ni-Ti-V **PGE pathfinders**	Differentiated mafic and ultra mafic (MUM) intrusions, in the form of sills which cross-cut synorogenic layered mafic complexes in proximity to major suture zones.
PC3	9,87	(iv) Placer/Paleoplacer (?) Carbonate-Hosted Cu (?) Sandstone Hosted U (?)	

Table 7: General PCA results and interpretations.

PC2 is interpreted as PGE mineralization. Primarily due to the presence of its pathfinders: *Cu-Cr-Co-Ni-Ti-V*. In this scenario, the potential PGE mineral deposit is correlated with a Mafic and Ultramafic (MUM) Complex. Specifically, this association is linked to differentiated MUM intrusions, often in the form of sills that are part of the magmatic delivery and storage system which cross-cut synorogenic layered mafic complexes in proximity to major suture zones.

Determining the specific mineralization events associated with PC3 proves to be challenging. However, it is important to highlight additional mineralization occurrences recorded in the broader vicinity of the study area within the Yukon-Tanana Uplands terrane. These include historical instances of mineralization such

as: Paleo placer Gold *(Au)*, Carbonate-Hosted *Cu (Co-Ag-Ge-Ga)* and Sandstone Hosted *U(V-Cu)*. These occurrences serve as valuable contextual information in understanding the broader mineralogical landscape in the region. **(Table 7)**

6.3.2 Bivariate Data Analysis Results

Utilizing the previously computed Pearson correlation matrix, the subsequent step involves verifying and quantifying the correlations associated to the REE and PGE mineralization respectively. Taking into account the 3 geochemical associations determined through the principal component analysis (PCA): (i), (ii) and (iii). The elements of each association are examined by using a bivariate approach, specifically employing scatter plots to visualize the relationships. For each pair of variables, a scatter plot is generated, accompanied by a linear regression line and the associated coefficient of determination R2. The aim is to understand how the values of one variable relate to the values of another variable in order to reveal patterns, associations, and dependencies among the elements.

REE Correlation Ranking		
Ranking	Variable	Correlation
1	Y	0,88
2	Th	0,87
3	Ga	0,76
4	Al	0,70
5	U	0,68
6	Nb	0,62
7	K	0,61
8	Rb	0,61
9	Hf	0,56
10	Li	0,56
11	Cs	0,56
12	Zr	0,53
13	B	0,52
14	Zn	0,51
15	Ta	0,49
16	P	0,46
17	Be	0,41
18	Bi	0,39
19	Pb	0,31

Table 8: *REE Correlation coefficients ranking.*

All elements exhibiting correlation coefficients greater than 0.5 with REE were arranged in a descending order based on their correlation strength, with the highest coefficient correlations highlighted in red. As a consequence, *Tantalum (Ta)* was not taken into account in the analysis due to its correlation coefficient falling below the threshold of 0.5. Instead, for the PGE, since the Platinum Group Elements were not directly measured in this geochemical survey, their pathfinders were identified through the PCA. **(Table 8**) Consequently, the coefficient correlations of the bivariate-scatter plots were employed for verifying that the PGE pathfinders identified previously are well correlated among them.

Correlation REE-Y: 0.88
Y(Log) = (0.9423)REE(Log)-0.7328
$R^2 = 0.7813$

Correlation REE-Th: 0.87
Th(Log) = (1.1211)REE(Log) -1.4546
$R^2 = 0.7635$

Correlation REE-U: 0.68
U(Log) = (1.1773)REE(Log) -2.0749
$R^2 = 0.4653$

Correlation REE-Nb: 0.62
Nb(Log) = (0.6615) REE(Log-0.3202
$R^2 = 0.3832$

Correlation REE-Hf: 0.56
Hf(Log) = (0.6378)REE(Log) -0.6062
$R^2 = 0.3168$

Correlation REE-Zr: 0.53
Zr(Log) = (0.5564)REE(Log)+1.1682
$R^2 = 0.2774$
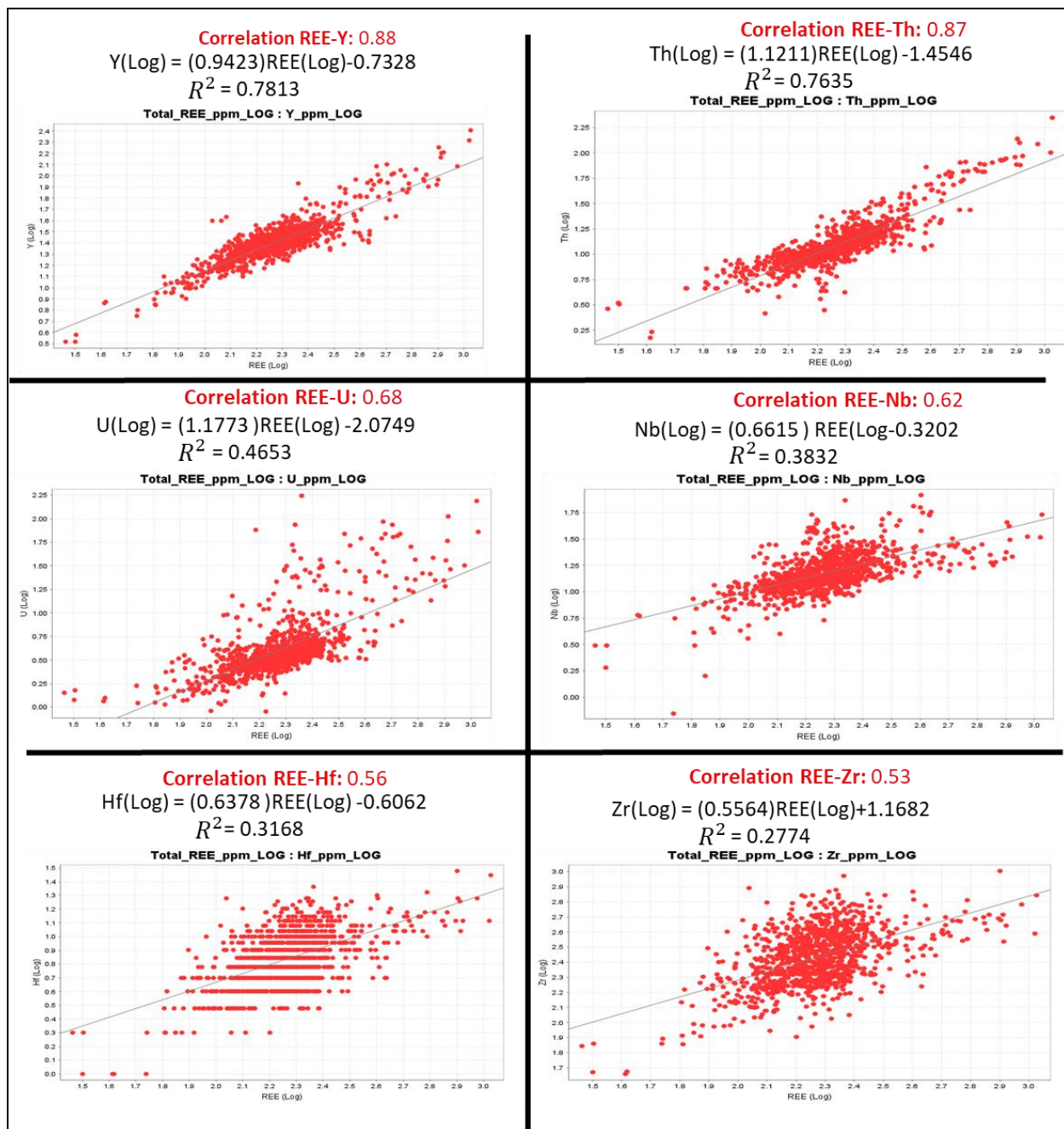
Figure 15: *Scatter plots and linear regression models for bivariate analysis of REE association*

Analyzing the REE scatter plots, the correlation of REE´s with its pathfinders *Y-Th-Nb-U-Zr* and *Hf* are positive, it indicates that all the pathfinders' concentrations increase as the REE concentration increases. However, the patterns, strength relationships and linear regression lines among them vary significantly. The correlation of REE´s with *yttrium(Y)* and *Thorium (Th)* is clearly linear and very strong. Exhibits a very good correlation, with values over 0.8 indicating a strong fit between the variables. As well as their regression lines show high R2 values. REE correlations associated with *Uranium(U)* and *Niobium (Nb)* indicate pseudo-linear and moderate to high correlations with values ranging from 0.6 to 0.7 and the associated linear regression lines yield R2 values of 0.46 and 0.38, respectively. *Hafnium (Hf) and*

Zirconium (Zr) stand out as elements characterized by the lowest coefficient correlations and R2 values, their scatter plots exhibit a dispersed, nearly non-linear arrangement of data points, lacking a clearly defined pattern, thus indicating a moderate correlation between these elements. **(Figure 15)**
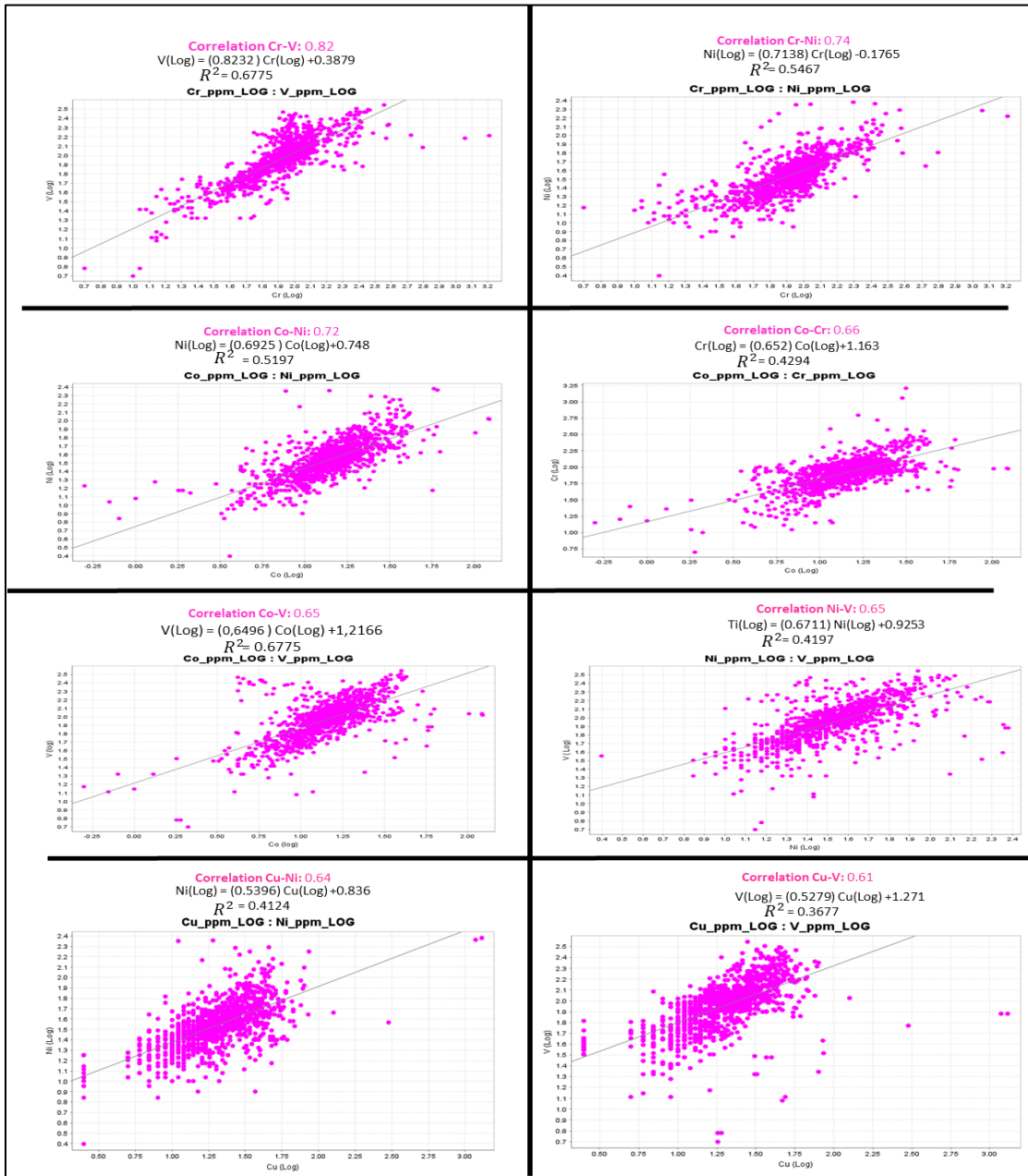
Figure 16: Scatter plots and linear regression models for bivariate analysis of PGE association, Part A

On the other hand, when assessing the PGE pathfinders' correlation coefficients among them, it becomes evident that Ni and V exhibit high correlations respect all the other elements, except with Ti. Moreover, Cr and Co present robust correlations with 3 out 5 elements and medium correlations with the remaining 2 elements. In contrast, *Copper (Cu)* and *Titanium (Ti)* emerge as the least correlated elements **(Table 9)**. Copper displays moderate correlations with all elements, while Titanium exhibits merely 3 moderate correlations and 2 relatively weak correlations within the set. In a broader context, the PGE pathfinders

exhibit notable correlations among them, with correlation coefficients spanning from 0.82 to 0.6. The sole element displaying a relatively poor level of correlation is Titanium (Ti). **(Figure 16 and 17)**
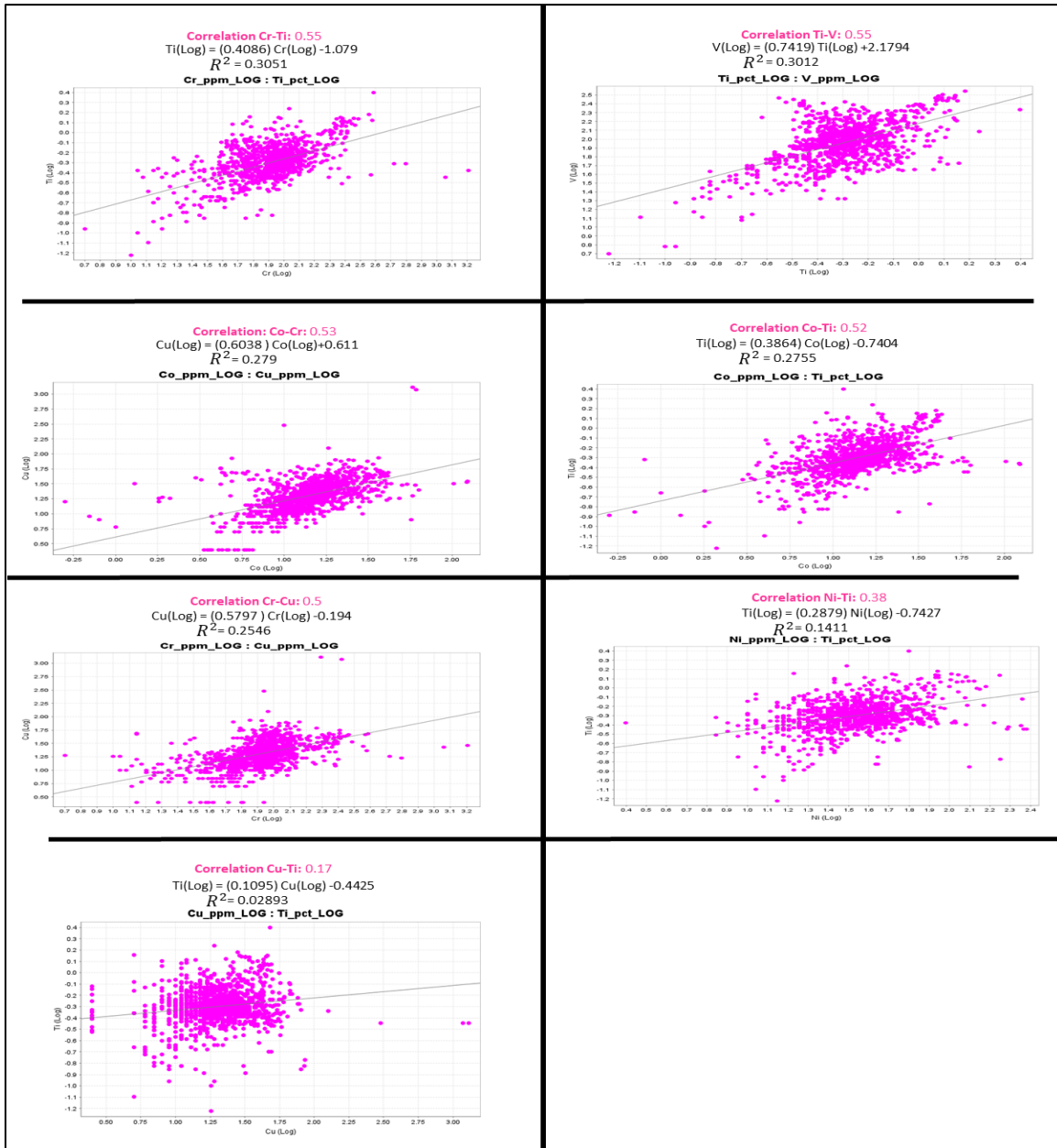
Figure 17: *Scatter plots and linear regression models for bivariate analysis of PGE association, Part B*

	Co (ppm)	Cr (ppm)	Cu (ppm)	Ni (ppm)	Ti (pct)	V ppm (LOG)
Co ppm (LOG)	1,00	0,66	0,53	0,72	0,52	0,65
Cr ppm (LOG)	0,66	1,00	0,50	0,74	0,55	0,82
Cu ppm (LOG)	0,53	0,50	1,00	0,64	0,17	0,61
Ni ppm (LOG)	0,72	0,74	0,64	1,00	0,38	0,65
Ti pct (LOG)	0,52	0,55	0,17	0,38	1,00	0,55
V ppm (LOG)	0,65	0,82	0,61	0,65	0,55	1,00

Table 9: *PGE pathfinders Correlation coefficients*

6.3.3 Univariate Geochemical maps

Summarizing the analytical process thus far, the multivariate analysis has revealed three distinct geochemical associations: *REE+Y*, *REE* pathfinders *(Th-Nb-U-Zr-Hf-Ta),* and *PGE* pathfinders (*Cu-Cr-Co-Ni-Ti-V)*. Subsequently, in the bivariate analysis, the correlations within these associations were rigorously verified, examined, and quantified. Remarkably, strong correlations were observed among all elements, except for Tantalum in the REE association and Titanium in the PGE association. Consequently, both Tantalum and Titanium were excluded from the final univariate analysis, as they demonstrated weaker associations compared to their counterparts. The univariate analysis involves the application of both descriptive statistics (in a non-spatial context) and geo statistics (within a spatial context) to construct geochemical maps for each association and individual element. These maps serve as a means to illustrate the spatial distribution of the selected chemical elements. They not only portray areas of equal concentration but also reveal geochemical anomalies, pinpointing locations with unusually elevated concentrations. The process of geochemical mapping was executed through two distinct methods:

6.1.1.1   IoGAS Geochemical Mapping

The initial method involved utilizing the ioGAS software to conduct an analysis using descriptive statistics, focusing on measures of central tendency and dispersion. A summary statistics table was calculated. Specifically, histograms were employed to assess and validate whether the data, which had undergone a prior log transformation, followed a normal distribution. Quantitative assessment of normality was executed by considering specific criteria, including: (1) Ensuring that the difference between the mean and median was less than 1. (2) Confirming that the absolute value of skewness fell within the range of 0 to 0.5. Following a normal distribution is a crucial aspect in this context, primarily due to the advantageous properties exhibited by a Gaussian distribution. In a Gaussian distribution, both the Interquartile Range (IQR) and the median demonstrate robustness, which, in turn, greatly simplifies the process of calculating geochemical anomalies. Furthermore, Probability plots play an important role in confirming the normality of the data distribution, while also serving as a valuable tool for identifying outliers or anomalies within the dataset

Boxplots play a crucial role in statistical analysis, serving multiple purposes, including the identification of central tendencies, the assessment of data variability, and the detection of outliers or anomalies. In these plots, key statistical measures are visually represented: a circle denotes the mean, a line signifies the median, Q1 and Q3 demarcate the lower and upper quartiles (Top and Botton box), and the whiskers establish the thresholds for anomalies. In the context of mining prospection, boxplots offer valuable insights as they define data classes essential for the development of geochemical maps. Specifically, four distinct classes are established: Background (represented by the mean), Threshold (defined by Q3), TH1 or second-order anomaly (calculated as Q3 + 1.5*IQR), and TH2 or first-order anomaly (computed as Q3 + 3*IQR). In the process of constructing geochemical maps, the software ioGAS employed an Inverse Distance Weighting (IDW) algorithm to generate interpolated values for grid cells. These resultant maps offer a representation with 7 data classes given by default by the software without possibility of modification.

6.1.1.2   ArcGIS Geochemical Mapping

The second method employed in the geochemical mapping process employed a geostatistical approach. Utilizing the geostatistical wizard available in ArcGIS, a kriging ordinary interpolation method was systematically applied to each association/element within the dataset. This process involved calculations and variogram modeling, culminating in the generation of geochemical contour maps, individually tailored for each element. Within the variogram modeling process, several essential steps were rigorously executed. Initially, the dataset underwent log-transformation, followed by a tailored trend removal procedure. Specifically, a first-order trend removal was applied to address linear tendencies, while a second-order trend

removal was employed to account for curve tendencies within the data. Following these steps, the software prompted the selection of an appropriate variogram model to align with the experimental variogram. The model chosen was determined by minimizing the Average Standard Error, thereby optimizing the fit of the model to the variogram points. In essence, this selection process prioritized the model that best captured and characterized the spatial distribution exhibited by the data, enhancing the overall accuracy of the geostatistical analysis.

Consequently, a geochemical map is generated, with contour lines based on the previously defined four classes. This map not only visualizes the anomalous values (TH1 and TH2) but also provides valuable insights into the presence of anisotropy and its directional orientation. Lastly, for every computed variogram, essential parameters including the sill, range, and nugget are determined. The average standard error serves as measure linked to the reliability of the model generated, closer to 0, closer to the real natural model.

6.1.1.3 REE Univariate Geochemical analysis

-Univariate Analysis of Rare Earth Elements (REE):
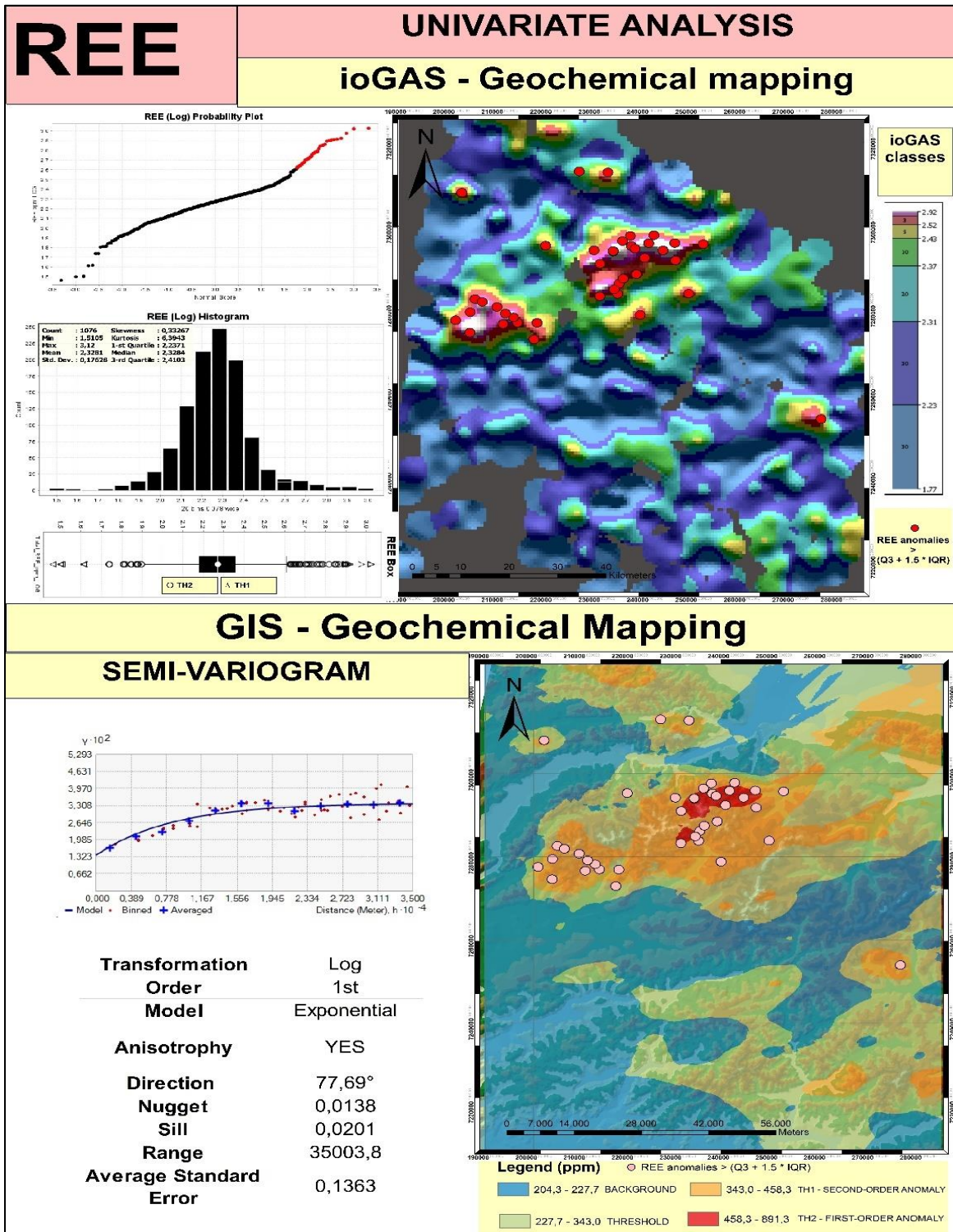
Figure 18: Univariate Analysis of Rare Earth Elements (REE)

-Univariate Analysis of Yttrium (Y):
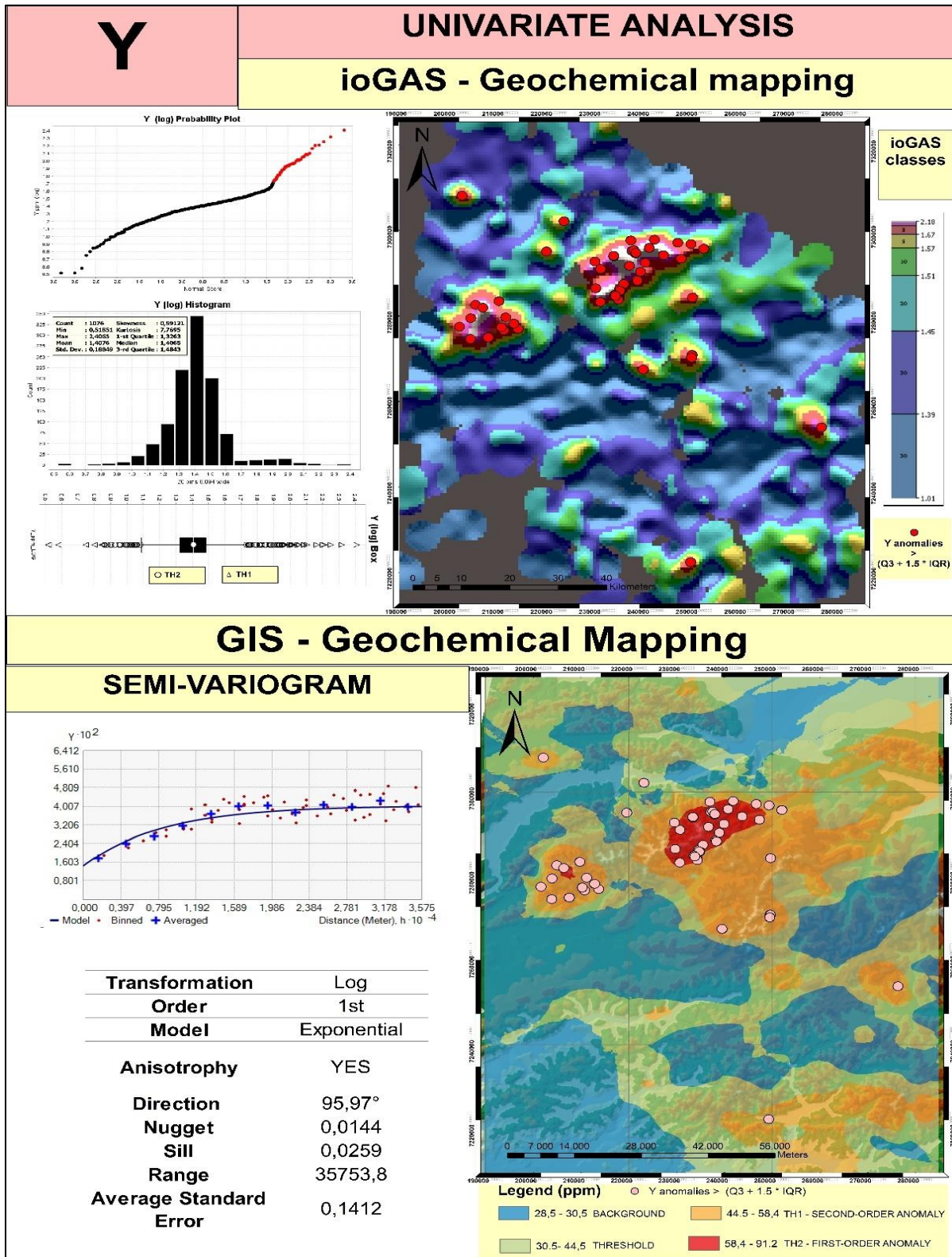
Figure 19: *Univariate Analysis of Yttrium (Y)*

- Univariate analysis of Thorium (Th):
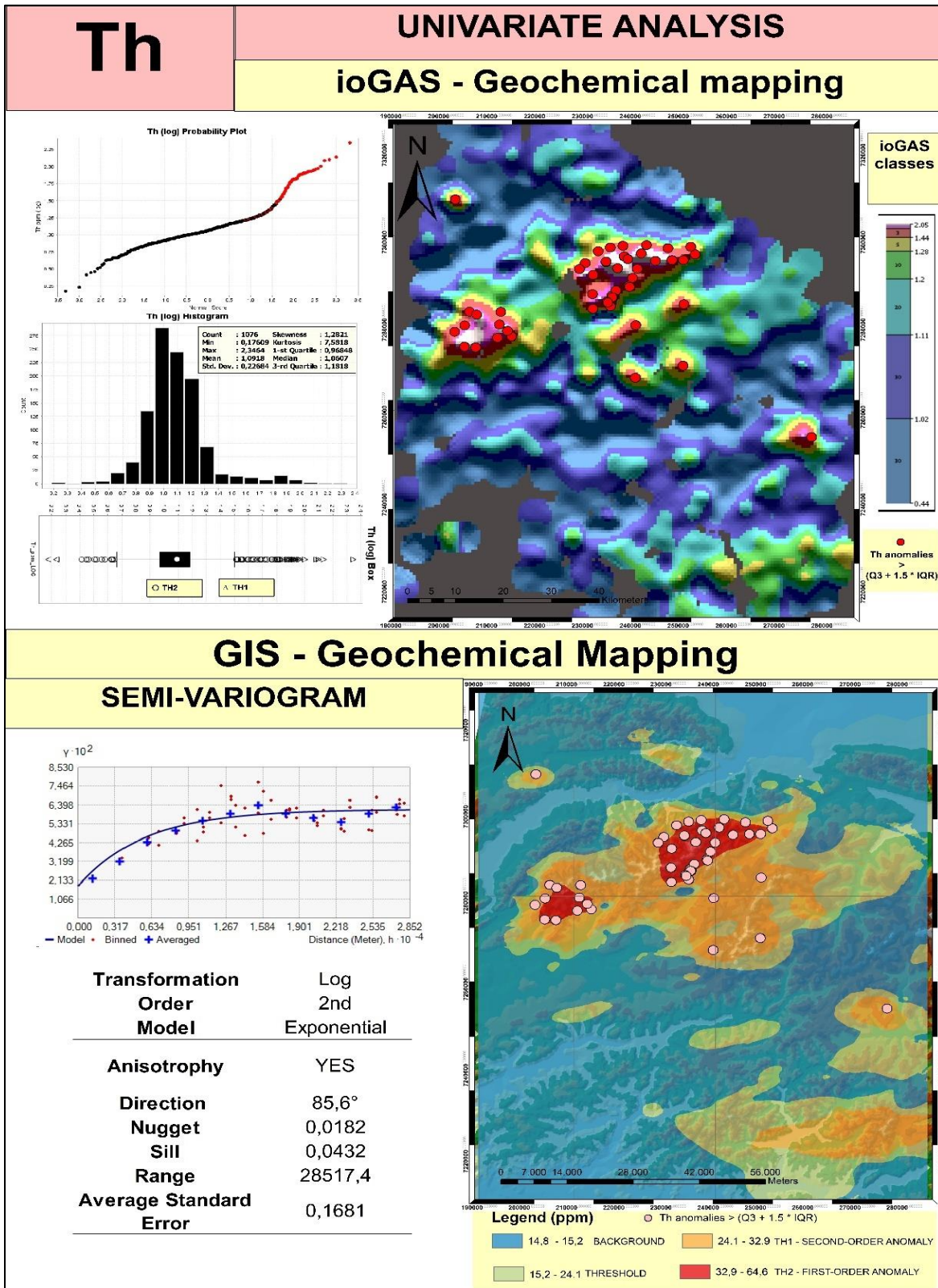
Figure 20: Univariate Analysis of Thorium (Th)

-Univariate Analysis of Uranium (U):
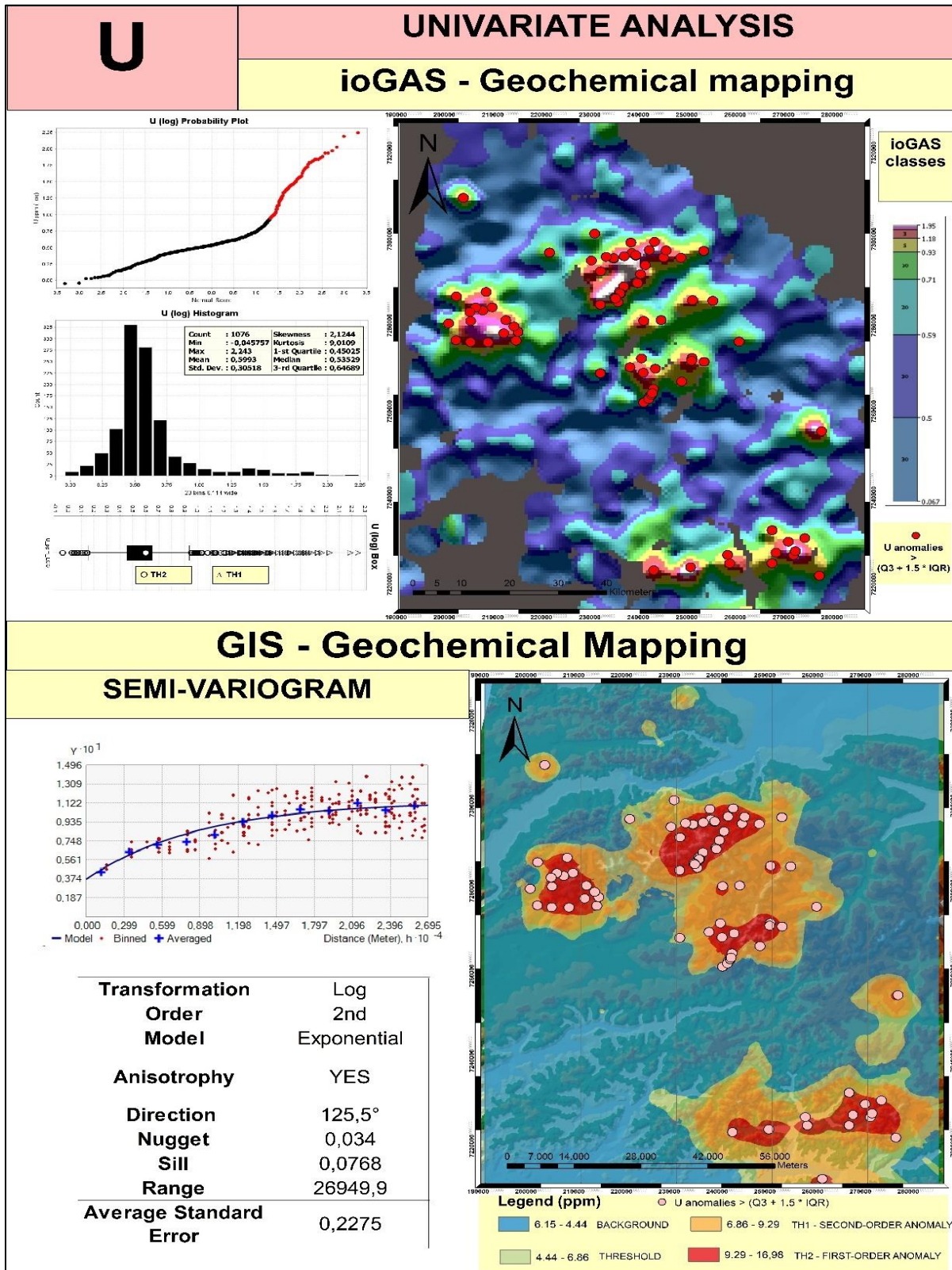
Figure 21: Univariate Analysis of Uranium (U)

-Univariate Analysis of Niobium (Nb):
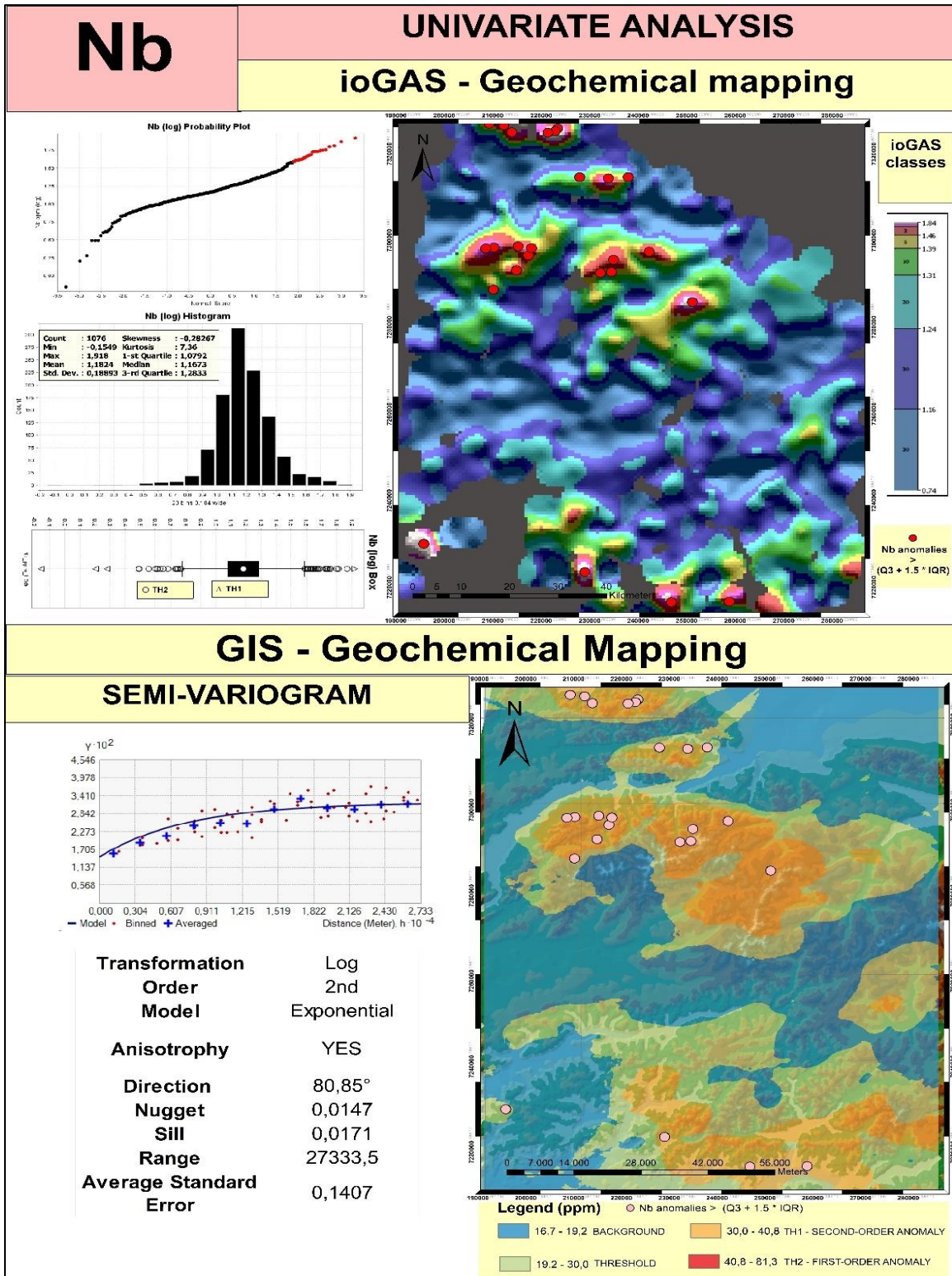
Figure 22: Univariate Analysis of Niobium (Nb)

-Univariate Analysis of Hafnium (Hf):
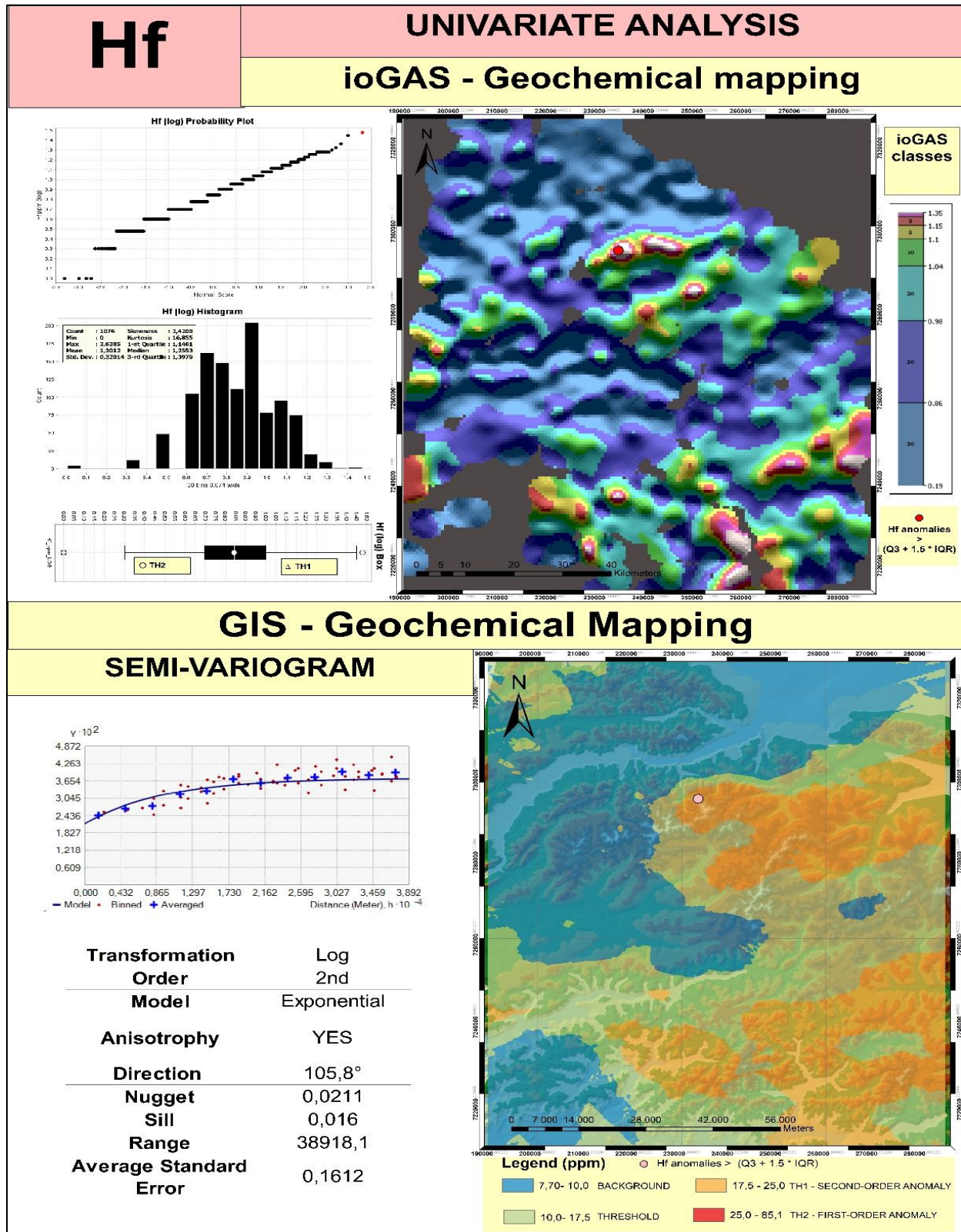
Figure 23: Univariate Analysis of Hafnium (Hf)

-Univariate Analysis of Zirconium (Zr):
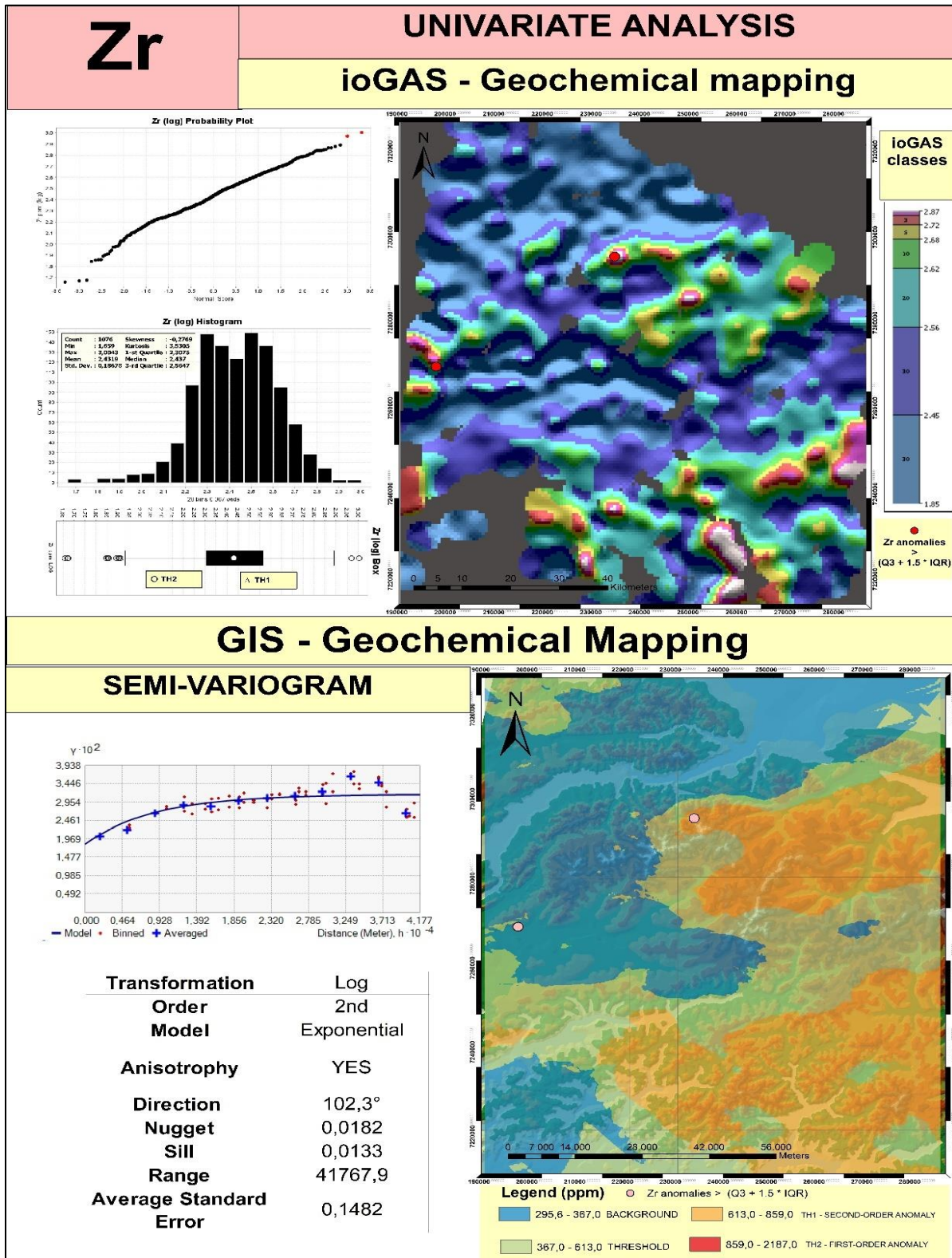
Figure 24: Univariate Analysis of Zirconium (Zr)

REE geochemical maps Comments

The REE association, along with its six associated pathfinder elements *(Y, Th, U, Nb, Hf, Zr),* demonstrated normal distributions as evidenced in both the histograms and probability plots. Furthermore, the variograms produced consistently low average standard errors, spanning from (0,1363) to (0,3186), affirming the reliability of the models employed. It is noteworthy that all the variograms employed the exponential model as the best fitting representation. In addition, the determination of common anisotropy orientation within the range of (77° - 125°) implies a North-East orientation for REE mineralization. This directional insight is significant in understanding the geological aspects of the deposit. In a broader context, the geochemical maps generated using both ioGAS (Inverse Distance Weighting Interpolation) and ArcGIS (Kriging Interpolation) exhibited similar patterns and trends. However, notable distinctions emerged in the data classes, with ioGAS maps revealing more zones of elevated concentration. Concerning the presence of anomalous values, a pattern emerged across the elements and REE components. All the maps and boxplots revealed the existence of more than 32 anomalous values distributed across multiple anomalous zones. However, Hafnium and Zirconium deviated from this trend, exhibiting 1 and 2 anomalous values, respectively. This observation highlighted the fact that within the REE pathfinder group, Hafnium and Zirconium exhibit the lowest degree of correlation, confirming the findings from the bivariate analysis. **(Figures 18,19,20,21,22,23 and 24)**

6.1.1.4   PGE Univariate Geochemical Analysis

- Univariate Analysis of Cobalt (Co):
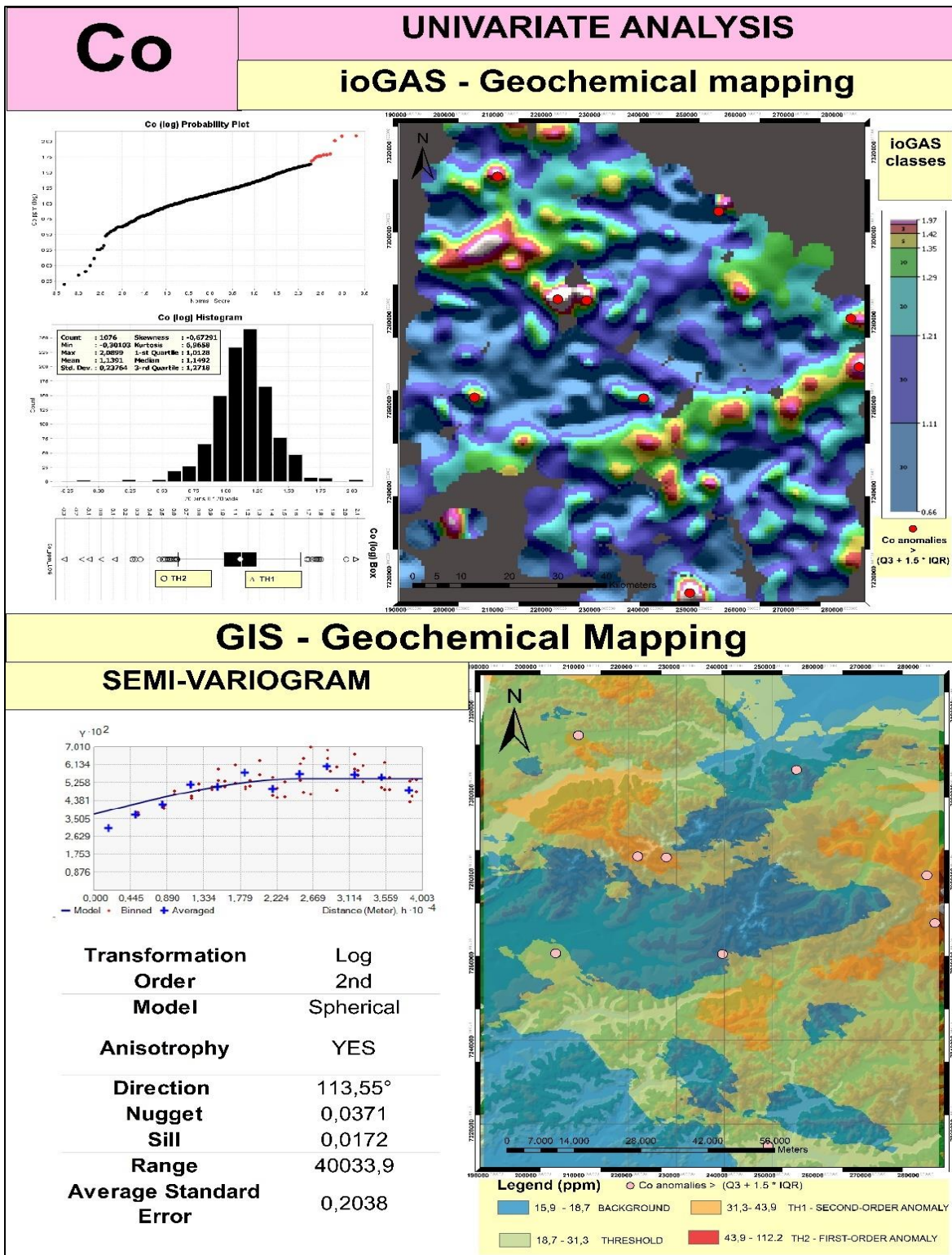
Figure 25: Univariate Analysis of Cobalt (Co)

-Univariate Analysis of Cooper (Cu):
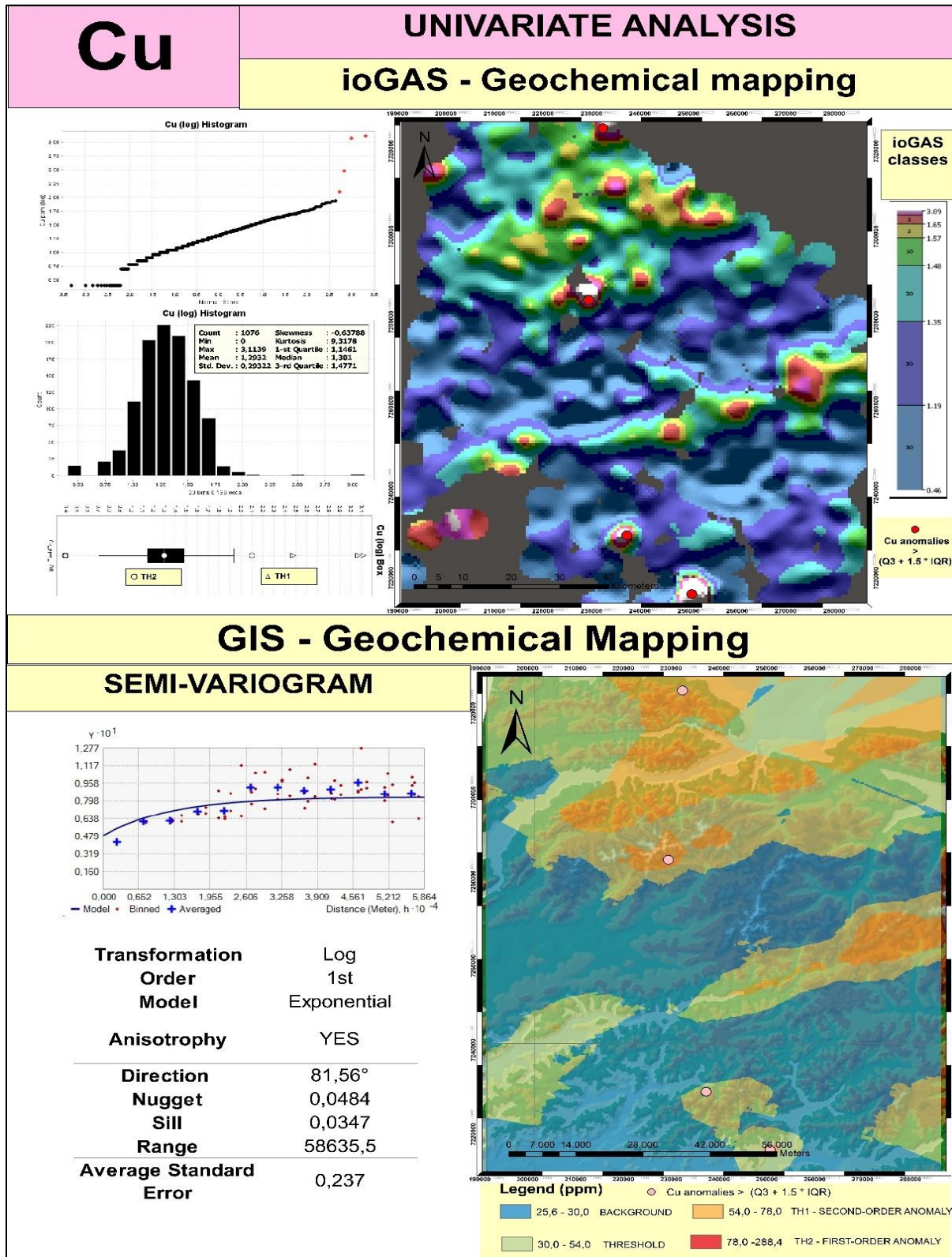
Figure 26: Univariate Analysis of Cooper (Cu)

-Univariate Analysis of Niquel (Ni):
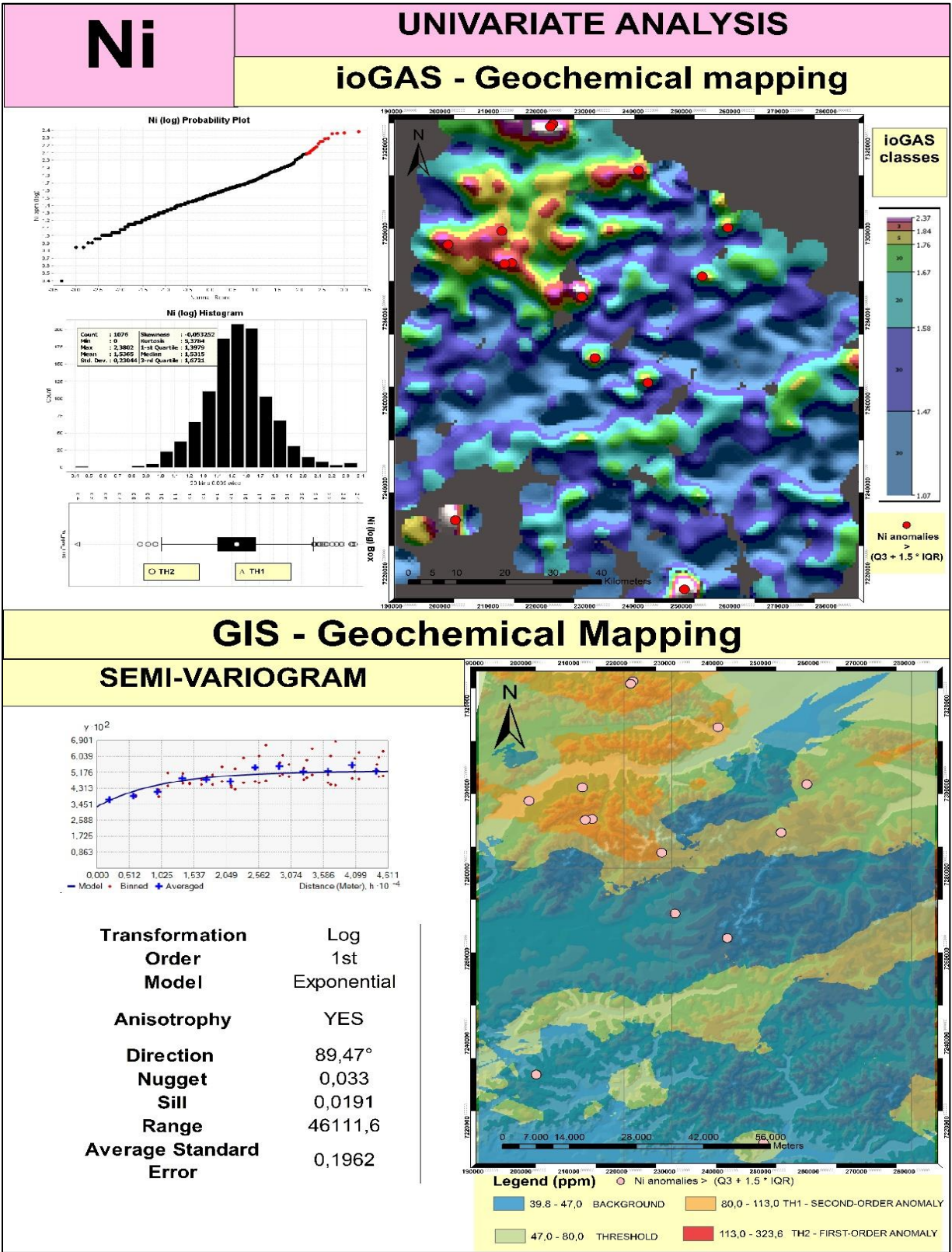
Figure 27: *Univariate Analysis of Niquel (Ni)*

-Univariate Analysis of Vanadium (V):
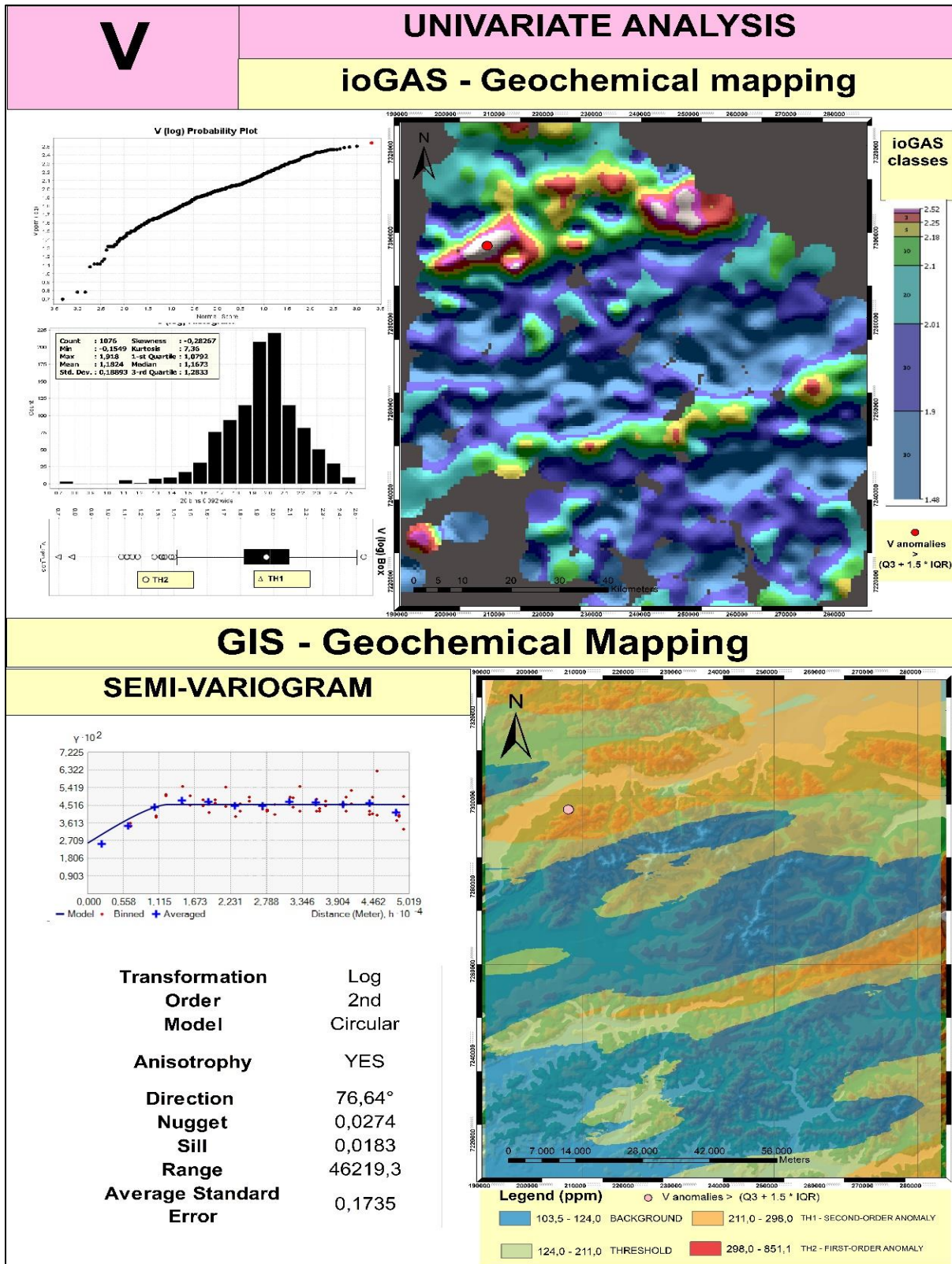
Figure 28: *Univariate Analysis of Vanadium (V)*

-Univariate Analysis of Chromium (Cr):
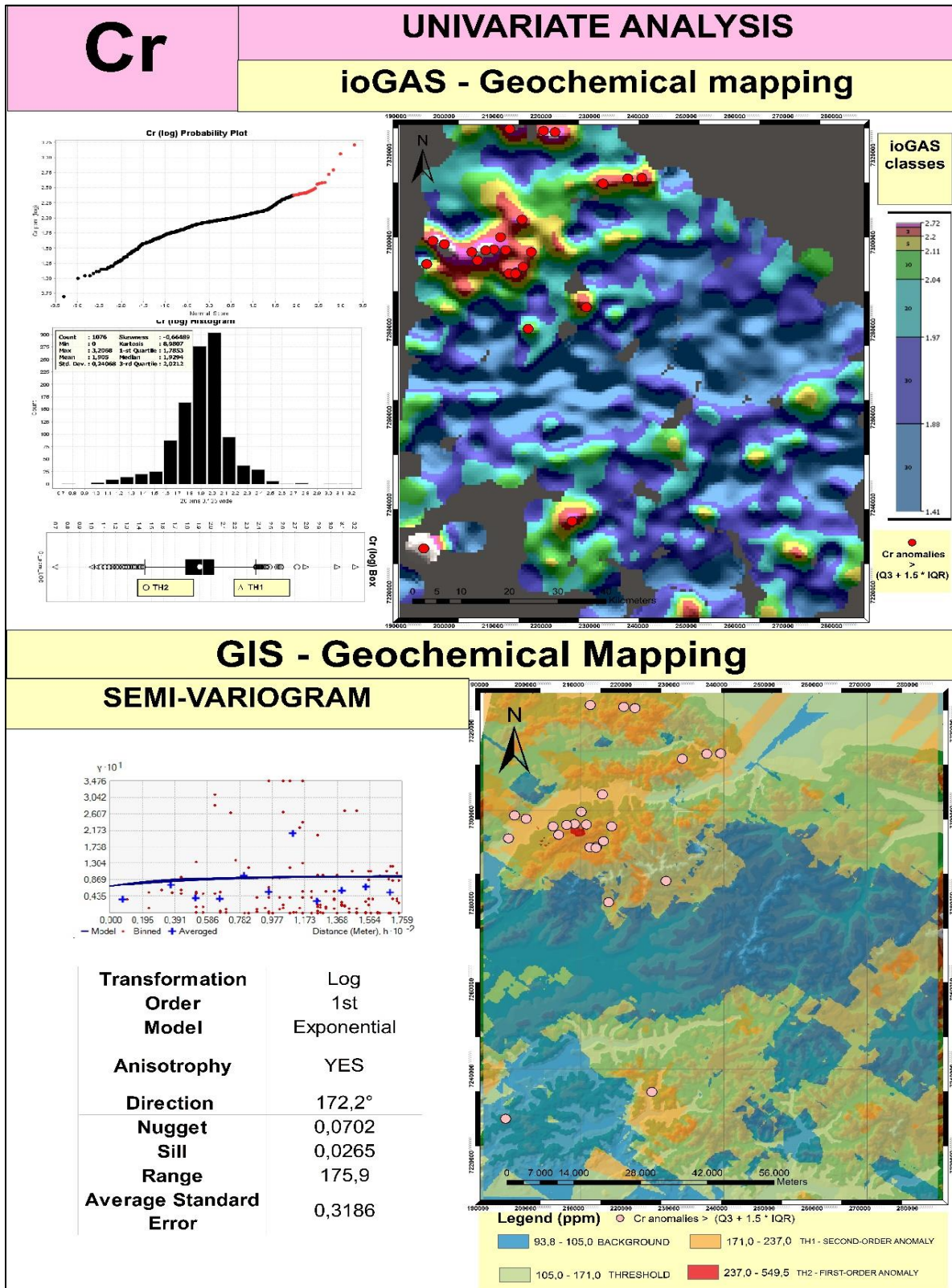
Figure 29: Univariate Analysis of Chromium (Cr)

PGE geochemical maps Comments

Each of the PGE pathfinders demonstrated a normal distribution, a fact verified through examination of their respective histograms and probability plots. Broadly, both the ioGAS and ArcGIS maps exhibit similarities in their patterns. However, when considering the individual elements within this group, it becomes evident that they do not share patterns or trends. For instance, notable variations arise in their anisotropy orientations, with Co, Cu, Ni, and V displaying anisotropy within the range of 76° to 113°. In contrast, Cr exhibits a distinct orientation leaning more toward the East at 172°. This divergence implies that the PGE mineralization assumes a North-East orientation, akin to the REE mineralization, although with notable variations among the individual pathfinder elements.

Within the Cr, Ni, and Cu Variograms, the most suitable model identified was the exponential, while for Co and V, the models of choice were the Spherical and Circular, respectively. Notably, only Cu and V exhibited a limited number of anomalous values, falling below the threshold of 5. It is worth mentioning that the average standard errors derived from these five variograms, though deemed acceptable, registered values higher than those observed within the REE association. This implies that the models and maps related to REE mineralization exhibit a higher level of reliability when compared to those of the PGE model and maps. Indeed, the maps and models of the PGE pathfinders exhibit a greater degree of irregularity and diminished clarity in contrast to the REE counterparts. Additionally, they encompass fewer anomalous values. Consequently, the process of correlation becomes more challenging, and the task of identifying coherent trends and patterns becomes more difficult. **(Figures 25,26,27,28 and 29)**

7. Mining potential maps

After the completion of the Exploratory Data Analysis (EDA), the results yield two distinct groups within the geochemical maps: (1) *REE-Y-Th-U-Nb-Hf-Zr* and (2) Co-Cu-Ni-V. As concluded in the Univariate analysis, Hafnium (Hf) and Zirconium (Zr) do not display the same spatial patterns and trends as their respective counterparts in group. A Similar scenario was observed among the Platinum Group Element (PGE) pathfinders, where *Chromium (Cr)* emerged as the sole element deviating from the common trend within its group. As a result, the final Mining Potential Maps do not include *Hafnium (Hf), Zirconium (Zr),* and *Chromium (Cr)* due to their distinct behavior, ensuring that the maps provide a more accurate and cohesive representation of the mineral potential in the studied area. Utilizing the Raster Calculator tool within ArcGIS, we conducted map sum operations, specifically, the summation of: *REE + Y + Th + U + Nb* and *Co + Cu + Ni + V*. This process resulted in the generation of two distinct final mining potential maps: one depicting the mineralization potential for REE and the other portraying the potential for Platinum Group Element (PGE) mineralization.
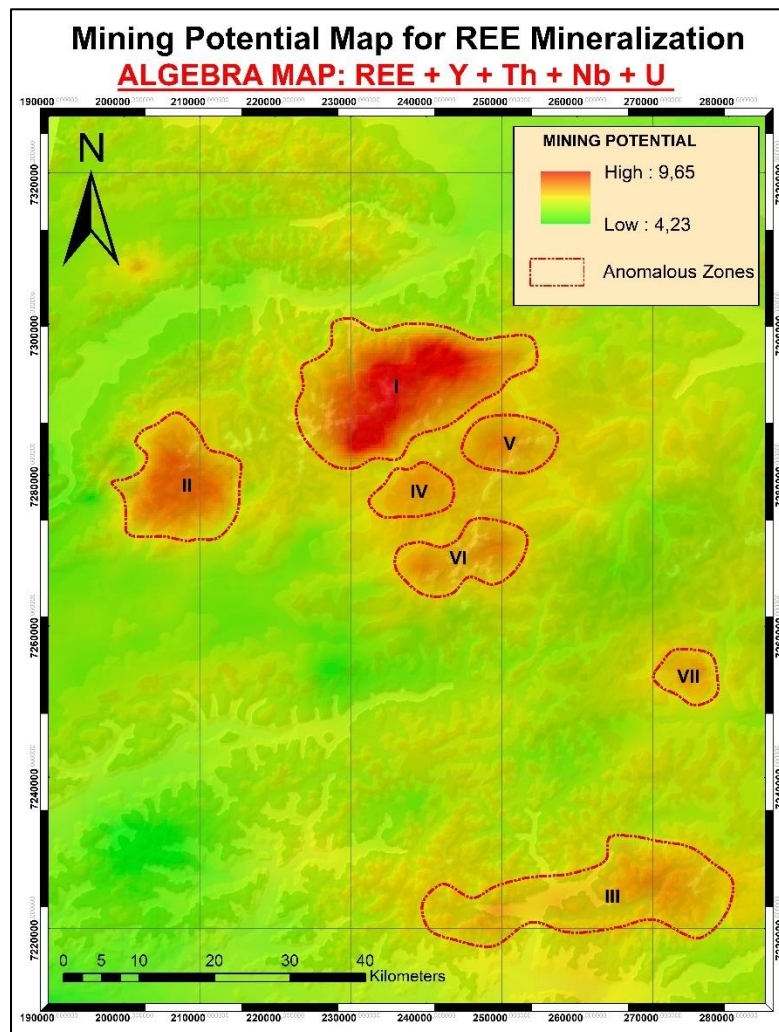
Figure 30: *Mining potential map for REE mineralization.*

7.1 Mining potential for REE mineralization

Upon analyzing the REE mining potential map, the presence of anomalous zones becomes evident. Notably, a significant cluster of these anomalous zones is situated in the north-central region of the study area. Furthermore, a notable cluster of such anomalous zones is situated in the north-central region of the study area. Furthermore, two additional anomalous zones are visualized in the southeastern section of the study area. Among the anomalous zones, only two zones, labeled as Zones I and II, displayed a notably high potential of REE and its associated pathfinder elements. These two zones stand out as prime candidates for REE mineralization, demonstrating robust potential. **(Figure 30)**
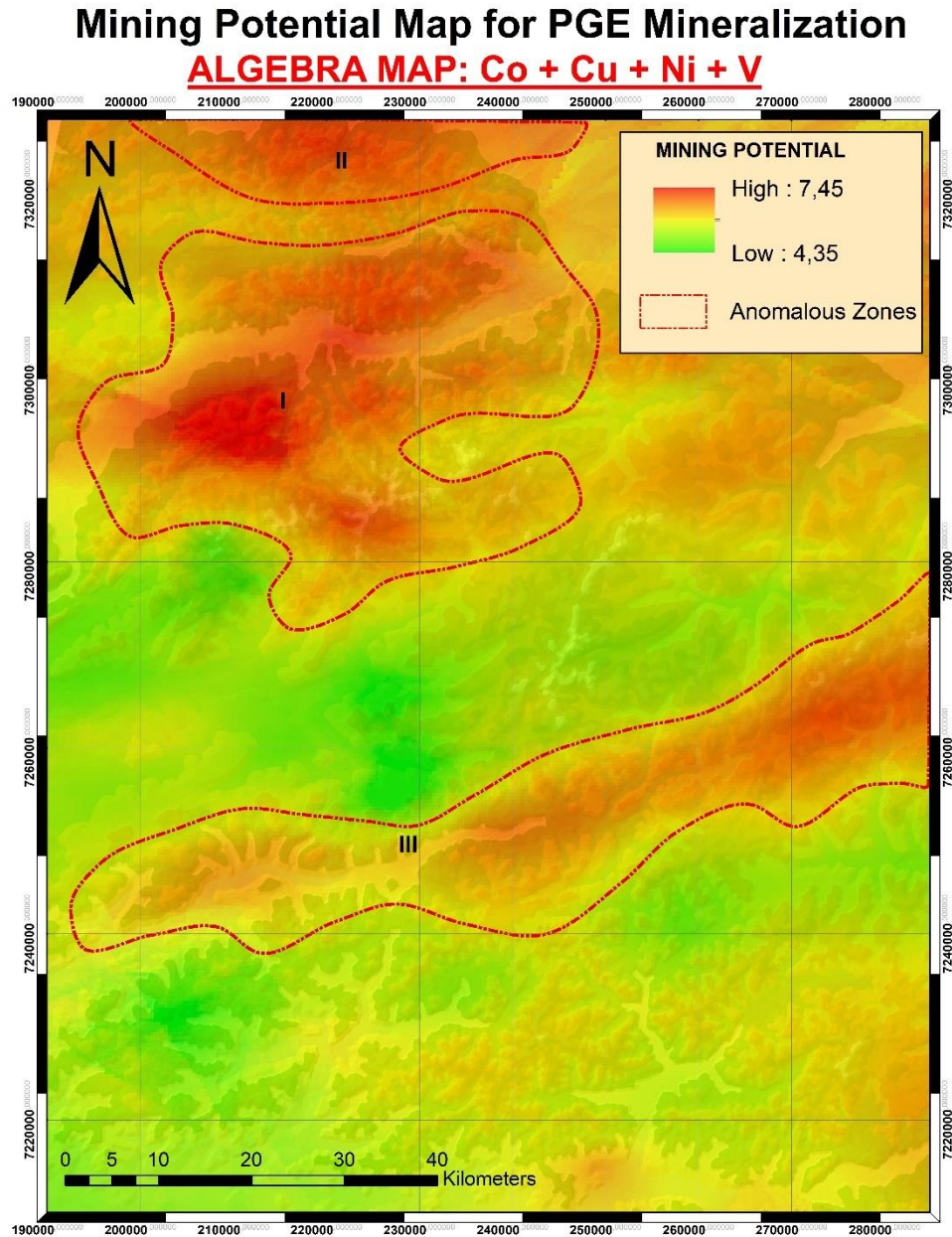
Figure 31: Mining potential map for PGE mineralization.

7.2 Mining potential for PGE mineralization

In reference to the Mining Potential Map for PGE Mineralization, it is evident that the number of anomalous zones is fewer in comparison to those in the REE category. These anomalous zones are characterized by their larger size, lack of uniformity, and irregular shape when contrasted with the REE anomalous zones. Notably, two significant zones are located in the northern region of the study area, while a third elongated zone extends across the study area in a northeast direction, aligning with the observed anisotropy of PGE pathfinders as revealed in the univariate maps Within the anomalous zones, only Zones I and II are considered as viable prospects for PGE mineralization, given that Zone III displays lower potentials compared to these two zones. **(Figure 31)**

8. Lithology Correlation

In addition to their primary use in prospecting for mining applications and their role as valuable inputs for subsequent mining exploration stages within the context of a mining project, mining potential maps can offer critical insights for establishing correlations with the lithological composition of a given area. This can be achieved by employing a compilation of geological units presented in the study zone and then overlaying the mining potential maps with the geological map. Through this process, it becomes possible to associate specific mineralizations with their corresponding rock types or categories.

8.1 REE lithology correlation

In the correlation of the Rare Earth Elements (REE) lithological map, it was observed that only one group of rocks exhibited a strong correspondence with the anomalous zone of REE mineralization. This group, denoted as 'Tkgi,' represents *the Granitic rocks of southern and interior Alaska*, which is a Cretaceous-Paleogene geological unit. This group comprises four distinct members: 'Undivided granitic rocks,' 'Peralkaline granite,' 'Felsic granitic rocks,' and 'Granodiorite to quartz monzodiorite. Among these rock types, the 'Peralkaline granite,' 'Undivided granitic rocks,' and 'felsic granitic rocks' have been identified as the lithologies most likely to host REE mineralization. This conclusion is drawn based on their geological characteristics and their association with typical peralkaline and alkaline rocks known to host REEs, such as syenite and nepheline-syenite. **(Figure 32)**
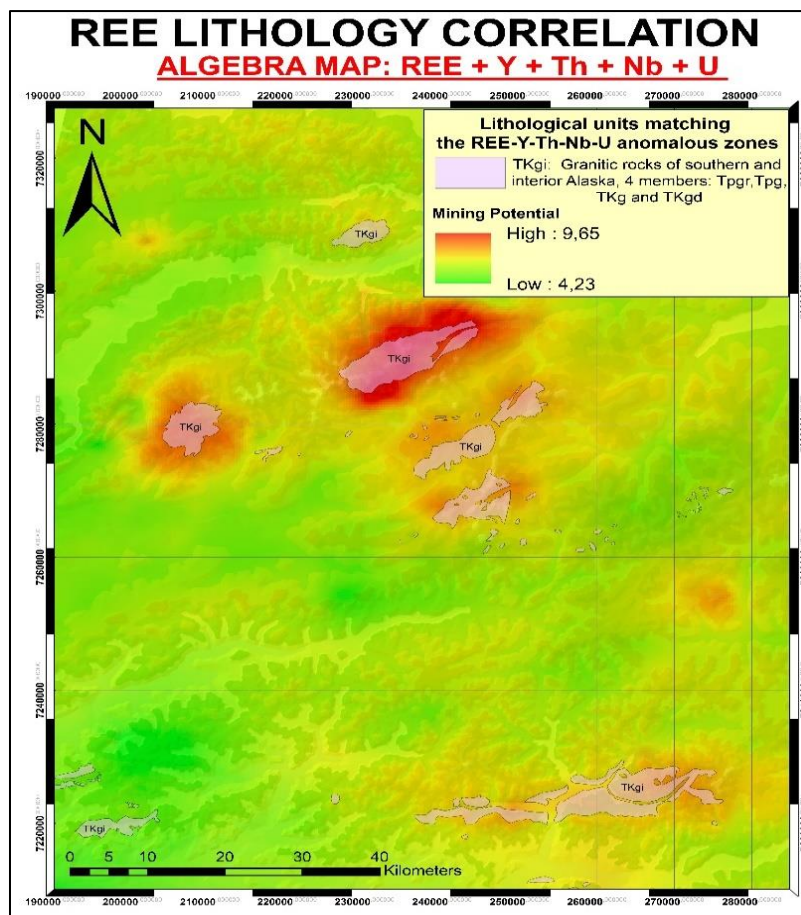
Figure 32: Lithology correlation for REE mineralization.

56

8.2 PGE lithology correlation

Analyzing the lithological correlations within the PGE anomalous zones presented a higher level of complexity due to their larger and irregular spatial extent. However, considering the geological context where PGE mineralization is typically associated with mafic or ultramafic rocks (referred to as MUM), often in the form of layered intrusions or ophiolite complexes, we undertook a deep examination of all the lithological units within the study area that exhibited the desired characteristics.

This investigation led to the identification of six geological units that are deemed the most probable hosts for PGE deposits.

(1) *Mafic Igneous Rocks, Central and Northeast Alaska (Early Paleozoic and/or Late Proterozoic) - (PzPmi):* This unit primarily comprises serpentinites intruded by dikes of clinopyroxene gabbro, microgabbro, and diorite.

(2) *Woodchopper Volcanics and Schwatka Unit of Weber and Others (1992) (Devonian) - (Dvec):* This unit contains amygdaloidal basalt, pillow basalt, and aquagene tuff interbedded with chert, argillite, quartzite, and limestone.

(3) *Fossil Creek Volcanics and Similar Rocks (Ordovician and Cambrian) - (OCv):* This unit consists of two members. The volcanic member comprises alkali basalt, agglomerate, and volcaniclastic conglomerate, while the sedimentary member contains well-rounded clasts of basalt, granite, quartzite, limestone, chert, and phyllite, along with basaltic tuff and mafic intrusive rocks.

(4) *Cascaden Ridge and Beaver Bend Combined Correlative Units (Devonian) - (Dcr):* While not an igneous rock unit, it exhibits conglomerate clasts composed of mafic and ultramafic rocks, as well as felsic volcanic rocks, chert, quartz, quartzite, argillite, slate, siltstone, and sandstone.

The units associated with the Yukon-Tanana Crystalline complex are the Eclogite and associated rocks (Paleozoic)—(Pze) and the Mafic schist and amphibolite (Devonian or older Paleozoic)—(Pzyms).

(5) *Eclogite and Associated Rocks (Paleozoic) - (Pze):* This unit features omphacite-bearing biotite-muscovite schist, micaceous marble, black quartzite, and amphibolite within a metamorphic sequence described as allochthonous. It also contains garnet-bearing quartz-biotite-muscovite schist, quartzite, and was derived from predominantly quartz-rich pelitic to calcareous pelitic sedimentary rocks, impure limestone, and associated mafic volcanic and volcaniclastic rocks.

(6) *Mafic Schist and Amphibolite (Devonian or Older Paleozoic) - (Pzyms):* This unit represents metamorphosed mafic pyroclastic rocks interbedded with schists. It includes hornblende metagabbro and metadiabase, as well as nonfoliated metaigneous rock with pseudomorphs of clinopyroxene and plagioclase, and minerals such as actinolite, chlorite, epidote, clinozoisite, and albite.

All six geological units contain mafic or ultramafic minerals, within different geological contexts. The first four units, located in the northern region, comprise original igneous rocks, with one group appearing as intrusive igneous formations and the other as volcanic rocks. However, the Dcr unit stands apart as it contains mafic and ultramafic clasts embedded within a sedimentary conglomerate. These clasts result from the weathering, erosion, transportation, and subsequent sedimentation of the original igneous rocks. The last two units, situated in the southern Yukon-Tanana Crystalline Complex, are associated with metamorphic processes. These rocks originated as mafic or ultramafic rocks and have undergone regional metamorphism. Eclogite is a distinctive indicator of high-pressure, high-temperature metamorphism. It forms under extreme pressures and temperatures, typically ranging from 600 to 800 degrees Celsius, and occurs at depths of 40 to 60 kilometers beneath the Earth's surface. This process is usually linked to tectonic plate collisions, where the pacific oceanic plate subduct beneath the North American continental plate. The protolith of eclogite typically consists of basaltic rock, characterized by its fine-grained, mafic igneous composition. Schist primarily arises from regional metamorphism, driven by elevated temperature and

pressure associated with tectonic processes, usually occurring in the deeper sections of the Earth's crust. The protolith of schist exhibits variability but is frequently derived from shale, slate, or phyllite, sedimentary rocks rich in clay minerals. Amphibolite, on the other hand, forms through medium- to high-grade regional metamorphism, characterized by increased temperatures and pressures, although not as extreme as those leading to eclogite. The protolith of amphibolite often comprises basalt, gabbro, or other mafic igneous rocks. **(Figure 33)**
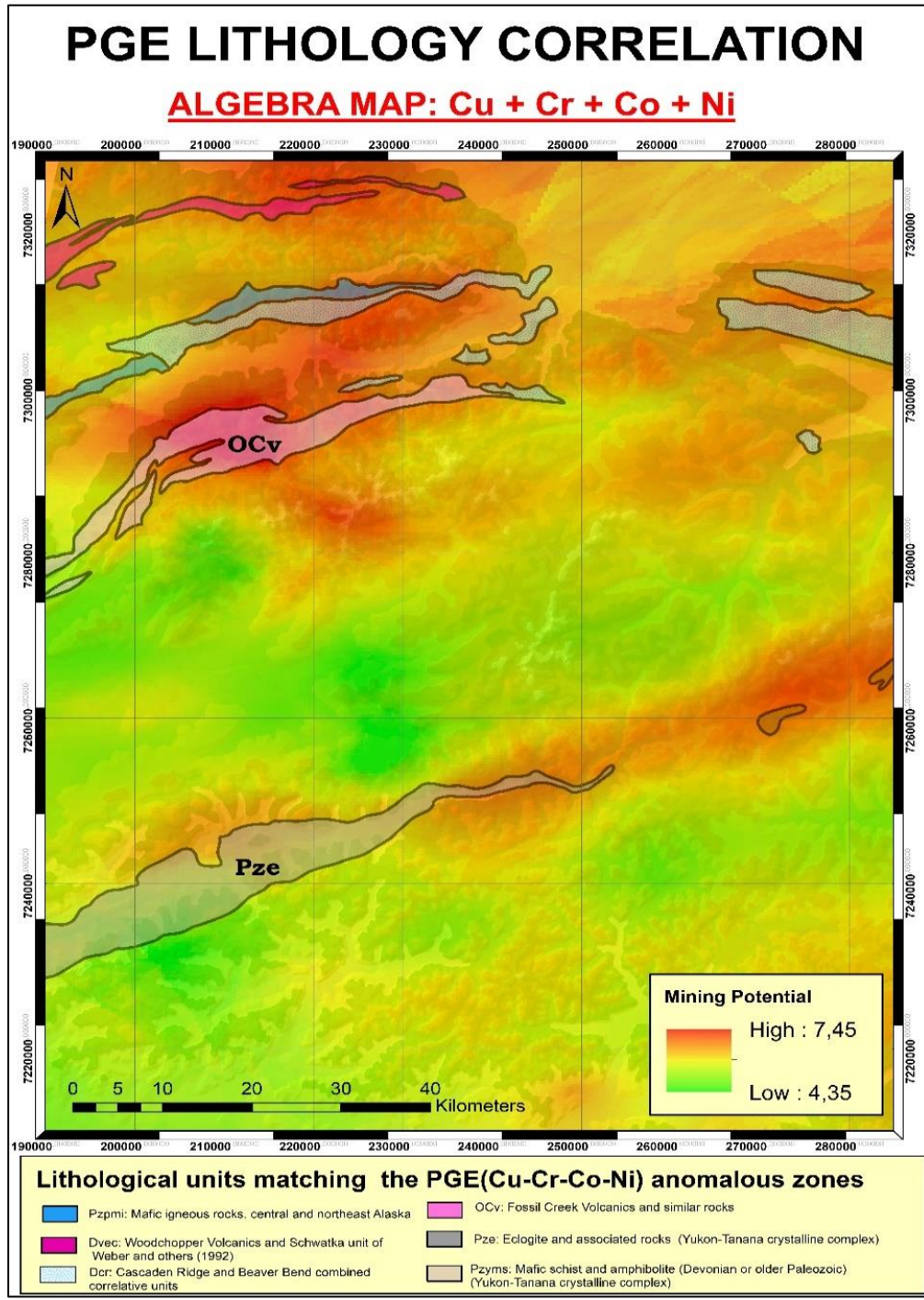
Figure 33: Lithology correlation for PGE mineralization.

9. Conclusions

The exploratory data analysis (EDA) techniques applied to the geochemical data presented interesting feedback about the REE and PGE mineralization and geological characteristics of the North central portion of Yukon Tanana Uplands.

Principal Component Analysis (PCA) has identified three significant geochemical associations: (i) *(REE~Eu)+Y* (ii) *(Th-Nb-U-Zr-Hf-Ta)* associated to a REE mineralization (PC1), and (iii) *Cu-Cr-Co-Ni-Ti-V* related to a PGE mineralization (PC2). These associations serve as pathfinders for specific mineralization events, with (ii) guiding REE mineralization and (iii) indicating PGE mineralization.

Bivariate analysis of geochemical associations revealed that only Tantalum (Ta) had a weak correlation with REEs, while the other pathfinders had stronger correlations. Similarly, Titanium (Ti) didn't exhibit a strong correlation within the Platinum Group Element (PGE) pathfinders, leading to the exclusion of Tantalum (Ta) and Titanium (Ti) from further analysis.

Two univariate mapping approaches - descriptive statistics with Inverse Distance Weighting Interpolation and geostatistics with Kriging Interpolation - resulted in two types of geochemical maps for REE (Y-Th-U-Nb-Zr-Hf) and PGE (Cu-Cr-Co-Ni-V) associations. Both maps had similar spatial trends but different data classes. Hafnium (Hf) and Zirconium (Zr) showed unique and different patterns with fewer anomalies in REE maps, while Chromium (Cr) deviated from typical PGE map patterns.

Using GIS raster calculations, two mining potential maps were created based on reduced geochemical data dimensions through EDA. The REE mining potential map revealed six anomalous zones, with only zones I and II considered viable candidates for hosting REE mineralization. In the PGE map, three anomalous zones were identified, and zones I and II were seen as potential prospects for PGE mineralization.

Since the potential mining maps serve as only one tool in the prospection stage, it is recommended to validate this information and results with additional surveys and methods such as: geophysics, Lidar, geological modelling, etc. In order to achieve more precise and accurate anomalous zones, especially in the PGE maps which presented Average Standard Errors higher than REE maps.

Overlaying mining potential maps with the geological map and lithological analysis revealed distinct findings: All REE anomalous zones correlated with Granitic rocks (Tkgi), known for hosting REE mineralization due to their peralkaline and alkaline rock types. For PGE, six lithological units were identified as host rocks across various geological contexts. There were igneous mafic intrusions, a primary source for PGE deposits. One unit featured a sedimentary conglomerate with mafic clastic material, while the other two comprised eclogite and amphibolite metamorphic rocks resulting from regional metamorphism of mafic and ultramafic substrates, which are common host rocks for PGE.

10.   Bibliography

[1] Clyde Wahrhaftig. (1965). "*Physiographic Divisions of Alaska*". *U.S*. Geological Survey Professional Paper. Page 24: https://dggs.alaska.gov/pubs/id/3872

[2] Pewe. T, Burbank. L, Mayo. L, (1967). "*Multiple Glaciation of the Yukon-Tanana Upland, Alaska*". Geological Survey, State of Alaska. General Map: https://pubs.usgs.gov/publication/i507

[3] Helen L. Foster. (1992). "*Geologic Map of The Eastern Yukon-Tanana Region, Alaska*". U.S. Geological. Survey Description of map units, pp 2-15: https://dggs.alaska.gov/pubs/id/11844

[4] Frederic H, Wilson. Chad P, Hults. Charles G, Mull. Susan M. Karl. (2015). "*Geologic Map of Alaska*". U.S. Geological Survey. Description of Map Units. Chapters: sedimentary, volcanic, intrusive and metamorphic map Units Descriptions: https://dggs.alaska.gov/pubs/id/29564

[5] RL Linnen. IM Samson. AE Williams-Jones. AR Chakhmouradian. (2014). "*Geochemistry of the REE, Nb, Ta, Hf, and Zr deposits*". Treatise on Geochemistry 2nd Edition. Pp 543-563. https://doi.org/10.1016/B978-0-08-095975-7.01124-4

[6] V, Balaram. (2022). "*Rare Earth Element Deposits: Sources, and Exploration Strategies*". Journal Geology Society of India. Edition 98: pp 1210-1216. https://doi.org/10.1007/s12594-022-2154-3

[7] Susan M. Karl, James V. Jones, III, and Timothy S. Hayes. (2016). "*GIS-Based Identification of Areas that have Resource Potential for Critical Minerals in Six Selected Groups of Deposit Types in Alaska*". U.S. Geological Survey in cooperation with the Alaska Division of Geological & Geophysical Surveys. Pp 19-28, 33-37: https://doi.org/10.3133/ofr20161191

[8] W.D. Maier. (2005). "*Platinum-group element (PGE) deposits and occurrences: Mineralization styles, genetic concepts, and exploration criteria*". Geological Society of Africa Presidential Review, No. 9. Pp 166-179. https://doi.org/10.1016/j.jafrearsci.2005.03.004

[9] Wolfgang D, Maier. Alexey A, Ariskin. (2016). "*Ni-Cu-PGE-Cr-V bearing layered mafic-ultramafic intrusions of Russia preface to a thematic issue*". Miner Deposita Chapter 51: pp 971–972. https://doi.org/10.1007/s00126-016-0699-z

[10] M, Komorowski, D. Marshall, J. Salciccioli. Y, Crutain. (2016). "*Exploratory Data Analysis*". Secondary Analysis of Electronic Health Records pp 185–203. https://doi.org/10.1007/978-3-319-43742-2_15

[11] M, Vigni, C, Durante. M, Cocchi. (2013). "*Exploratory Data Analysis*". Department of Chemical and Geochemical Sciences, University of Modena and Reggio Emilia, Modena, Italy. Pp 4-60. https://iris.unimore.it/retrieve/handle/11380/971504/91060/Exploratorypostprint.pdf

[12] Mateus, A. (2011). "*Análisis Geoestadístico por el Método de Kriging Ordinario Aplicado a Muestras de Sedimentos Fluviales en el Distrito Minero Azuay*". Universidad San Francisco De Quito, Ecuador. Máster Thesis. Chapters V and VI. Availabe in PDF.

[13] A, Macheyeki. X, Li. D, Kafumu. F, Yuan. (2020). "*Applied Geochemistry: Advances in Mineral Exploration Techniques*". Netherlands: Elsevier. Chapter: Conventional and nonconventional exploration techniques principles pp 87-148. Available in PDF.

[14] X, Emery. (2007). "*Apuntes de Geoestadistica*". Facultad de Ciencias Físicas y Matemáticas, Universidad de Chile. Chapters: 1,2,3,6,7 and 8. Available in PDF.

[15] ReflexNow Company. (2019). "*IMDEX ioGAS Quick Start Tutorial*": https://reflexnow.com/wp-content/uploads/2019/11/ioGAS-Quick-Start-Tutorial-7.1.pdf

11. Annexes

11.1 Pearson Correlation Matrix

	Al	Ca	Fe	K	Mg	P	Si	Ti	As	B	Ba	Bi	Cd	Co	Cr	Cs	Cu	Ga	Ge	Hf	Li	Mn	Nb	Ni	Pb	Rb	Sb	Sc	Sn	Sr	Ta	Th	Tl	U	V	W	Y	Zn	Zr	REE	LREE	HREE
Al	1,00	0,37	0,54	0,71	0,52	0,47	-0,16	0,37	-0,25	0,49	0,45	0,15	0,18	0,55	0,51	0,55	0,35	0,93	0,21	0,38	0,70	0,55	0,59	0,41	0,05	0,55	-0,25	0,70	0,17	0,45	0,38	0,53	0,35	0,41	0,54	-0,03	0,65	0,45	0,36	0,70	0,70	0,67
Ca	0,37	1,00	0,47	-0,09	0,77	0,70	-0,49	0,49	-0,25	0,20	0,40	-0,22	0,23	0,56	0,67	-0,06	0,27	0,30	0,09	0,31	0,01	0,58	0,50	0,47	-0,18	-0,21	-0,26	0,69	-0,22	0,77	0,22	0,02	-0,19	0,09	0,64	-0,19	0,40	0,32	0,32	0,29	0,28	0,40
Fe	0,54	0,47	1,00	0,17	0,70	0,63	-0,40	0,53	0,17	0,37	0,58	0,06	0,29	0,73	0,70	0,12	0,69	0,50	0,22	0,14	0,27	0,50	0,45	0,68	0,05	-0,03	0,18	0,78	-0,13	0,48	0,16	0,01	0,03	-0,04	0,78	-0,09	0,31	0,45	0,15	0,32	0,32	0,33
K	0,71	-0,09	0,17	1,00	0,04	0,15	0,12	-0,12	-0,03	0,39	0,32	0,38	0,16	0,19	0,04	0,72	0,23	0,71	0,16	0,17	0,74	0,29	0,28	0,11	0,30	0,88	-0,06	0,20	0,38	0,08	0,24	0,65	0,63	0,50	0,10	0,18	0,47	0,35	0,13	0,61	0,62	0,49
Mg	0,52	0,77	0,70	0,04	1,00	0,65	-0,55	0,64	-0,24	0,20	0,53	-0,26	0,18	0,74	0,77	-0,01	0,43	0,44	0,06	0,19	0,15	0,59	0,55	0,63	-0,25	-0,17	-0,20	0,81	-0,25	0,65	0,20	-0,08	-0,17	-0,09	0,77	-0,27	0,26	0,35	0,21	0,25	0,25	0,28
P	0,47	0,70	0,63	0,15	0,65	1,00	-0,37	0,45	0,02	0,39	0,64	0,03	0,44	0,56	0,66	0,17	0,54	0,45	0,19	0,26	0,21	0,56	0,55	0,56	0,05	0,00	0,05	0,68	-0,11	0,62	0,23	0,17	0,01	0,20	0,74	-0,06	0,50	0,54	0,26	0,46	0,45	0,50
Si	-0,16	-0,49	-0,40	0,12	-0,55	-0,37	1,00	-0,26	0,08	-0,09	-0,26	0,08	-0,17	-0,41	-0,39	-0,01	-0,31	-0,19	0,06	0,05	0,03	-0,29	-0,24	-0,32	0,10	0,17	0,10	-0,43	0,11	-0,41	-0,05	0,11	0,09	0,02	-0,40	0,15	-0,15	-0,22	0,03	-0,11	-0,10	-0,15
Ti	0,37	0,49	0,53	-0,12	0,64	0,45	-0,26	1,00	-0,21	0,23	0,26	-0,28	-0,01	0,52	0,55	-0,16	0,17	0,32	-0,03	0,45	0,06	0,40	0,66	0,38	-0,31	-0,31	-0,12	0,60	-0,12	0,48	0,45	-0,11	-0,38	-0,14	0,55	-0,08	0,21	0,13	0,50	0,19	0,18	0,21
As	-0,25	-0,25	0,17	-0,03	-0,24	0,02	0,08	-0,21	1,00	0,16	0,00	0,54	0,34	-0,06	-0,09	0,13	0,35	-0,19	0,25	-0,16	-0,05	-0,15	-0,21	0,09	0,61	0,02	0,81	-0,14	0,10	-0,11	-0,11	-0,01	0,22	0,02	-0,10	0,47	-0,12	0,18	-0,19	-0,07	-0,06	-0,11
B	0,49	0,20	0,37	0,39	0,20	0,39	-0,09	0,23	0,16	1,00	0,23	0,44	0,28	0,33	0,24	0,43	0,33	0,50	0,31	0,44	0,43	0,41	0,37	0,26	0,25	0,38	0,10	0,36	0,19	0,20	0,37	0,44	0,29	0,43	0,29	0,33	0,55	0,33	0,41	0,52	0,51	0,54
Ba	0,45	0,40	0,58	0,32	0,53	0,64	-0,26	0,26	0,00	0,23	1,00	-0,08	0,36	0,46	0,60	0,18	0,51	0,42	0,19	-0,01	0,24	0,36	0,37	0,51	-0,07	0,09	0,13	0,56	-0,16	0,50	0,05	0,03	0,14	0,01	0,78	-0,27	0,23	0,39	0,00	0,29	0,30	0,24
Bi	0,15	-0,22	0,06	0,38	-0,26	0,03	0,08	-0,28	0,54	0,44	-0,08	1,00	0,38	-0,09	-0,16	0,58	0,35	0,23	0,23	0,06	0,38	0,01	0,04	0,01	0,68	0,53	0,39	-0,08	0,52	-0,17	0,19	0,55	0,59	0,56	-0,15	0,67	0,38	0,37	-0,01	0,39	0,39	0,39
Cd	0,18	0,23	0,29	0,16	0,18	0,44	-0,17	-0,01	0,34	0,28	0,36	0,38	1,00	0,31	0,27	0,30	0,53	0,23	0,30	-0,07	0,24	0,34	0,23	0,42	0,57	0,18	0,34	0,22	0,10	0,16	0,12	0,24	0,34	0,31	0,28	0,16	0,35	0,75	-0,10	0,31	0,30	0,36
Co	0,55	0,56	0,73	0,19	0,74	0,56	-0,41	0,52	-0,06	0,33	0,46	-0,09	0,31	1,00	0,66	0,12	0,53	0,53	0,14	0,20	0,28	0,75	0,46	0,72	-0,04	0,01	-0,02	0,71	-0,19	0,51	0,15	0,02	-0,02	-0,03	0,65	-0,16	0,30	0,43	0,22	0,32	0,32	0,33
Cr	0,51	0,67	0,70	0,04	0,77	0,66	-0,39	0,55	-0,09	0,24	0,60	-0,16	0,27	0,66	1,00	0,01	0,50	0,44	0,20	0,21	0,15	0,47	0,46	0,74	-0,12	-0,16	-0,04	0,79	-0,29	0,59	0,10	-0,03	-0,10	-0,06	0,82	-0,23	0,30	0,38	0,23	0,30	0,29	0,32
Cs	0,55	-0,06	0,12	0,72	-0,01	0,17	-0,01	-0,16	0,13	0,43	0,18	0,58	0,30	0,12	0,01	1,00	0,29	0,59	0,19	0,07	0,76	0,19	0,21	0,11	0,39	0,82	0,04	0,13	0,44	0,01	0,21	0,63	0,69	0,64	0,05	0,37	0,50	0,43	0,02	0,56	0,55	0,52
Cu	0,35	0,27	0,69	0,23	0,43	0,54	-0,31	0,17	0,35	0,33	0,51	0,35	0,53	0,53	0,50	0,29	1,00	0,35	0,24	-0,08	0,28	0,36	0,21	0,64	0,36	0,10	0,43	0,53	-0,05	0,25	-0,01	0,07	0,24	0,07	0,61	0,05	0,26	0,59	-0,10	0,25	0,25	0,28
Ga	0,93	0,30	0,50	0,71	0,44	0,45	-0,19	0,32	-0,19	0,50	0,42	0,23	0,23	0,53	0,44	0,59	0,35	1,00	0,30	0,35	0,70	0,51	0,61	0,39	0,13	0,64	-0,18	0,62	0,23	0,34	0,40	0,60	0,41	0,45	0,49	0,04	0,69	0,48	0,33	0,76	0,76	0,71
Ge	0,21	0,09	0,22	0,16	0,06	0,19	0,06	-0,03	0,25	0,31	0,19	0,23	0,30	0,14	0,20	0,19	0,24	0,30	1,00	0,06	0,18	0,09	0,18	0,26	0,33	0,23	0,25	0,23	0,02	0,07	0,12	0,23	-0,07	0,07	0,19	0,10	0,27	0,28	0,04	0,29	0,29	0,28
Hf	0,38	0,31	0,14	0,17	0,19	0,26	0,05	0,45	-0,16	0,44	-0,01	0,06	-0,07	0,20	0,21	0,07	-0,08	0,35	0,06	1,00	0,12	0,33	0,47	-0,02	0,02	0,09	-0,22	0,32	0,16	0,37	0,49	0,49	-0,07	0,37	0,11	0,25	0,58	0,07	0,98	0,56	0,56	0,58
Li	0,70	0,01	0,27	0,74	0,15	0,21	0,03	0,06	-0,05	0,43	0,24	0,38	0,24	0,28	0,15	0,76	0,28	0,70	0,18	0,12	1,00	0,36	0,41	0,22	0,18	0,74	-0,08	0,28	0,40	0,07	0,36	0,57	0,54	0,54	0,18	0,21	0,52	0,44	0,08	0,56	0,56	0,52
Mn	0,55	0,58	0,50	0,29	0,59	0,56	-0,29	0,40	-0,15	0,41	0,36	0,01	0,34	0,75	0,47	0,19	0,36	0,51	0,09	0,33	0,36	1,00	0,34	0,49	-0,02	0,15	-0,14	0,56	0,02	0,49	0,30	0,20	0,07	0,22	0,49	-0,04	0,46	0,47	0,32	0,40	0,39	0,45
Nb	0,59	0,50	0,45	0,28	0,55	0,55	-0,24	0,66	-0,21	0,37	0,37	0,04	0,23	0,46	0,46	0,21	0,21	0,61	0,18	0,47	0,41	0,47	1,00	0,34	0,00	0,20	-0,18	0,53	0,19	0,50	0,73	0,40	0,12	0,34	0,45	0,11	0,59	0,43	0,48	0,62	0,61	0,59
Ni	0,41	0,47	0,68	0,11	0,63	0,56	-0,32	0,38	0,09	0,26	0,51	0,01	0,42	0,72	0,74	0,11	0,64	0,39	0,26	0,22	0,41	0,49	0,34	1,00	0,08	-0,03	0,14	0,60	-0,21	0,34	0,03	-0,03	0,05	-0,07	0,65	-0,15	0,21	0,55	0,00	0,23	0,23	0,23
Pb	0,05	-0,18	0,05	0,30	-0,25	0,05	0,10	-0,31	0,61	0,25	-0,07	0,68	0,57	-0,04	-0,12	0,39	0,36	0,13	0,33	0,02	0,22	-0,02	0,00	0,08	1,00	0,40	0,50	0,53	0,29	0,50	0,07	0,44	0,12	0,41	-0,21	0,45	0,26	0,54	-0,03	0,31	0,31	0,29
Rb	0,55	-0,21	-0,03	0,88	-0,17	0,00	0,17	-0,31	0,02	0,38	0,09	0,53	0,18	0,01	-0,16	0,82	0,10	0,64	0,23	0,09	0,74	0,15	0,20	-0,03	0,40	1,00	-0,05	-0,02	0,53	-0,13	0,25	0,76	0,77	0,66	-0,12	0,31	0,52	0,34	0,03	0,61	0,61	0,53
Sb	-0,25	-0,26	0,18	-0,06	-0,20	0,05	0,10	-0,12	0,81	0,10	0,13	0,39	0,34	-0,02	-0,04	0,04	0,43	-0,18	0,25	-0,22	-0,08	-0,14	-0,18	0,14	0,50	-0,05	1,00	-0,07	0,04	-0,15	-0,13	-0,11	0,18	-0,11	0,06	0,27	-0,15	0,17	-0,24	-0,12	-0,11	-0,14
Sc	0,70	0,69	0,78	0,20	0,81	0,68	-0,43	0,60	-0,14	0,36	0,56	-0,08	0,22	0,71	0,79	0,13	0,53	0,62	0,23	0,32	0,53	0,56	0,53	0,60	-0,11	-0,02	-0,07	1,00	-0,19	0,65	0,20	0,10	-0,05	0,06	0,84	-0,19	0,47	0,36	0,32	0,44	0,43	0,49
Sn	0,17	-0,22	-0,13	0,38	-0,25	-0,11	0,11	-0,12	0,10	0,19	-0,16	0,52	0,10	-0,19	-0,29	0,44	-0,05	0,23	0,02	0,16	0,40	0,02	0,19	-0,21	0,29	0,53	0,04	-0,19	1,00	-0,19	0,47	0,53	0,49	0,56	-0,27	0,52	0,38	0,21	0,11	0,36	0,35	0,36
Sr	0,45	0,77	0,48	0,08	0,65	0,62	-0,41	0,48	-0,11	0,20	0,50	-0,17	0,16	0,51	0,59	0,01	0,25	0,34	0,07	0,07	0,49	0,50	0,34	0,49	-0,09	-0,13	-0,15	0,65	-0,19	1,00	0,25	0,07	-0,14	0,11	0,59	-0,12	0,35	0,23	0,38	0,35	0,35	0,37
Ta	0,38	0,22	0,16	0,24	0,20	0,23	-0,05	0,45	-0,11	0,37	0,05	0,19	0,12	0,15	0,10	0,21	-0,01	0,40	0,12	0,49	0,36	0,30	0,73	0,03	0,07	0,25	-0,13	0,20	0,47	0,25	1,00	0,44	0,18	0,46	0,08	0,34	0,51	0,27	0,45	0,49	0,48	0,50
Th	0,53	0,02	0,01	0,65	-0,08	0,17	0,11	-0,11	0,44	0,03	0,55	0,24	0,02	-0,03	0,63	0,07	0,60	0,23	0,49	0,57	0,20	0,40	-0,03	0,44	0,76	-0,11	0,10	0,53	0,07	0,44	0,18	1,00	0,59	0,83	-0,07	0,43	0,81	0,41	0,43	0,87	0,87	0,83
Tl	0,35	-0,19	0,03	0,63	-0,17	0,01	0,09	-0,38	0,22	0,29	0,14	0,59	0,34	-0,02	-0,10	0,69	0,24	0,41	-0,07	-0,07	0,54	0,07	0,12	0,05	0,12	0,77	0,18	-0,05	0,49	-0,14	0,18	0,59	1,00	0,57	-0,32	0,41	0,39	-0,15	0,46	0,46	0,46	0,42
U	0,41	0,09	-0,04	0,50	-0,09	0,20	0,02	-0,14	0,02	0,43	0,01	0,43	0,01	0,56	0,31	-0,03	-0,06	0,64	0,07	0,45	0,18	0,37	0,54	0,22	0,34	-0,07	0,41	0,66	-0,11	0,06	0,56	0,11	0,46	1,00	-0,09	0,43	0,76	0,42	0,30	0,68	0,67	0,76
V	0,54	0,64	0,78	0,10	0,77	0,74	-0,40	0,55	-0,10	0,29	0,78	-0,15	0,28	0,65	0,82	0,05	0,61	0,49	0,19	0,11	0,18	0,49	0,45	0,65	-0,21	-0,12	0,06	0,84	-0,27	0,59	0,08	-0,07	-0,07	-0,09	1,00	-0,32	0,32	0,36	0,13	0,30	0,30	0,33
W	-0,03	-0,19	-0,09	0,18	-0,27	-0,06	0,15	-0,08	0,47	0,33	-0,27	0,67	0,16	-0,16	-0,23	0,37	0,05	0,04	0,10	0,25	0,21	-0,04	0,11	-0,15	0,45	0,31	0,27	-0,19	0,52	-0,12	0,34	0,43	0,32	0,43	-0,32	1,00	0,27	0,15	0,21	0,28	0,28	0,27
Y	0,65	0,40	0,31	0,47	0,26	0,50	-0,15	0,21	-0,12	0,55	0,23	0,38	0,35	0,30	0,30	0,50	0,26	0,69	0,27	0,58	0,52	0,46	0,59	0,21	0,26	0,52	-0,15	0,47	0,38	0,35	0,51	0,41	0,41	0,76	0,32	0,27	1,00	0,52	0,53	0,88	0,86	0,99
Zn	0,45	0,32	0,45	0,35	0,35	0,54	-0,22	0,13	0,18	0,33	0,39	0,37	0,75	0,43	0,38	0,43	0,59	0,48	0,28	0,07	0,44	0,47	0,43	0,55	0,54	0,34	0,17	0,36	0,21	0,23	0,27	0,41	0,39	0,42	0,36	0,15	0,52	1,00	0,04	0,51	0,50	0,53
Zr	0,36	0,32	0,15	0,13	0,21	0,26	0,03	0,50	-0,19	0,41	0,00	-0,01	-0,10	0,22	0,23	0,02	-0,10	0,33	0,04	0,98	0,08	0,32	0,48	0,00	-0,03	0,03	-0,24	0,32	0,11	0,38	0,45	0,43	-0,15	0,30	0,13	0,21	0,53	0,04	1,00	0,53	0,52	0,53
REE	0,70	0,29	0,32	0,61	0,25	0,46	-0,11	0,19	-0,07	0,52	0,29	0,39	0,31	0,32	0,30	0,56	0,25	0,76	0,29	0,56	0,56	0,40	0,62	0,23	0,31	0,61	-0,12	0,44	0,36	0,35	0,49	0,35	0,46	0,68	0,30	0,28	0,88	0,51	0,53	1,00	1,00	0,92
LREE	0,70	0,28	0,32	0,62	0,25	0,45	-0,10	0,18	-0,06	0,51	0,30	0,39	0,30	0,32	0,29	0,55	0,25	0,76	0,29	0,56	0,56	0,39	0,61	0,23	0,31	0,61	-0,11	0,43	0,35	0,35	0,48	0,48	0,46	0,67	0,30	0,28	0,86	0,50	0,52	1,00	1,00	0,90
HREE	0,67	0,40	0,33	0,49	0,28	0,50	-0,15	0,21	-0,11	0,54	0,24	0,39	0,36	0,33	0,32	0,52	0,28	0,71	0,28	0,58	0,52	0,45	0,59	0,23	0,29	0,53	-0,14	0,49	0,36	0,37	0,50	0,83	0,42	0,76	0,33	0,27	0,99	0,53	0,53	0,92	0,90	1,00

11.2 PCA Eigenvectors

Eigenvectors	PC1	PC2	PC3	PC4	PC5
Al	0,17	0,06	0,04	0,20	0,03
Ca	0,10	0,21	0,03	-0,13	0,13
Fe	0,10	0,20	-0,15	0,04	-0,13
K	0,13	-0,10	-0,01	0,30	0,03
Mg	0,09	0,26	-0,01	0,02	0,06
P	0,13	0,17	-0,08	-0,04	-0,02
Si	-0,04	-0,15	0,05	0,02	-0,11
Ti	0,07	0,21	0,07	-0,15	-0,11
Ag	-0,03	-0,10	-0,27	-0,23	-0,10
As	-0,01	-0,08	-0,29	-0,09	-0,35
B	0,13	-0,01	-0,04	-0,02	-0,21
Ba	0,09	0,17	-0,12	0,17	0,03
Be	0,09	-0,17	-0,02	-0,08	0,25
Bi	0,08	-0,19	-0,18	-0,01	-0,16
Cd	0,09	0,00	-0,24	-0,02	0,03
Co	0,10	0,20	-0,09	0,04	0,01
Cr	0,10	0,23	-0,08	0,00	0,01
Cs	0,12	-0,13	-0,06	0,27	-0,04
Cu	0,09	0,10	-0,28	0,07	-0,06
Ga	0,17	0,03	0,02	0,20	0,00
Ge	0,07	-0,02	-0,12	0,01	-0,18
Hf	0,12	0,01	0,17	-0,28	-0,12
In	0,03	-0,07	-0,20	-0,17	0,38
Li	0,13	-0,07	-0,01	0,29	0,00
Mn	0,12	0,13	-0,02	0,01	0,10
Mo	0,04	-0,01	-0,24	-0,03	0,20
Nb	0,15	0,09	0,05	-0,08	0,01
Ni	0,08	0,18	-0,18	0,08	-0,03
Pb	0,06	-0,17	-0,25	-0,09	-0,06
Rb	0,12	-0,19	-0,01	0,28	0,04
Re	0,02	-0,03	-0,07	-0,07	0,19
Sb	-0,02	-0,05	-0,31	-0,08	-0,27
Sc	0,13	0,22	-0,02	0,03	-0,05
Se	0,01	-0,03	-0,22	-0,15	0,32
Sn	0,07	-0,19	0,03	0,02	-0,03
Sr	0,10	0,19	0,02	-0,10	0,03
Ta	0,11	-0,03	0,09	-0,14	-0,05
Te	-0,01	-0,05	-0,23	-0,21	0,24
Th	0,16	-0,17	0,06	0,01	0,00
Tl	0,10	-0,18	-0,13	0,20	0,09
U	0,15	-0,17	0,04	-0,01	0,06
V	0,10	0,25	-0,08	0,08	-0,01
W	0,05	-0,18	-0,06	-0,15	-0,26
Y	0,20	-0,05	0,06	-0,07	0,04
Zn	0,13	0,01	-0,19	0,03	0,09
Zr	0,11	0,03	0,18	-0,29	-0,12
Ce	0,19	-0,06	0,05	0,00	-0,03
Dy	0,20	-0,04	0,05	-0,07	0,02
Er	0,19	-0,06	0,07	-0,08	0,04
Eu	0,14	0,18	-0,05	-0,01	-0,14
Gd	0,20	-0,02	0,03	-0,03	0,00
Ho	0,20	-0,05	0,06	-0,07	0,03
La	0,19	-0,06	0,04	0,01	-0,04
Lu	0,19	-0,07	0,09	-0,11	0,03
Nd	0,20	-0,04	0,03	0,00	-0,04
Pr	0,19	-0,05	0,04	0,00	-0,04
Sm	0,20	-0,04	0,03	-0,02	-0,02
Tb	0,20	-0,04	0,03	-0,04	0,02
Tm	0,19	-0,07	0,08	-0,09	0,04
Yb	0,19	-0,07	0,09	-0,10	0,04
Eigenvalues	22,87	9,42	5,92	3,24	2,08
Variance (%)	38,11	15,69	9,87	5,40	3,47
Variance accumlative	38,11	53,80	63,68	69,08	72,54

11.3 Summary Descriptive Statistics Table

Elements	Mean	Median	Standard Deviation	Sample Variance	Kurtois	Skewness	Sum Count	Min	Q1	Q3	IQR	TH1	TH2	Max	UCC
Al (pct)	6,26	6,27	1,35	1,83	0,98	-0,45	1076	0,84	5,44	7,24	1,80	9,93	12,62	10,80	8,15
Ca (pct)	0,98	0,70	1,47	2,18	103,46	8,71	1076	-0,01	0,39	1,17	0,78	2,34	3,51	22,60	2,56
Fe (pct)	3,71	3,54	1,30	1,69	4,25	1,32	1076	0,65	2,89	4,33	1,44	6,49	8,65	11,90	3,52
K (pct)	1,92	1,84	0,68	0,46	5,53	1,22	1076	0,25	1,44	2,31	0,87	3,61	4,91	6,70	2,32
Mg (pct)	0,98	0,86	0,71	0,50	24,70	4,12	1076	0,05	0,64	1,10	0,46	1,79	2,48	6,98	1,49
P (pct)	0,07	0,06	0,05	0,00	23,28	3,48	1076	-0,01	0,04	0,08	0,04	0,14	0,20	0,55	0,105
Si (pct)	30,88	30,80	3,98	15,87	4,91	-0,62	1076	5,54	28,80	33,00	4,20	39,30	45,60	45,40	28,2
Ti (pct)	0,54	0,50	0,23	0,05	7,76	1,88	1076	0,06	0,41	0,63	0,22	0,96	1,29	2,50	0,38
Ag (ppm)	-0,27	-1,00	5,36	28,78	162,41	11,95	1076	-1,00	-1,00	-1,00	0,00	-1,00	-1,00	83,00	0,075
As (ppm)	364,29	11,00	4946,42	24489839,90	277,16	16,48	1076	-5,00	7,00	17,00	10,00	32,00	47,00	89500,00	4,48
B (ppm)	96,18	86,00	43,94	1932,17	6,89	1,82	1076	12,00	68,00	113,00	45,00	180,50	248,00	467,00	10
Ba (ppm)	919,09	712,50	800,89	642020,78	14,08	3,39	1076	75,40	505,00	949,25	444,25	1615,63	2282,00	6670,00	624
Be (ppm)	-3,97	-5,00	4,12	16,98	25,61	4,68	1076	-5,00	-5,00	-5,00	0,00	-5,00	-5,00	37,00	2,1
Bi (ppm)	0,39	0,20	0,85	0,72	92,41	7,99	1076	-0,10	0,10	0,30	0,20	0,60	0,90	14,50	0,16
Cd (ppm)	0,54	0,30	1,58	2,50	189,13	12,20	1076	-0,20	-0,20	0,68	0,88	1,99	3,30	27,70	0,09
Ce (ppm)	86,83	78,85	45,28	2052,45	17,89	3,46	1076	12,50	63,23	97,30	34,08	148,41	199,53	444,00	66,5
Co (ppm)	15,89	14,10	9,79	95,94	32,87	4,02	1076	0,50	10,50	18,70	8,40	31,30	43,90	123,00	17,3
Cr (ppm)	93,77	85,00	76,45	5850,79	178,67	10,55	1076	-10,00	61,00	105,00	44,00	171,00	237,00	1610,00	92
Cs (ppm)	4,92	3,90	3,48	12,09	14,61	2,82	1076	0,40	2,70	6,00	3,30	10,95	15,90	36,70	4,9
Cu (ppm)	25,60	20,00	54,87	3013,42	452,28	20,46	1076	-5,00	14,00	30,00	16,00	54,00	78,00	1300,00	28
Dy (ppm)	5,27	4,71	3,45	11,95	41,44	5,30	1076	0,71	3,85	5,60	1,75	8,23	10,85	47,90	5,2
Er (ppm)	3,07	2,75	2,02	4,09	46,09	5,59	1076	0,37	2,28	3,27	0,99	4,75	6,23	28,90	3,5
Eu (ppm)	1,23	1,22	0,43	0,19	5,24	1,12	1076	0,21	0,95	1,46	0,51	2,23	2,99	4,33	2
Ga (ppm)	16,42	16,55	4,00	16,04	0,53	-0,17	1076	2,09	13,70	19,10	5,40	27,20	35,30	30,30	17,5
Gd (ppm)	6,12	5,69	3,43	11,76	23,29	3,91	1076	0,82	4,49	6,73	2,24	10,09	13,45	39,90	6,2
Ge (ppm)	1,74	2,00	0,81	0,66	5,17	-1,72	1076	-1,00	2,00	2,00	0,00	2,00	2,00	5,00	1,5
Hf (ppm)	7,70	7,00	3,54	12,54	2,89	1,23	1076	1,00	5,00	10,00	5,00	17,50	25,00	30,00	5,3
Ho (ppm)	1,04	0,94	0,68	0,46	44,76	5,50	1076	0,13	0,77	1,11	0,34	1,62	2,13	9,45	1,3
In (ppm)	-0,16	-0,20	0,55	0,30	345,64	18,46	1076	-0,20	-0,20	-0,20	0,00	-0,20	-0,20	10,70	0,25
La (ppm)	42,91	39,50	21,50	462,67	14,44	3,11	1076	6,20	31,30	48,10	16,80	73,30	98,50	203,00	39
Li (ppm)	42,59	40,00	18,95	359,51	4,07	1,22	1076	-10,00	29,00	51,00	22,00	84,00	117,00	159,00	21
Lu (ppm)	0,45	0,40	0,30	0,09	45,53	5,47	1076	0,06	0,33	0,49	0,16	0,72	0,96	4,39	0,8
Mn (ppm)	878,11	702,50	965,28	932623,88	103,23	8,23	1076	-10,00	467,50	996,50	529,00	1790,00	2583,50	15500,00	774
Mo (ppm)	-0,88	-2,00	4,28	18,30	183,77	11,89	1076	-2,00	-2,00	-2,00	0,00	-2,00	-2,00	70,00	1,1
Nb (ppm)	16,74	14,70	8,27	68,43	11,02	2,58	1076	0,70	12,00	19,20	7,20	30,00	40,80	82,80	12
Nd (ppm)	36,38	33,80	18,23	332,55	15,37	3,15	1076	5,10	26,80	41,10	14,30	62,55	84,00	180,00	41,5
Ni (ppm)	39,77	34,00	25,39	645,14	16,90	3,22	1076	-5,00	25,00	47,00	22,00	80,00	113,00	240,00	47
Pb (ppm)	42,46	18,00	230,88	53355,73	271,75	15,80	1076	-5,00	14,00	25,00	11,00	41,50	58,00	4350,00	17
Pr (ppm)	9,82	8,96	5,30	28,10	17,34	3,40	1076	1,41	7,06	11,18	4,11	17,34	23,51	53,10	9,2
Rb (ppm)	104,30	91,90	56,65	3211,96	6,33	2,10	1076	11,70	66,33	123,00	56,68	208,01	293,03	449,00	84
Re (ppm)	-0,02	-0,02	0,01	0,00	159,07	11,92	1076	-0,02	-0,02	-0,02	0,00	-0,02	-0,02	0,09	0,0007
Sb (ppm)	14,95	1,20	118,52	14060,93	205,91	13,00	1076	-0,10	0,80	2,38	1,58	4,74	7,10	2410,00	0,4
Sc (ppm)	11,86	12,00	5,18	26,84	4,95	0,11	1076	-5,00	9,00	14,00	5,00	21,50	29,00	44,00	14
Se (ppm)	-4,88	-5,00	1,42	2,02	163,84	12,40	1076	-5,00	-5,00	-5,00	0,00	-5,00	-5,00	18,00	0,05
Sm (ppm)	6,77	6,20	3,78	14,31	21,47	3,81	1076	1,00	4,90	7,40	2,50	11,15	14,90	41,50	7,05
Sn (ppm)	8,22	3,50	18,50	342,63	56,82	6,50	1076	-1,00	2,00	6,00	4,00	12,00	18,00	224,00	2,1
Sr (ppm)	132,69	118,00	79,52	6329,96	59,32	5,70	1076	18,30	88,68	162,00	73,33	271,99	381,98	1090,00	320
Ta (ppm)	1,22	1,10	1,02	1,05	18,63	2,48	1076	-0,50	0,80	1,50	0,70	2,55	3,60	12,00	2
Tb (ppm)	0,90	0,82	0,57	0,32	34,20	4,79	1076	0,12	0,65	0,98	0,33	1,48	1,97	7,44	1,2
Te (ppm)	-0,45	-0,50	0,63	0,40	296,17	16,83	1076	-0,50	-0,50	-0,50	0,00	-0,50	-0,50	11,10	0,001
Th (ppm)	14,84	11,50	14,46	209,30	56,46	6,17	1076	1,50	9,30	15,20	5,90	24,05	32,90	222,00	10,5
Tl (ppm)	0,54	0,60	1,02	1,04	40,38	3,98	1076	-0,50	-0,50	0,90	1,40	3,00	5,10	12,00	2,7
Tm (ppm)	0,46	0,40	0,32	0,10	51,02	5,88	1076	0,06	0,34	0,48	0,14	0,69	0,90	4,76	0,52
U (ppm)	6,15	3,43	12,08	146,10	71,56	7,33	1076	0,90	2,82	4,44	1,62	6,86	9,29	175,00	2,7
V (ppm)	103,54	95,00	53,72	2888,54	2,05	1,25	1076	5,00	66,00	124,00	58,00	211,00	298,00	350,00	97
W (ppm)	5,43	2,00	32,44	1053,35	694,55	24,28	1076	-1,00	1,00	3,00	2,00	6,00	9,00	958,00	1,25
Y (ppm)	28,53	25,50	18,54	344,22	42,01	5,32	1076	3,30	21,20	30,50	9,30	44,45	58,40	255,00	21
Yb (ppm)	3,07	2,70	2,07	4,28	47,64	5,69	1076	0,40	2,30	3,20	0,90	4,55	5,90	29,80	3,2
Zn (ppm)	132,26	95,00	195,84	38389,74	239,83	13,50	1076	25,00	75,00	134,00	59,00	222,50	311,00	3870,00	67
Zr (ppm)	295,60	273,50	126,70	16068,20	1,97	1,09	1076	45,60	203,00	367,00	164,00	613,00	859,00	1010,00	193
REE (ppm)	204,34	186,19	105,12	11060,29	18,31	3,49	1076	29,10	150,80	227,67	76,87	342,97	458,27	1063,24	100-300
LREE (ppm)	183,94	168,09	93,69	8786,11	16,61	3,32	1076	26,42	134,25	205,10	70,86	311,39	417,67	912,51	94
HREE (ppm)	20,40	18,42	12,69	161,20	38,58	5,09	1076	2,68	15,09	21,95	6,86	32,23	42,51	172,54	3,01

(LREE): Light rare earth elements (La - Eu)

(HREE): Heavy rare earth elements (Gd-Lu)

(UCC): Mean upper crust concentration values reported by Rudnick and Gao (2014)

(TH1): Threshold separating the background concentration range from the second-order anomaly (outliers) range (Q3 + 1.5 * IQR).

(TH2): Threshold separating the second-order anomaly range from first-order anomaly range (Q3 + 3 * IQR).